

TOPICAL REVIEW

Open Heavy Flavor in QCD Matter and in Nuclear Collisions

Francesco Prino

INFN Torino, Via Pietro Giuria 1, I-10125 Torino, Italy

E-mail: prino@to.infn.it

Ralf Rapp

Cyclotron Institute and Department of Physics and Astronomy, Texas A&M University, College Station, TX 77843-3366, USA

E-mail: rapp@comp.tamu.edu

Abstract. We review the experimental and theoretical status of open heavy-flavor (HF) production in high-energy nuclear collisions at RHIC and LHC. We first overview the theoretical concepts and pertinent calculations of HF transport in QCD matter, including perturbative and non-perturbative approaches in the quark-gluon plasma, effective models in hadronic matter, as well as implementations of heavy-quark (HQ) hadronization. This is followed by a brief discussion of bulk evolution models for heavy-ion collisions and initial conditions for the HQ distributions which are needed to calculate HF spectra in comparison to observables. We then turn to a discussion of experimental data that have been collected to date at RHIC and LHC, specifically for the nuclear suppression factor and elliptic flow of semileptonic HF decays, D mesons, non-prompt J/ψ from B -meson decays, and b -jets. Model comparisons to HF data are conducted with regards to extracting the magnitude, temperature and momentum-dependence of HF transport coefficients from experiment.

Contents

1	Introduction	2
1.1	QCD Matter and Heavy-Ion Collisions	2
1.2	Diagnostic Potential of Heavy-Flavor Particles	4
1.3	Brief Outline	5
2	Theoretical Descriptions of Heavy Flavor in Medium	6
2.1	Frameworks for Heavy-Flavor Transport	7
2.2	Calculations of Heavy-Flavor Transport	10
2.2.1	Quark-Gluon Plasma I: Elastic Interactions	10
2.2.2	Quark-Gluon Plasma II: Radiative Interactions	14
2.2.3	Hadronic Matter	16
2.2.4	Lattice QCD	17
2.2.5	Comparison of Spatial Diffusion Coefficients	18
2.2.6	Hadronization	20
2.2.7	Pre-Equilibrium and Mean-Field Transport	23
2.3	Bulk Medium Evolution Models for URHICs	25
3	Experimental Results and Comparison to Models	26
3.1	Experimental Facilities and Techniques	26
3.1.1	Accelerators	26
3.1.2	Open Heavy-Flavor Production Measurement Techniques	28
3.1.3	Experimental observables	32
3.2	Open Heavy-Flavor Data in pp and p-A (d-A) Collisions	35
3.2.1	Production in pp and Comparison to pQCD Calculations	35
3.2.2	Results from p-A (d-A) collisions and Cold-Nuclear-Matter Effects	44
3.3	Results from A-A Collisions and Model Comparisons	52
3.3.1	Heavy-flavor decay leptons	54
3.3.2	Charm hadrons	63
3.3.3	Beauty production	71
3.4	Summary of Model-to-Data Comparisons and Implications for HF Transport	75
4	Conclusions and Outlook	79

1. Introduction*1.1. QCD Matter and Heavy-Ion Collisions*

The investigation of strongly interacting matter under extreme conditions of temperature and energy density is at the forefront of modern nuclear physics research. On the one hand, this research improves our understanding of the hot medium that

prevailed in the first few microseconds of the early universe, as well as of the interior of neutron stars where a compression of several times normal nuclear matter density is realized at small temperatures. On the other hand, it remains a formidable challenge to map out the phase structure of Quantum Chromodynamics (QCD) as part of the standard model of elementary particle physics, based on the many-body physics of quarks and gluons and/or suitable effective degrees of freedom. In particular, the asymptotic freedom of the QCD coupling strength suggests that hadronic matter, which prevails at low temperatures and densities, will change into a quark-gluon plasma (QGP) at high temperatures.

Collision experiments of heavy atomic nuclei at high energies provide the unique opportunity to create and study the properties of QCD matter in the laboratory. Due to the transient nature of the medium produced in these reactions, which explodes with large collective velocities, its systematic investigation is not easy. Nevertheless, progress has been made over about 30 years of ultrarelativistic heavy-ion collisions (URHICs) due to a concerted effort of experiment and theory. The basic picture that has emerged for the reaction dynamics is that of an expanding fireball which rapidly reaches near local equilibrium within about $1 \text{ fm}/c$ after the initial collision, a pressure-driven expansion for about $10\text{--}15 \text{ fm}/c$ and a subsequent rather sudden freezeout into free-streaming hadrons which are observed in the detectors, cf. Refs. [1–3] for recent overviews. Analyses of bulk-hadron momentum distributions provide a snapshot of the fireball at its break-up stage, revealing a “thermal freezeout” at a temperature, $T_{\text{fo}} \simeq 100 \text{ MeV}$, and an average collective expansion velocity of more than half the speed of light [4, 5]. The analysis of abundances of different hadron species, the so-called hadro-chemistry, reveals a higher temperature, $T_{\text{ch}} \simeq 160 \text{ MeV}$, characterizing the “chemical freezeout” of the hadronic system. This temperature is close to the pseudo-critical temperature of the chiral transition computed in lattice-QCD, $T_{\text{pc}} = 155 \pm 10 \text{ MeV}$ [6, 7], although the transition from partons to hadrons probably occurs over an extended temperature window. Electromagnetic radiation from the medium further supports the formation of matter at and above the transition; in particular, dilepton invariant-mass spectra show that the ρ -meson, as a “prototype” light hadron, strongly broadens in hadronic matter and dissolves in the vicinity of T_{pc} [8].

A fundamental question that remains open thus far is how the quark-hadron transition emerges from the underlying in-medium QCD force, and how the latter determines the transport properties of the QGP. The heavy charm and bottom quarks ($Q = c, b$) play a special role in this context. In the present review we will elaborate on the physics of open heavy-flavor (HF) probes in URHICs, focusing on recent developments pertaining to theoretical modeling, the first round of LHC data as well as the most recent RHIC data (see, *e.g.*, Ref. [9–11] for recent reviews). While the physics of the open HF sector bears intimate connections to the hidden HF (quarkonium) sector, which are increasingly exploited, we will here concentrate on the former and refer to recent overviews on in-medium quarkonium physics in Refs. [11–15].

1.2. Diagnostic Potential of Heavy-Flavor Particles

The masses of charm and bottom quarks (as well as hadrons containing them) are much larger than both the QCD scale parameter and the pseudo-critical temperature of the QCD phase transition, $m_{c,b} \gg \Lambda_{\text{QCD}}, T_{\text{pc}}$. In the vacuum, this has long been recognized as an effective expansion tool to formulate a potential theory of the fundamental QCD force. The potential approach was originally motivated by phenomenological descriptions of quarkonium spectroscopy in vacuum, but is now accurately confirmed by lattice QCD (lQCD) calculations [16].

In the context of QCD matter studies in heavy-ion collisions, the large heavy-quark (HQ) mass, m_Q , together with flavor conservation in strong interactions, has several important implications:

(a) $Q\bar{Q}$ production is essentially restricted to the primordial nucleon-nucleon collisions in the reaction, since the production threshold is much higher than the typical medium temperatures.

(b) Since the HQ mass is much larger than the pseudo-critical temperature, charm and bottom quarks retain their “identity” through the hadronization transition in URHICs; this renders them an excellent probe of hadronization mechanisms down to small momenta, *i.e.*, whether they pick up a light anti-/quark from the surrounding medium or fragment independently.

(c) The typical momentum exchange of HF particles with the heat bath, $\bar{q}^2 \simeq T^2$, is parametrically small compared to the thermal HF momentum, $p_Q^{\text{th}} \simeq \sqrt{2m_Q T}$; HF particles thus execute a “Brownian motion” with many, relatively small momentum kicks from the medium.

(d) The typical thermal energy transfer on the HF particle is parametrically small compared to the momentum transfer, $q_0^2 \sim \bar{q}^4/m_Q^2 \ll \bar{q}^2$; therefore, the 4-momentum transfer $q^2 = q_0^2 - \bar{q}^2$ is essentially spacelike, which is characteristic of potential-type interactions.

(e) The thermal relaxation time of HF particles, $\tau_Q \simeq \tau_{\text{th}} m_Q/T$, is much longer than the thermalization time, τ_{th} , of the bulk medium; thus, in connection with item (a) and the possibility that τ_Q is comparable to (or longer than) the fireball lifetime, τ_{FB} , HF spectra in heavy-ion collisions retain a memory of their interaction history. If so, their finally observed modifications can serve as a gauge of the HF coupling strength to the medium.

As a further benefit for phenomenology, various quantities which characterize the interactions of heavy flavor in medium can be computed in thermal lattice QCD, *e.g.*, the HF diffusion coefficient [17, 18], HQ susceptibilities [19] and mesonic correlation functions [20]. Even if these quantities are not directly applicable to experiment, they can serve as valuable constraints for model calculations which provide a bridge to experimental observables [21]. The above features provide for a promising framework to determine the basic QCD force in the medium and its emergent phenomena of HF transport in QCD matter, by combining lattice QCD, model calculations and the

phenomenological analysis of experimental data in a controllable way.

For sufficiently high momenta, $p_Q \gg m_Q$, heavy quarks will behave as light particles, transitioning into the regime of energy loss dominated by gluon radiation. It currently remains an open question at which momenta this transition occurs, whether it coincides with a transition from non-perturbative to perturbatively calculable mechanisms, and how the quark mass effect establishes itself prior to reaching the ultrarelativistic regime.

1.3. Brief Outline

The remainder of this review is organized as follows.

In Sec. 2 we review general frameworks for the theoretical description of HF propagation through QCD matter and their implementations into the phenomenology of heavy-ion collisions. We start by recalling the basic elements of HF transport approaches, in particular simulations based on the Boltzmann and relativistic Langevin equations, and critically discuss their virtues and limitations as well as respective regimes of applicability (Sec. 2.1). We then survey and compare different mechanisms of HF transport through QCD matter including perturbative and non-perturbative elastic HQ interactions in the QGP, perturbative radiative HQ energy loss, heavy-meson scattering in hadronic matter, analyses using thermal lQCD, as well as transport through the quark-hadron transition and pre-equilibrium phases of heavy-ion collisions (Sec. 2.2). This is followed by a discussion of further ingredients needed to make realistic contact with data (Sec. 2.3), pertaining to the initial conditions for the HQ spectra and the space-time evolution of the bulk medium formed in heavy-ion collisions.

In Sec. 3 we summarize the current status of experimental HF measurements in light- and heavy-ion collisions and their theoretical interpretation through model comparisons. We first survey the relevant accelerator facilities, experimental tools and types of HF observables (Sec. 3.1), followed by a presentation of the current data on HF production in pp collisions and their modification in proton/deuteron-nucleus (pA/dA) collisions (Sec. 3.2). The compilation of HF data in nucleus-nucleus (AA) systems (Sec. 3.3) is organized into three parts, dedicated to HF decay lepton, charmed-hadron, and beauty production, each of them reviewing the results on the modification of transverse-momentum (p_T) spectra and the elliptic flow in Au-Au and Cu-Cu collisions at RHIC and Pb-Pb collisions at the LHC. The discussion of the data is accompanied by model comparisons which we attempt to translate into qualitative and quantitative information about the mechanisms and magnitudes of HF interactions and transport coefficients in QCD matter (Sec. 3.4).

We summarize and give an outlook in Sec. 4.

2. Theoretical Descriptions of Heavy Flavor in Medium

As alluded to in the introduction, the motion of HF particles (both quarks and hadrons) through the QCD medium at temperatures relevant for URHICs is akin to a Brownian motion, where a heavy *probe* is injected into a background medium of light particles. The subsequent diffusion process of the probe particle is governed by its coupling to the medium, schematically given by an average displacement squared,

$$\langle \vec{r}^2 \rangle = (2d)D_s t \quad (1)$$

(t : time). The transport properties of the medium are encoded in the spatial diffusion coefficient, D_s (the prefactor $2d$, where d is the number of spatial dimensions, is a convention). A small value of D_s characterizes a strong coupling: frequent rescattering limits the spatial dispersion of the Brownian particle. The spatial diffusion coefficient is directly related to the thermal relaxation (or equilibration) time, τ_{eq} , of the heavy particle via

$$\tau_{\text{Q}} = \frac{m_{\text{Q}}}{T} D_s . \quad (2)$$

This relation makes explicit the “time delay” in the HF thermalization process by the HQ mass to temperature ratio, m_{Q}/T , and further suggests that D_s is a generic medium property. When scaling D_s by the thermal wavelength of the medium, $\lambda_{\text{th}} = 1/2\pi T$, one obtains a dimensionless quantity which has been suggested to be proportional to the widely discussed ratio of viscosity to entropy density of the medium [9, 22],

$$D_s(2\pi T) \propto \frac{\eta}{s}(4\pi) . \quad (3)$$

The numerical coefficient in this relation is, however, not unique, varying, *e.g.*, from ~ 1 in strongly-coupled conformal field theory (CFT) [23–25] to $2/5$ in kinetic theory for a weakly coupled ultrarelativistic gas [26].

In the remainder of this section we first discuss two of the most commonly employed transport approaches to HF propagation in QCD matter, namely relativistic Langevin processes and Boltzmann simulations (Sec. 2.1). In particular, we revisit their regimes of applicability in relation to both the large mass limit of the HF particle and the nature of the background medium. We then turn to microscopic calculations of HF transport coefficients in QCD matter (Sec. 2.2), encompassing elastic and inelastic interactions in both perturbative and nonperturbative approaches, for both QGP (Secs. 2.2.1 and 2.2.2) and hadronic matter (Sec. 2.2.3). This will be followed by a discussion of lQCD computations (Sec. 2.2.4), the spatial HF diffusion coefficient (Sec. 2.2.5), hadronization mechanisms and their relation to diffusion processes (Sec. 2.2.6), and pre-equilibrium as well as mean-field effects on HQ propagation (Sec. 2.2.7). Finally, we discuss further model components needed for quantitative phenomenology of HF data in URHICs (Sec. 2.3), focusing on properties of the bulk medium evolution pertinent to HF transport. Another component, namely initial conditions for the HQ spectra, will be discussed in more detail in connection with pp and pA data in Sec. 3.2. Throughout Sec. 2 we will adopt natural units with $\hbar = c = 1$.

2.1. Frameworks for Heavy-Flavor Transport

In kinetic theory, the starting point for describing the motion of HF particles through QCD matter is the Boltzmann equation. Since there is no principal difference between HF hadrons in hadronic matter and heavy quarks in QGP, we focus our formal discussion in this section on the latter. The space-time evolution of the HQ phase space distribution function, f_Q , is then governed by the integro-differential equation

$$\left[\frac{\partial}{\partial t} + \frac{\vec{p}}{E_p} \frac{\partial}{\partial \vec{x}} + \vec{F} \frac{\partial}{\partial \vec{p}} \right] f_Q(t, \vec{x}, \vec{p}) = C[f_Q], \quad (4)$$

where $E_p = \sqrt{m_Q^2 + \vec{p}^2}$ denotes the HQ on-shell energy (reflecting the inherently classical nature of the Boltzmann equation). In a static medium in equilibrium the distribution function approaches the Boltzmann distribution, $f_Q = d_Q \exp(-E_p/T)$, where T is the temperature and $d_Q=6$ the HQ degeneracy.

The space-time evolution of f_Q is generated by the first two terms on the left-hand side (*lhs*) of Eq. (4). The third term represents the effects due to a force \vec{F} induced by an external (or mean) field, *e.g.*, (chromo-) electric and/or magnetic fields as could be relevant in the early phases of a heavy-ion collision. Examples of those will be discussed in Sec. 2.2.7.

The right-hand side (*rhs*) of the Boltzmann equation is the collision integral. For $2 \rightarrow 2$ scattering of a heavy quark off thermal partons it takes the form

$$C[f_Q] = \frac{1}{2E_p} \int \tilde{d}k \int \tilde{d}p' \int \tilde{d}k' \frac{1}{d_Q} \sum_{m=q,\bar{q},g} |\mathcal{M}_{Qm}|^2 (2\pi)^4 \delta^{(4)}(p+k-p'-k') \times [f_Q(E_{p'}) f_m(\omega_{k'}) - f_Q(E_p) f_m(\omega_k)]. \quad (5)$$

where $\tilde{d}k \equiv d^3k/(2\omega_k(2\pi)^3)$ are the standard Lorentz-invariant phase space differentials and \mathcal{M}_{Qm} is the HQ-parton scattering amplitude with \vec{p} (\vec{p}') and \vec{k} (\vec{k}') the 3-momenta of the incoming (outgoing) heavy quark Q and medium parton m (quark, antiquark or gluon), respectively; the f_m are the latter's thermal distribution functions and $\omega_{k,k'}$ their on-shell energies (quantum effects can be included through the use of Fermi/Bose distribution functions and final-state blocking/enhancement factors, and are implicit in field-theoretical evaluations of the scattering amplitude). In a dilute medium, the collision integral can be approximated by using particle cross sections. For large scattering rates the definition of asymptotic states becomes problematic and a formulation in terms of scattering probabilities is preferable. The inclusion of radiative processes is more challenging, especially if interference effects for subsequent scatterings become significant, due to the inherent off-shell nature of these processes, see, *e.g.*, Refs. [27, 28] for recent work in the HQ context. As is well known, electromagnetic Bremsstrahlung off heavy fermions is suppressed by the fourth power of their mass. It is currently an open question at which HQ momenta and QGP temperatures radiative processes take over from elastic ones. We will return to this question below.

As discussed in the introduction, for large quark masses and moderate temperatures, the typical momentum transfer from the heat bath to the heavy quark

is parametrically small, $\vec{q}^2 \ll \vec{p}^2$ where $\vec{q} = \vec{p} - \vec{p}' = \vec{k}' - \vec{k}$. In addition, the energy transfer is further suppressed, $q_0^2 \ll \vec{q}^2$. These conditions imply that the heavy quark is undergoing soft but incoherent collisions characteristic for Brownian motion. The scattering rate in the collision integral can then be expanded in powers of the momentum transfer. Carrying this out to second order, the Boltzmann equation can be transformed into the Fokker-Planck equation,

$$\frac{\partial}{\partial t} f_Q(t, \vec{p}) = \frac{\partial}{\partial p_i} \left\{ A_i(\vec{p}) f_Q(t, \vec{p}) + \frac{\partial}{\partial p_j} [B_{ij}(\vec{p}) f_Q(t, \vec{p})] \right\} , \quad (6)$$

which now is only a differential equation for the HQ phase space distribution function. Its key ingredients are the transport parameters A and B . In a medium in (local) thermal equilibrium they simplify to three a priori independent coefficients,

$$A_i(\vec{p}) = A(p) p_i , \quad (7)$$

$$B_{ij}(\vec{p}) = B_0(p) P_{ij}^\perp(\vec{p}) + B_1(p) P_{ij}^\parallel(\vec{p}) , \quad (8)$$

characterizing momentum friction and diffusion, respectively, of the propagating heavy quark ($P_{ij}^\perp = \delta_{ij} - p_i p_j / \vec{p}^2$ and $P_{ij}^\parallel = p_i p_j / \vec{p}^2$ are the standard 3D transverse and longitudinal projectors, respectively). They correspond to the first and second moments of the thermally weighted scattering amplitude,

$$A(p) = \left\langle 1 - \frac{\vec{p} \cdot \vec{p}'}{\vec{p}^2} \right\rangle , \quad (9)$$

$$B_0(p) = \frac{1}{4} \left\langle \vec{p}'^2 - \frac{(\vec{p}' \cdot \vec{p})^2}{\vec{p}^2} \right\rangle , \quad (10)$$

$$B_1(p) = \frac{1}{2} \left\langle \frac{(\vec{p}' \cdot \vec{p})^2}{\vec{p}^2} - 2\vec{p}' \cdot \vec{p} + \vec{p}^2 \right\rangle , \quad (11)$$

where the definition of the brackets follows from the collision term in the Boltzmann equation,

$$\begin{aligned} \langle X(\vec{p}') \rangle &= \frac{(2\pi)^4}{2E_p d_Q} \int \tilde{d}k \tilde{d}k' \tilde{d}p' \\ &\quad \times \sum_m |\mathcal{M}_{Qm}|^2 \delta^{(4)}(p + k - p' - k') f_m(\omega_k) X(\vec{p}') . \end{aligned} \quad (12)$$

In the non-relativistic limit of 3-momentum independent transport coefficients, $\gamma \equiv A(p) = \text{const}$ and $D_p \equiv B_0(p) = B_1(p) = \text{const}$, the Fokker-Planck equation takes the simpler form

$$\frac{\partial}{\partial t} f_Q(t, p) = \gamma \frac{\partial}{\partial p_i} [p_i f_Q(t, p)] + D_p \Delta_{\vec{p}} f_Q(t, p) \quad (13)$$

($\Delta_{\vec{p}}$: 3-momentum Laplace operator). For large times, this equation has the solution

$$f_Q(t, p) = \left(\frac{2\pi D_p}{\gamma} \right)^{3/2} \exp \left(-\frac{\gamma \vec{p}^2}{2D_p} \right) . \quad (14)$$

Matching this to the non-relativistic equilibrium limit one obtains the Einstein relation (or dissipation-fluctuation theorem),

$$D_p = m_Q \gamma T , \quad (15)$$

highlighting the intimate relation between momentum friction and diffusion, and their role in imprinting the temperature of the heat bath on the HQ distribution.

In URHICs, the Fokker-Planck equation can be implemented to simulate HF motion through QCD matter via a Langevin process. The latter consists of a “deterministic” drag and “stochastic” diffusion part, defined via momentum and position updates as

$$\begin{aligned} dp_j &= -\Gamma(p, T)p_j dt + \sqrt{dt}C_{jk}\rho_k \\ dx_j &= \frac{p_j}{E} dt . \end{aligned} \quad (16)$$

The C 's are uniquely related to the diffusion coefficients,

$$C_{jk} = \sqrt{2B_0(p)}P_{jk}^\perp(\vec{p}) + \sqrt{2B_1(p)}P_{jk}^\parallel(\vec{p}) , \quad (17)$$

and are weighted with a random Gaussian noise distribution, $P(\vec{\rho}) = \exp(-\vec{\rho}^2/2)/(2\pi)^{3/2}$. The precise relation of Γ to the friction coefficient, $\Gamma(p) = A(p, T) + \mathcal{O}(T/m_Q)$, depends on the numerical scheme to carry out the Langevin process [29, 30]. In the so-called post-point scheme, the relativistic version of the Einstein relation takes the form $B_0(p) = B_1(p) = TE_p\Gamma(p)$. The latter is not automatically satisfied for microscopically calculated transport coefficients, but rather becomes an important tool to ensure their consistency [22, 31] and, consequently, the proper equilibrium limit when implementing them into Langevin simulations. In both perturbative [22] and non-perturbative approaches [31] for calculating the transport coefficients from underlying microscopic interactions, the Einstein relation was found to be rather well satisfied for the friction and transverse diffusion coefficient. Significant deviations were found to develop for the longitudinal coefficient toward higher momenta, presumably due to the specific kinematics of the scattering processes (*e.g.*, pQCD scattering is typically strongly peaked at forward angles). To ensure the correct equilibrium limit in Langevin simulations of the Fokker-Planck equation, B_1 is then corrected for by its value obtained from the Einstein relation [32–34] in terms of the friction coefficient; alternatively, the latter is readjusted by the diffusion coefficients $B_{0,1}$ [22, 35, 36].

One may wonder how accurate the Fokker-Planck approximation due to the expansion in the momentum transfer is, especially for charm quarks at high temperatures. This question has recently been revisited by comparing the results of HQ Boltzmann and Langevin simulations using leading-order pQCD cross section for heavy-light parton scattering [37]. It was found that for charm quarks with $m_c = 1.3$ GeV in a heat bath of $T = 0.4$ GeV, appreciable deviations of several 10's of percent develop in the momentum spectra after an evolution time of $\Delta t = 2$ fm. For bottom quarks with $m_b = 4.2$ GeV, the deviations are below $\sim 5\%$ even after $\Delta t = 6$ fm, and also for c quarks at $T = 0.2$ GeV the agreement is much improved. This suggests that for ratios $M_Q/T \gtrsim 6$ the Langevin approximation is quite reliable. In fact, if the dissipation-fluctuation theorem is enforced for the pQCD transport coefficients in the Langevin simulation, the discrepancies with the Boltzmann results are further reduced by up to a factor of ~ 2 [37].

Another feature of the Boltzmann equation that is not easily implemented in Langevin simulations is that of off-equilibrium effects in the surrounding medium. In the

Boltzmann equation, such effects on the medium parton distribution functions can be treated on the same footing as for the HQ distribution, as done, *e.g.*, in Refs. [38–40]. On the other hand, the simulations of the bulk medium in the Boltzmann approach usually rely on quasi-particles with vanishing widths. In the Langevin approach, the underlying transport coefficients can be calculated with finite-temperature field theory techniques, where the inclusion of quantum effects through the use of broad spectral functions for the bulk medium constituents is in principal straightforward. The Langevin approach is thus better suited for situations where the medium is strongly coupled (as implicit in hydrodynamic medium evolutions), as long as the “Brownian” particle is still a reasonably well-defined quasi-particle, *i.e.*, with an energy much larger than its width, $E_p \gg \Gamma_Q(p)$ (here, Γ_Q denotes the scattering rate, not equilibration rate, characterizing the width of the quasi-particle peak in the HQ spectral function).

2.2. Calculations of Heavy-Flavor Transport

2.2.1. Quark-Gluon Plasma I: Elastic Interactions

Early evaluations of HQ transport coefficients in deconfined matter were carried out using perturbative Born diagrams for cross sections off thermal partons, with a Debye screening mass $m_D = gT$ introduced as an infrared regulator into the (dominant) t -channel gluon exchange propagator [41],

$$D_g = \frac{1}{(t - m_D^2)}, \quad (18)$$

where t is the 4-momentum transfer in the scattering. Subsequently, these calculations have been routinely repeated to serve as a benchmark, and will be referred to as “schematic LO pQCD” in the following. Even for a coupling constant as large as $\alpha_s = g^2/4\pi = 0.4$, which produces appreciable total cross sections of a few millibarns, the predominantly forward scattering results in friction coefficients for charm (bottom) quarks reaching about $A(p=0) \simeq 12(5)$ MeV, with a weak momentum dependence. The corresponding thermal relaxation times, $\tau_Q \simeq 15\text{-}20(40)$ fm/ c (translating into a spatial diffusion coefficient $D_s(2\pi T) \simeq 30$), are quite a bit longer than the typical QGP lifetime of about 5–10 fm/ c in central heavy-ion collisions at RHIC and LHC energies [42]. When first RHIC data on HF spectra and elliptic flow in Au-Au collisions at $\sqrt{s_{\text{NN}}}=200$ GeV were published [43, 44], it became clear that much shorter thermalization times are required to account for the strong medium modifications implied by these data (and subsequently by LHC data). A non-perturbative resonance model [31, 32], which gave a fair description of these first data, led to an initial estimate of the diffusion coefficient of $D_s(2\pi T) \simeq 4\text{-}6$.

Several developments in the perturbative framework have been carried out since then. In Refs. [45, 46], the schematic screening in eq. (18) has been improved following the methods of Ref. [47] by matching a hard-thermal loop calculation of the gluon self-energy for small momentum transfers, t , to a perturbative (unscreened) calculation at large t . This effectively leads to a reduction in the screening of the gluon exchange

propagator, which may be represented as

$$D_g = \frac{1}{t - rm_D^2} . \quad (19)$$

Numerically, the effective reduction parameter turns out to be quite small, $r \simeq 0.2$, which produces a substantial increase (by about a factor of 2) of the energy loss of a heavy quark for a typical strong coupling constant of $\alpha_s \simeq 0.2$. It has furthermore been argued [45, 46] that the running of the QCD coupling constant ought to be accounted for down to soft scales, rising up to values of $\alpha_s \simeq 1$ for small $|t|$. When combining the running coupling with the reduced Debye screening, the charm-quark friction coefficient (or thermalization rate) increases by a factor of 5-10 over the schematic fixed-coupling/-Debye mass scheme at small charm-quark momenta [46]. A matching of the HTL calculations at low $|t|$ to pQCD scattering at high $|t|$ has also been utilized in the calculations of the transport coefficients by the Torino group (or POWLANG approach) [36, 48], but with a fixed Debye mass as obtained from weak-coupling calculations and a coupling constant running with temperature (not with momentum transfer) [49]; in particular, the calculated longitudinal diffusion coefficient has been used to fix the friction coefficient via the Einstein relation. This leads to a significantly smaller thermalization rate at zero charm-quark momentum, but also to a different momentum dependence which is initially rising with p .

In a spirit similar to the implementation of Refs. [45, 46], the HQ-medium interactions have been calculated in the dynamical quasiparticle model using elastic Born cross sections with infrared enhanced coupling constant [50]. In this calculation the HQ transport is coupled to a bulk medium whose equation of state is consistent with lQCD. The results for the charm-quark relaxation rate in this approach are smaller by about a factor of $\sim 2-3$ compared to the HTL-inspired scheme with running coupling and reduced Debye mass. These transport coefficients have been subsequently employed in the PHSD transport model [40, 51].

A large increase in the HQ thermalization rate raises the question of higher order corrections. In Ref. [52] the convergence of the perturbative expansion for the HQ transport coefficient has been scrutinized. It was found that even for a strong coupling constant as small as $\alpha_s = 0.03$ (corresponding to $g_s = 0.6$) the NLO correction is around a factor of 2 (and further growing for larger values of α_s). This gives little hope for a rigorous perturbative evaluation of HQ transport, but rather calls for non-perturbative methods. For example, it would be of interest to carry out a ladder resummation of the infrared-augmented one-gluon exchange interaction and check for the appearance of bound-state solutions.

A large running coupling toward small momentum transfers in the one-gluon exchange interaction corresponds to a strong Coulomb force on the heavy quark at large distances. However, in the QCD vacuum, the long-distance part of the potential between a static color charge and its anti-charge is characterized by a linearly increasing “string” interaction, presumably induced by gluonic condensates. The pertinent Cornell

potential,

$$V(r) = -\frac{4}{3} \frac{\alpha_s}{r} + \sigma r , \quad (20)$$

was originally inferred from a successful description of the vacuum charmonium and bottomonium spectra [53] and is now well established from lQCD [16]. A key question in QGP research is how this fundamental force changes in the medium. Lattice-QCD computations of the free energy at finite temperature indicate that remnants of the confining force survive in the QGP, possibly up to $2 T_c$ [54]. Thus, string-like interactions are likely to play an important role for HQ interactions when approaching T_c from above. As elaborated in Sec. 1.2, an extension of the potential model to finite temperature may provide an opportunity to include non-perturbative interactions in the description of open and hidden HF particles in QCD matter at moderate temperatures. This can be realized in the thermodynamic T -matrix formalism, which has been widely used in other contexts, such as the nuclear many-body problem [55], electromagnetic plasmas [56], or cold atomic gases [57]. In Ref. [58] the T -matrix formalism has been deployed to selfconsistently evaluate HQ and quarkonium properties in the QGP. With additional relativistic (magnetic) corrections to the static potential [59], and an approximate description of vacuum spectroscopy, a comprehensive treatment of HF properties in the QGP can be carried out. Euclidean correlators, susceptibilities and spectral functions can be calculated and tested against lQCD results, as well as transport properties which can be implemented into URHIC phenomenology. In particular, the in-medium T -matrix for heavy-light parton scattering can be straightforwardly implemented to calculate HQ transport coefficients using eq. (12) [58, 60, 61]. A critical input to this approach is the two-body interaction kernel, *i.e.*, the HQ potential. Ideally, one could take it directly from lQCD. However, lQCD computations rather provide the free ($F_{Q\bar{Q}}$) and internal ($U_{Q\bar{Q}}$) energies, which strictly speaking are not potentials. However, they have been used to bracket the uncertainty in the potential definition; the internal energy leads to much stronger interactions and is clearly preferred over the free energy when carrying out quarkonium [62–64] and open HF phenomenology [65] at RHIC and LHC energies. Most notably, when using the free energy, the calculated suppression of the $Y(1S)$ state is larger than observed [66, 67], and, pertinent to the present topic, the calculated elliptic flow of open HF observables is much too small [68]. Recent progress in determining the underlying HQ potential has been made by directly calculating the static free and internal energies from the T -matrix [70]. It turns out that large imaginary parts in the single HQ selfenergies as well as in the potential induce substantial deviations from the free energy (the latter emerges as potential in the limit of small imaginary parts, *e.g.*, in the weak-coupling limit). Remarkably, the in-medium potential, V , gives rise to a long-range (non-Coulombic) force which is neither present in F nor in U , cf. Fig. 1. This has important consequences for the HQ transport coefficient, which for low momenta turns out to be larger than when U is assumed as potential. These results are not unlike the ones found in Ref. [54] where a 2-parameter ansatz for the spectral function with a functional form adopted from HTL perturbation theory was

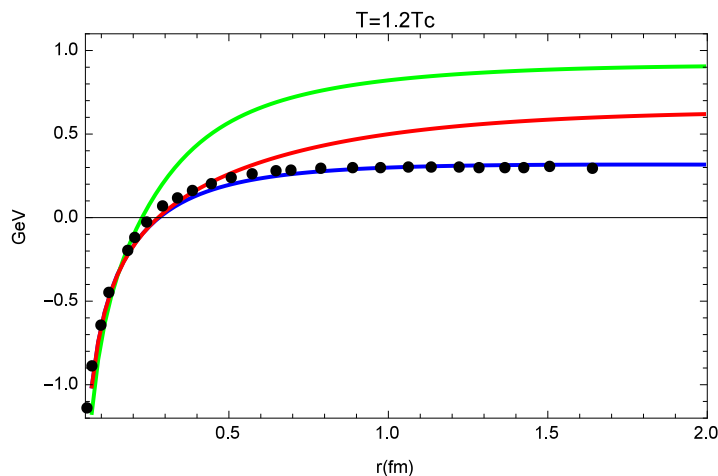


Figure 1. Fit of a T -matrix calculation of the free energy (blue line) to IQCD data [69] (black points) at $T=240$ MeV, and the resulting internal energy (green line) and in-medium input potential (red line). Figure taken from Ref. [70].

used for the extraction of the potential. On the other hand, in Ref. [71] the (real part of the) potential turns out to be close to the free energy. More work is needed to clarify the differences in these findings.

An in-medium Cornell potential is also underlying the collisional dissociation approach for HF propagation in the QGP adopted in the model by Vitev *et al.* [72]: the propagating heavy quarks can form in-medium D - and B -meson bound states which subsequently dissociate again, and so on. As in Refs. [31, 60], the presence of such mesonic correlations in the QGP has been found to be instrumental in generating sufficient suppression of the HF spectra at RHIC, and later LHC [72].

The momentum dependence of the charm-quark friction coefficient (or thermalization rate) is summarized in Fig. 2 for several of the above discussed approaches, as a function of 3-momentum and for several temperatures. The schematic LO pQCD approach [41] with fixed coupling ($\alpha_s=0.4$) and Debye mass gives relatively small values of around 0.05/fm, with a weak momentum dependence. In the HTL approach of the Torino group (as implemented in the POWLANG HF transport approach for URHICs) [36, 48], much larger values are found (by factor of ~ 3 -4 at low p), which is in part due the improved treatment of the screening and in part due to the procedure of inferring $A(p)$ from the longitudinal momentum diffusion coefficient, $B_1(p)$ (also, the charm-quark mass is $m_c=1.3$ GeV). In particular, the latter produces a momentum dependence of the friction coefficient which increases with p before approximately leveling off. On the contrary, the increase in soft HQ interactions due to a reduced screening mass and running coupling constant at low momentum transfers [45, 46] (as implemented in the MC@sHQ+EPOS [73, 74] and BAMPS [38, 75] HF transport approach) leads to a marked enhancement of the friction coefficient at low charm-quark momenta, by up to an order of magnitude over the schematic LO pQCD benchmark, while at high mo-

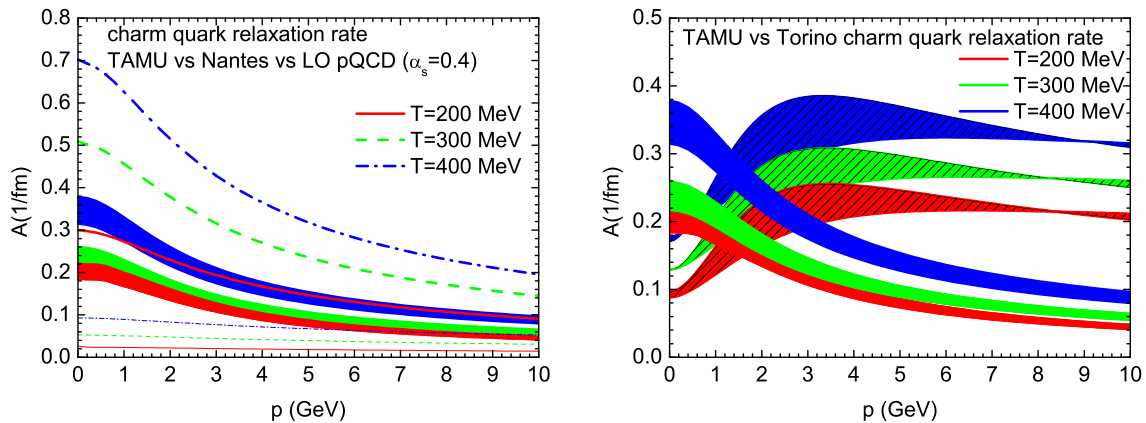


Figure 2. Charm-quark friction coefficient calculated from different underlying elastic interactions in the QGP. Left panel: schematic LO pQCD calculations with fixed Debye mass and coupling constant (thin lines), pQCD Born calculations with reduced Debye mass (from HTL/pQCD matching) and running coupling constant [46] (thick lines), and in-medium T -matrix calculations for HQ-parton scattering using internal energies from thermal IQCD as potential [58, 61] (bands with a 20% uncertainty range due to different IQCD inputs). Right panel: pQCD calculations in the HTL-pQCD matched approach (Torino) used in POWLANG where the friction coefficient has been inferred from the longitudinal diffusion coefficient [36, 48] (shaded bands with uncertainty due to different matching scales), compared to the same T -matrix results as in the left panel.

menta it falls below the HTL approach of Refs. [36, 48]. The T -matrix approach (as used in the TAMU HF transport approach [65, 76]) also predicts a marked low-momentum enhancement of the thermalization rate, but generated by near-threshold resonances as a consequence of the ladder resummation. At high momenta it tends toward the schematic pQCD results. The T -matrix results have a slightly different temperature dependence [58, 60] than the pQCD-like approaches, with a relatively larger interaction strength near T_c , falling off at higher T as the resonances dissolve. This is even more pronounced with the newly derived potential [70] where the low-momentum friction coefficient *decreases* with temperature.

2.2.2. Quark-Gluon Plasma II: Radiative Interactions

Radiative ($2 \rightarrow 3$) scattering processes are suppressed compared to elastic scattering with increasing mass of the incoming particle(s). For example, in electrodynamics, the radiative energy loss of a muon is parametrically suppressed relative to an electron by the fourth power of the mass ratio, $(m_e/m_\mu)^4$. The reason is the suppression of the energy relative to the momentum transfer, $q_0^2 \sim \vec{q}^4/m_Q^2 \ll \vec{q}^2$ (as discussed in the introduction), which renders the emission of an on-shell gluon (or photon) with $q^2 = 0$ unfavorable, at least as long as the 3-momentum transfer is small. Within QCD, the pertinent suppression of forward-angle gluon emission was termed the “dead cone”

effect [77]; subsequently, it was argued that medium-induced gluon radiation can fill this dead cone, while a depletion persists for large energies of the emitted gluon [78, 79]. For sufficiently energetic heavy quarks, the mass effect is expected ‘ to cease and the radiative energy loss to take over from the elastic one, since the energy tends to be radiated in large quantities per scattering event. On the other hand, at the level of the nuclear modification factor in URHICs, also elastic scatterings with typically smaller energy loss can lead to a significant suppression effect due to the rather steeply falling initial spectra. Even for light-parton jet quenching, the quantitative role of elastic scattering has not been settled yet; *e.g.*, in a pQCD thermal-field theory framework, the elastic contribution to the nuclear modification factor, R_{AA} (see Sec. 3.1.3 for its definition), of pions remains significant at high p_T , despite the much smaller energy loss [80].

Heavy-flavor observables at intermediate and high p_T thus provide an excellent tool to map out the transition from a predominantly elastic- to radiative-scattering regime (and, in principle, as a function of temperature). The availability of two different HQ masses (charm and bottom) adds a further handle to determine this transition and test underlying mechanisms. Toward this end, several strategies have been pursued thus far. In Refs. [32, 36, 40, 48, 60, 76, 81] (UrQMD, POWLANG, PHSD and TAMU models), an absolute determination of the elastic contribution is attempted to infer the onset of radiative contributions by deviations from the experimental data beyond a certain p_T . Alternatively, in the MC@sHQ+EPOS [46, 73], Vitev *et al.* [72], BAMPS [28, 38], and Cao *et al.*/Duke [82, 83] models, both elastic and radiative contributions are included in a simultaneous best fit to data. Early on it was already realized that radiative energy loss alone, which was able to describe light-hadron suppression at RHIC, is insufficient to account for the suppression of HF decay electrons at RHIC [84].

The evaluation of HQ radiative energy loss has thus far been mostly based on pQCD. One starts from the elastic heavy-light parton scattering diagrams, augmented with the radiation of a gluon, albeit in different approximation schemes. In Ref. [85], within the HTL framework, the radiative energy loss rate for a heavy quark has been expanded in the number of HQ scattering events, *i.e.*, in its inverse mean-free path. This is also known as an opacity expansion which, in particular, accounts for a finite size of the QCD medium, as originally developed for light-parton jet quenching [86]. The extension to heavy quarks [85] includes recoil effects of the plasma partons and the possibility that the initial heavy quark is produced off its mass shell and goes on-shell by radiating a gluon. The approach used in MC@sHQ+EPOS [73, 87] and BAMPS [28] utilizes the Born diagrams for elastic parton scattering with a radiated gluon [88] extended to a heavy quark in a regime of “intermediate” energies where the mass effect can be argued to largely suppress coherence effects known to be important for light partons. In this framework the radiative $2 \rightarrow 3$ cross section can be approximately cast into a factorized form of an elastic cross section times a probability of radiating an extra gluon ($P_g \propto \alpha_s$), schematically given as

$$d\sigma(Qp \rightarrow Qpg) \simeq d\sigma(Qp \rightarrow Qp) P_g \quad (p = q, \bar{q}, g) . \quad (21)$$

To account for interference effects, in particular for a suppression of gluon emission if the latter is characterized by a formation time longer than the time between subsequent HQ scatterings, a practical prescription has been implemented in the BAMPS model [28]. It amounts to vetoing the gluon emission process if the HQ mean-free path, λ , is shorter than a fraction x_{LPM} of the gluon formation time, τ_{form} , *i.e.*, $\lambda < x_{\text{LPM}}\tau_{\text{form}}$, with $0 < x_{\text{LPM}} < 1$ a free parameter. A different implementation of coherence effects is used in the MC@sHQ+EPOS model [89], where a suppression factor has been deduced assuming that multiple scatterings during the formation time can be represented by a single “effective” scattering center with modified formation length. Further quantitative differences in these two implementations include the choice of charm-quark mass, $m_c=1.5$ GeV [89] vs. 1.3 GeV [28], and the use of finite vs. zero mass for the radiated gluons, respectively.

2.2.3. Hadronic Matter

Investigations of D -meson properties in hadronic matter have been carried out in several approaches to date, *e.g.*, QCD sum rules [90,91] and many-body theory [92–94]. Until rather recently, their focus was mostly on D -meson spectral properties, including mass shifts and in-medium broadening, while transport properties did not receive much attention. In the year 2011 a series of works were conducted to investigate the latter.

In Ref. [95] heavy-meson chiral perturbation theory was used to calculate the D -meson diffusion constant in a low-temperature pion gas using the π - D scattering amplitude to lowest order in the couplings (Born amplitudes). When extrapolated up to a temperature of $T=100$ MeV (which might be beyond the applicability of the approximations), a relaxation rate of $\gamma_D \simeq 0.05/\text{fm}$ for zero-momentum D mesons was found. In Ref. [96] scattering amplitudes of D mesons off pseudoscalar (π , K , η) and vector mesons (ρ , ω , K^*) as well as baryons and anti-baryons (N , \bar{N} , Δ , $\bar{\Delta}$) were adopted from existing calculations based on effective lagrangians. The resummation (unitarization) underlying these amplitudes led to significantly smaller values for the $p=0$ relaxation rate, by about a factor of 10 at $T=100$ MeV (where essentially only pions contribute). However, when extrapolated to temperatures around T_c , the D -meson relaxation rate increases to $\sim 0.08/\text{fm}$, or a relaxation time of ~ 12 fm/ c , which is comparable to the fireball lifetime in URHICs. The pertinent spatial diffusion coefficient amounts to $D_s(2\pi T) \simeq 6$, not far from estimates on the QGP side within the T -matrix formalism [58]. In Ref. [97] a similar set of hadronic scattering partners was employed with the amplitudes treated in Born approximation. At $T=100$ MeV the relaxation rate was calculated to be rather large, $\gamma_D \simeq 0.08/\text{fm}$, although the temperature dependence is more mild than in Ref. [95], cf. Fig. 3. Furthermore, using unitarized amplitudes with interaction vertices from HQ chiral perturbation theory, a pion gas result of $\gamma_D \simeq 0.005/\text{fm}$ was found in Ref. [98], consistent with Ref. [96]. A more complete calculation [99] including scattering off the light pseudoscalar octet as well as nucleons and Δ 's led to good agreement with the full results of Ref. [96], cf. Fig. 3. This suggests that the use of resummed amplitudes, as well as excited states in hadronic matter, is

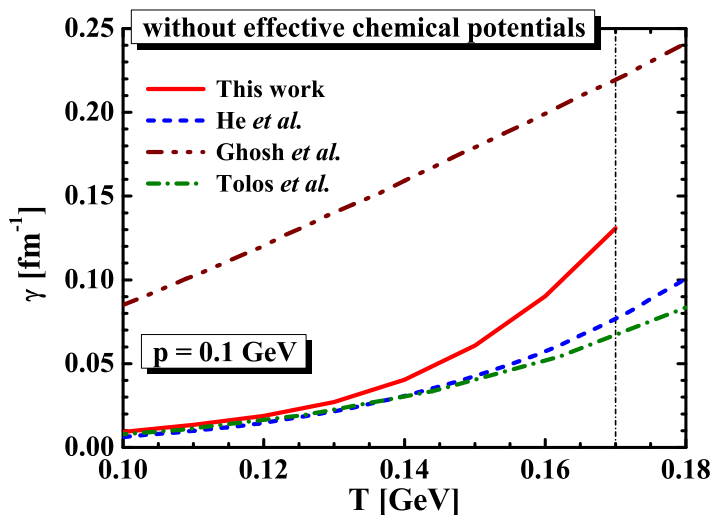


Figure 3. Thermal relaxation rate of low-momentum D -mesons in hadronic matter in chemical equilibrium, computed in the approaches of Refs. [96] (dashed line), [97] (dash-double-dotted line), [99] (dash-dotted line) and [100] (solid line). Figure taken from Ref. [100].

critical to arrive at reliable results.

The effects of higher excited hadronic states were estimated in Ref. [100] using the idea [96] that D -meson cross sections for scattering off light mesons (m) and baryons (b) can be approximated by $\sigma_{Dm}=7\text{-}10\text{ mb}$ and $\sigma_{Db}=10\text{-}15\text{ mb}$, respectively. These values, motivated by constituent light-quark counting arguments, were found to reproduce the results of the microscopic calculations for γ_D in Ref. [96] reasonably well. Up to $T=130\text{ MeV}$ the contribution of excited states is found to be negligible, but it increases the D -meson relaxation rate by up to $\sim 60\%$ at $T=170\text{ MeV}$, cf. Fig. 3.

The transport of B mesons in hadronic matter was also studied in due course. In Ref. [101] Born amplitudes off pseudoscalar mesons from heavy-meson chiral perturbation theory were employed, leading to a small relaxation rate of $\gamma_B \simeq 0.001/\text{fm}$ at $T=100\text{ MeV}$ (the D -meson rate was found to be only slightly larger in this framework). In the unitarized calculation of Ref. [102], a significantly larger value was obtained, close to $\gamma_B=0.003/\text{fm}$, almost a factor of 2 smaller than for D -mesons in the same framework [98]. A more complete calculation [103] including B^* resonances and scattering off N and Δ 's gave similar results at $T=100\text{ MeV}$, but a significant increase of $\gtrsim 50\%$ for $T \geq 140\text{ MeV}$.

2.2.4. Lattice QCD

The extraction of transport coefficients in lQCD is rather challenging, but progress is being made. For the HF case one usually computes the euclidean $Q\bar{Q}$ correlation function in the vector channel, transforms it to the spectral function in Minkowski space (requiring an inverse integral transform), and then takes the zero-energy limit to extract the friction coefficient and from it the spatial diffusion coefficient, D_s . This

has been carried out in quenched QCD [104], yielding a result of $D_s(2\pi T) \simeq 2 \pm 1$ without a significant temperature dependence over the range $T=1.4-3 T_c$. Alternatively, in the static limit the diffusion coefficient can be extracted from the color-electric field correlator which has been simulated in quenched QCD in Ref. [17]. Here the computed diffusion coefficient turned out to be $D_s(2\pi T) \simeq 6 \pm 2$ for $T=1.1-1.5 T_c$ and possibly increasing at higher T . A more recent quenched IQCD extraction based on the electric-field correlator method gives $D_s(2\pi T) \simeq 3.7-7$ for $T=1.5 T_c$ [105], consistent with the previous analysis [17].

Important questions remain about the microscopic mechanisms underlying the rather small values of the spatial HF diffusion coefficient, D_s . Detailed comparisons to model calculations are one way to gain insights, which will be done in Sec. 2.2.5 in connection with Fig. 4. Alternatively, within IQCD, information about the effective degrees of freedom of the QGP at given temperature can be obtained from generalized susceptibilities. These can be used to correlate the (conserved) charm quantum number with other conserved quantum numbers (*e.g.*, baryon charge or strangeness), to test whether the prevalent degrees of freedom carrying charm are mesonic/diquark-like, or if they are quark-like. This has been scrutinized in a recent work [107], and it was found that hadronic degrees of freedom play a significant role in contributing to the partial charm-generated pressure above T_c , up to at least $T \simeq 1.2 T_c \simeq 200$ MeV. This finding is quite consistent with the picture that broad D -meson resonances gradually dissolve with increasing temperature of the QGP, as predicted within the T -matrix approach [58, 60, 108]. It is furthermore quite intriguing that the corresponding T -matrix calculations of the HQ diffusion coefficient [58, 60] are comparable to the IQCD results discussed above.

2.2.5. Comparison of Spatial Diffusion Coefficients

In Fig. 4 we present a summary of results for the spatial diffusion coefficient, D_s , scaled by the thermal wavelength. We compare the quenched IQCD results from Sec. 2.2.4 to various model calculations of elastic charm-quark scattering in the QGP as discussed in Sec. 2.2.1, corresponding to the $p \rightarrow 0$ limit of the friction coefficients displayed in Fig. 2. The schematic LO pQCD calculations with fixed coupling constant ($\alpha_s=0.4$) and Debye mass ($m_D=gT$), as well as the T -matrix calculations with the free energy as potential, are significantly above the IQCD values. On the other hand, the T -matrix results with the internal energy as potential, the Torino and Nantes HTL/pQCD calculations, as well as the infrared-enhanced pQCD implementation into the dynamical quasiparticle model [50] (not shown), are largely within the range of the quenched IQCD data. The T -matrix and Torino results show a significant temperature dependence, while the IQCD results are currently inconclusive on this aspect. Also shown is the calculation of the D -meson diffusion coefficient in hadronic matter based on effective interactions [96]. As mentioned earlier, its temperature dependence and values extrapolated to the pseudo-critical region are suggestive for a continuous transition into the quark-based calculations, together with a shallow minimum structure around

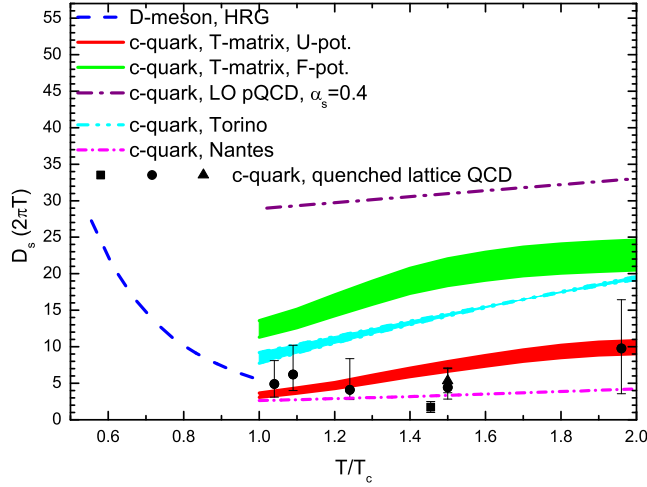


Figure 4. Charm-quark diffusion coefficients from quenched IQCD (circles [17], squares [104], and triangle [105]) compared to model calculations based on different elastic interactions in the QGP (corresponding to the $A(p=0)$ limit in Fig. 2): T -matrix calculations with either free (green band) or internal energy (red band) as potential [58,61], pQCD Born calculations from HTL/pQCD matching using a reduced Debye mass and running coupling (Nantes [45, 46], pink dash-dotted line) or with perturbative Debye mass and fixed coupling (Torino [36, 48], cyan band), as well as schematic LO pQCD with fixed coupling and Debye mass $m_D=gT$ (purple dash-dotted line). The blue-dashed line below T_c is a calculation of D -meson diffusion in hadronic matter from elastic scattering off various mesons and anti-/baryons [96].

T_{pc} [96, 106]. We also note that calculations of D_s based on the bottom-quark friction coefficients [31, 36, 46, 58, 61] give similar results to the charm-quark ones, within 20% for most of the approaches; in other words, the charm- and bottom-quark friction coefficients, $A(p=0)$, differ by approximately the mass ratio m_b/m_c . Since the masses are divided out in converting $A(p=0)$ to D_s , the latter can indeed serve as a reasonably universal measure of the (HQ) interaction strength in the QGP.

The diffusion coefficient has also been computed in the strong-coupling limit of conformal field theories (CFTs) by using the AdS/CFT correspondence principle. The result for the HQ drag (or friction) coefficient in a Super-Yang Mills (SYM) plasma with N_c fundamental charges has been worked out as [23–25]

$$\gamma_Q^{\text{SYM}} = \frac{\pi\sqrt{\lambda}T_{\text{SYM}}^2}{2m_Q}, \quad (22)$$

which turns out to be proportional to the square root of the 't Hooft coupling, $\lambda = g_{\text{SYM}}^2 N_c$, highlighting its nonperturbative nature. Interestingly, the AdS/CFT friction coefficient (thermalization rate) exhibits the factor T/m_Q characteristic for the time delay in the thermalization of a Brownian particle. Several caveats arise in converting this result into an estimate for the QCD plasma [109]. When rescaling the

temperature of the SYM plasma to match the degrees of freedom (energy density) of the QCD plasma, and matching the coupling constant to an α_s estimated from the lQCD HQ free energies, one obtains $\gamma_Q = CT^2/m_Q$ with $C \simeq 1.5$ -2.5, yielding $\gamma_Q \simeq 0.3$ -0.5 /fm at $T=250$ MeV. The pertinent diffusion coefficient (not shown in Fig. 4) turns out to be rather similar to the pQCD results with running coupling and reduced Debye mass [45, 46] (Nantes, pink dash-dotted line in Fig. 4).

2.2.6. Hadronization

The diffusion of heavy flavor in the QGP and hadronic phase of URHICs needs to be interfaced by a transition of the degrees of freedom, from charm and bottom quarks to HF hadrons. Unlike in a macroscopic modeling of the bulk evolution, *e.g.*, with hydrodynamics, where this transition is encoded in the equation of state, the hadronization mechanism for HF transport requires a microscopic treatment. This is both a challenge and an opportunity to learn about this fundamental process in QCD.

In the vacuum, the common procedure to hadronize quarks at high momentum is the use of an empirical fragmentation function, $D_q^h(z)$, which describes the probability distribution of producing a hadron of momentum p_h from a parent quark of momentum p_q , with the momentum fraction $z = p_h/p_q$. Different quark species (as well as gluons) are modeled with different distributions which, once fixed (say, in e^+e^- annihilation), are assumed to be universal for other collision systems. For HQ fragmentation a widely adopted form is the Peterson fragmentation function [110],

$$D_Q^H(z; \epsilon_Q) = \frac{N}{z[1 - (1/z) - \epsilon_Q/(1 - z)]^2}, \quad (23)$$

where N is a normalization factor to ensure $\int D(z)dz = 1$. The parameter ϵ_Q controls the hardness of the distribution, with a maximum at $z \simeq 1 - 2\epsilon_Q$ and a width of $\sim \epsilon_Q$. A standard choice is $\epsilon_c=0.04$ and $\epsilon_b = 0.005$, in line with the expected behavior of $\epsilon_Q \propto 1/m_Q^2$ [110]. An alternative, more involved modeling of the HQ fragmentation function has been developed in connection with fixed-order-next-to-leading-logarithm (FONLL) calculations of HQ production [111, 112], where the Peterson framework does not straightforwardly apply.

At low momentum, the fragmentation picture breaks down, and other mechanisms must set in. In particular, a recombination of heavy quarks with surrounding light anti-/quarks has been suggested [113, 114] and found to account for flavor asymmetries in D -meson production in elementary hadronic reactions, especially at forward rapidities through recombination with valence anti-/quarks of the projectile [115, 116]. The recombination picture is even more compelling within a QGP cooling through the transition temperature, where an ample abundance of thermal light quarks and anti-quarks provides a natural source to color-neutralize heavy quarks. Initial works have implemented this idea using an instantaneous approximation using 3D space-momentum Wigner functions to convert charm quarks into D -mesons (or charmonia) with comoving light quarks [117, 118]. Despite the fact that the major momentum fraction is carried by the heavy quark, a large effect on the D -meson elliptic flow in URHICs at low

and intermediate momenta was found, as being imprinted by recombination with light quarks. One expects this mechanism to reach out to higher transverse momenta than for light hadrons since, at comparable momenta, the velocity of heavy quarks is smaller than for light quarks thus facilitating recombination with comoving thermal partons. A more rigorous implementation of the recombination mechanism at low and intermediate p_T should account for energy conservation (*i.e.*, be formulated as a *rate*) and satisfy thermal equilibrium as the correct long-time limit. This is particularly important in situations with significant space-momentum correlations as is the case in non-central heavy-ion collisions with a collectively expanding partonic source with elliptic flow [119]. Such correlations are not accounted for in coalescence formalisms with global (momentum-space only) or factorized momentum- and coordinate-space distribution functions (such as usually done with 3D Wigner distributions). In the “resonance recombination model” (RRM) the hadronization of heavy quarks is described by scattering off thermal light quarks into broad D -meson like resonances [120, 121], which by construction conserves 4-momentum and recovers the thermal-equilibrium limit. In the HF context the RRM was implemented on a hydrodynamic hypersurface with elliptic flow [76]; it was shown that a HQ distribution in local equilibrium, with an elliptic flow as dictated by the hydrodynamic velocity fields, indeed maps into a D -meson distribution in local equilibrium with the correct mesonic elliptic flow \ddagger . Utilizing the heavy-light quark T -matrix interactions, which generate resonances close to T_c , to compute the HQ recombination rates within RRM [76, 106] puts the hadronization process on the same footing as the non-perturbative HQ diffusion processes (we recall in passing that the confining force plays an essential role in these interactions). In this picture, hadronization is simply a manifestation of the increasing strength of HQ interactions with the partonic medium as T_c is approached from above.

A quantitative treatment of HQ recombination processes needs to allow for the possibility of forming higher excited hadrons, in particular D^* mesons, Λ_c baryons and D_s mesons in the charm sector (and likewise for bottom). Even if these particles are not measured, they can have a significant impact on the D -meson abundance through depleting the charm quarks available for D -meson recombination, the so-called “chemistry effect” (hadrons containing more than one anti-/charm quark, including double-charm baryons and charmonia, give small corrections in this context as their abundance only constitutes up to a few percent of the total charm yield). For example, the fraction of D_s and Λ_c could be significantly enhanced in URHICs relative to pp collisions in the presence of coalescence processes.

A “hybrid” in-medium hadronization scheme, which embeds fragmentation into an environment of thermal partons, has recently been implemented into the POWLANG transport approach [122]. Here, the hadronization of a heavy quark propagating in a hydrodynamic background is carried out once it enters a fluid cell which has cooled down

\ddagger For example, for sufficiently large radial flow, a single charm-quark distribution with strictly positive $v_2^c(p_t)$ implemented into RRM gives rise to a charmonium distribution with $v_2^\psi(p_T)$ dipping into negative values at small p_T , reflecting the well-known mass effect in the v_2 behavior of heavy particles.

to a pseudo-critical temperature of $T_{pc}=155$ MeV. The thermal light- and strange-quark distributions in the rest frame of the fluid cell are sampled and boosted into the lab frame where a string is constructed by joining the endpoints of the heavy- and light-quark positions. These configurations are then passed to PYTHIA 6.4 [123] to simulate the fragmentation of the string into hadrons. In this way the HF fragmentation process inherits collective flow of the expanding medium. By the nature of the fragmentation process, where the strings, once formed, are hadronized as in vacuum, the HF hadro-chemistry remains rather similar to that in the vacuum; in particular, it does not induce a sizeable enhancement of the D_s^+/D or Λ_c^+/D ratios relative to pp collisions.

In practice, the question arises how to disentangle the effects of the QGP phase, hadronization (via coalescence) and hadronic phase from HF observables in URHICs. In Ref. [106] it has been suggested that heavy-strange mesons (D_s and B_s) can help in this respect, based on two main ideas. First, the suppression of strangeness in elementary (pp) collisions is lifted in heavy-ion collisions reflected in the near-equilibrium level of strange-particle production (quantified by a strangeness fugacity $\gamma_s \simeq 1$). Consequently, if HF recombination is effective, it would manifest itself as an increase in the D_s/D (or B_s/B) ratio in AA relative to pp collisions. Moreover, the p_T dependence of this ratio could reveal how far out coalescence mechanisms are operative, especially since the small mass difference between strange and non-strange mesons renders a splitting in their R_{AA} due to collective flow a small effect. Second, it is expected that hadronic rescattering is much weaker for D_s than for D mesons, based on the picture that the coupling to the heat bath is mostly driven by the light-quark content of the hadron (the approximate constituent light-quark scaling of the D -meson interactions with light hadrons referred to in Sec. 2.2.3 is one indication thereof; another one is the apparent earlier kinetic decoupling of multi-strange hadrons in the hadronic phase of URHICs, see, *e.g.*, Refs. [124, 125] for recent works on this issue). This implies that the difference between the v_2 of D and D_s mesons can serve as a measure of the elliptic flow imprinted on the D during the hadronic phase, and thus serve as a measure of its hadronic transport coefficient. It furthermore turns out that the hadronic interactions do not have a large effect on the R_{AA} of the D -mesons, presumably due to a compensation between the dropping temperature and increasing flow of the medium. This would be fortunate as to conserve the comparison of the D - and D_s -meson R_{AA} 's as a measure of coalescence processes.

We finish this section by illustrating the results for the coalescence probabilities of charm quarks as a function of their (transverse) momentum in URHICs for some of the implementations employed in the literature, cf. Fig. 5. The three examples are based on rather different ingredients. The TAMU model [65, 76] (left panel) utilizes RRM [120] with mesonic resonance rates for charm quarks of mass $m_c=1.7$ -1.8 GeV interacting with constituent thermal light quarks on a hydro hypersurface at $T=170$ MeV, assuming a thermal hadro-chemistry. The Duke model [82] employs an instantaneous Wigner function approach [126] for charm quarks of mass $m_c=1.27$ GeV with constituent thermal light quarks at $T=165$ MeV where transverse-flow effects are simulated through an

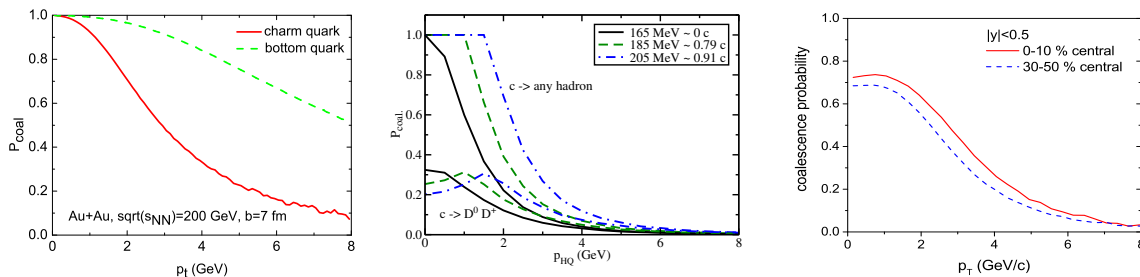


Figure 5. Coalescence probabilities of charm quarks in heavy-ion collisions as a function of their (transverse) momentum in the lab frame using (a) the resonance recombination model [120] within the TAMU transport approach [76] at RHIC (left panel, for c and b quarks), (b) an instantaneous coalescence model with Wigner functions [126] within the Duke transport approach [82] (middle panel), and (c) a stochastic sampling of Wigner functions within the PHSD transport approach [40, 51] (right panel).

effective medium temperature; a hadro-chemistry is accounted for by coalescence into the ground and first excited states of D mesons and charmed baryons. In the PHSD transport model [40, 51], a Wigner function coalescence is implemented by a stochastic sampling of the local environment with charm quarks of mass $m_c=1.5$ GeV, as given by the light-parton phase space distributions; the sampling is carried out when the PHSD bulk medium evolves through energy densities around $\epsilon_{pc} \simeq 0.5$ GeV/fm³, representing the pseudo-transition region; also here the hadro-chemistry is accounted for through the inclusion of higher charm resonance states. The calculated coalescence probabilities in all three approaches share basic features, such as a maximum at low momentum and decreasing over a momentum range of a few times the HQ mass. The normalization of $P_{\text{coal}}(p_t \rightarrow 0)$ has been put to one in the TAMU and Duke models, while in the PHSD model it is below one and significantly depends on the assumed hadron radius in the Wigner function. A more rigorous way to determine the absolute normalization remains to be developed. The drop of $P_{\text{coal}}(p_t)$ with increasing momentum is strongest in the Duke model, while it is weaker for PHSD and TAMU, possibly caused (at least in part) by the larger charm-quark masses used in the latter two models. We also note that other features of the coalescence process have significant impact on experimental observables, *e.g.*, how the HQ momentum translates into a hadron momentum. In the Duke model, the net effect of heavy-light coalescence on D -meson observables turns out to be quite small, while is noticeable in PHSD, and still larger in the TAMU model. More detailed studies are needed to unravel the origin of these differences.

2.2.7. Pre-Equilibrium and Mean-Field Transport

In this section we return to the role that a “mean-field” induced force could play in the propagation of heavy quarks in URHICs. The canonical environment for such a formulation are the earliest, off-equilibrium phases in the collision, where a high occupancy of gluonic modes is suggestive for a field description, or, from a

slightly different viewpoint, a description in terms of a strongly coupled fluid without quasiparticle structure.

The latter approach has been adopted in Ref. [127], by employing the AdS/CFT duality to study the force needed to drag a heavy quark at constant velocity through an environment of two colliding (longitudinally Gaussian and transversely uniform) sheets of energy. When comparing the required force in this highly off-equilibrium medium to that of the equilibrium limit in the $\mathcal{N}=4$ super-Yang-Mills plasma, it was found that the results are quite similar (within a few 10's of percent) if evaluated at the same energy densities (or, equivalently, at the same “pseudo”-temperatures extracted from different diagonal elements of the off-equilibrium stress-energy tensor). This suggests that the effects of the initial off-equilibrium phases on HQ diffusion in URHICs can be reasonably well approximated by the standard transport approach with coefficients extrapolated from the equilibrium theory at corresponding energy densities. In addition, a characteristic time delay in the impact of the initial medium on the HQ motion was found, on the order of 0.1-0.2 fm/c, which could serve as the absolute starting time for the transport simulation.

The gluon saturation approach has been followed in Ref. [128], by converting the gluonic field configurations obtained within the IP-glasma model [129] into off-equilibrium quantum-statistical gluon distribution functions, associated with a typical timescale of the inverse saturation momentum, $\tau_{\text{glasma}} \sim 1/Q_s \sim 0.1\text{-}0.2$ fm/c (not unlike the delay time found in the AdS/CFT approach discussed in the previous paragraph). This distribution has then been inserted into eq. (12) to evaluate the HQ transport coefficients using the schematic LO pQCD matrix elements. The findings parallel those of the AdS/CFT approach, in that the HQ drag coefficient turns out to be very similar to the one in equilibrium provided the same total gluon density is enforced. It turns out to be larger than for a chemically equilibrated QGP at the same parton number (or energy) density, primarily due to the larger color factor in the pQCD HQ-gluon scattering amplitude relative to HQ-quark scattering.

A genuine mean-field contribution can also occur in later stages of the fireball evolution, *e.g.*, due to an effective in-medium quark mass, $m_Q^*(T)$, when the quark propagates through regions with non-zero temperature gradient. The HQ mass is generally expected to increase with decreasing temperature of the QGP, as borne out of both perturbative and non-perturbative calculations (see, *e.g.*, Ref. [15]). Thus, for a heavy quark propagating through an expanding fireball where the temperature decreases both with time and in outward direction, its 3-momentum is reduced due the pertinent mean-field force. This effect has been studied in relativistic Langevin simulations using the transport coefficients of Ref. [58] and found to soften the momentum spectrum while slightly reducing the elliptic flow, although both effects are quantitatively small (a few percent) [130]. Generally speaking, for large HQ scattering rates, corresponding to large imaginary parts in the self-energy, real parts tend to be rather structureless (by means of a dispersion integral) and the corresponding mean-field forces small. Repulsive forces on heavy quarks due to a vector mean-field in the QGP have been studied in the PHSD

approach [51] and found to induce a hardening of the final D -meson spectra, enhancing the “flow bump” in their R_{AA} and shifting it to slightly higher p_T .

2.3. Bulk Medium Evolution Models for URHICs

To implement the HF transport properties as discussed in the preceding section into the phenomenology of URHICs, two additional ingredients are required. The first one concerns the initial conditions for the HQ phase space distribution. Here one usually adopts pQCD calculations fit to experimental p_T spectra of HF particles in elementary pp collisions (augmented with suitable fragmentation functions). In an AA collision, their spatial distribution is usually assumed to follow the NN collision profile, while the p_T distributions are possibly modified due to nuclear modifications in the parton distribution functions (and constrained by pA data). A more detailed discussion of these issues will be given in Sec. 3.2 below.

The second ingredient beyond the HQ interactions with the medium is the space-time evolution of the latter. The Fokker-Planck/Langevin framework, with transport coefficients depending on temperature (possibly chemical potentials) and 3-momentum in the rest frame of the medium, is naturally implemented into hydrodynamic (or fireball) models based on local thermal equilibrium. A minimal requirement for state-of-the-art evolution models for HF transport simulations is the description of light-hadron (π , K , p) multiplicities, p_T spectra and their elliptic-flow coefficient, $v_2(p_T)$, at least approximately and up to a typical transverse momentum of $p_T \simeq 2$ GeV, which encompasses $\sim 90\%$ or more of the produced bulk particles. However, even within this constraint, an appreciable uncertainty in the space-time evolution of the temperature and the collective flow field (in particular the elliptic flow) remains. For example, an initial study of this issue [131], comparing charm-quark Langevin simulations within the original Kolb-Heinz (KH) 2+1D hydrodynamic model [132] and a parameterized expanding thermal fireball model, revealed significant deviations between the results for the charm-quark v_2 at the end of the quark-hadron mixed phase (using the same transport coefficients). A large part of the discrepancy originated from the different build-up of the radial and elliptic flow in the two evolution models, proceeding significantly slower (“softer”) in the KH hydro. Retuning the fireball to agree with the inclusive light-quark v_2 of the KH hydro at the end of the mixed phase leads to much closer agreement for the resulting charm-quark v_2 [76] (see also Ref. [36] for a comparison of HF spectra from different hydro evolutions). Typical components of a “soft” hydro evolution include a standard initial participant profile for the entropy density, vanishing initial-flow velocity at the thermalization time, and an equation-of-state (EoS) with a quark-hadron mixed-phase. Among the consequences of a “soft” expansion are that the bulk- v_2 builds up rather slowly and receives sizable contributions from the hadronic phase (30-40%), that multi-strange particles need to freeze out well inside the hadronic phase, and that the pion HBT radii disagree with experiment. All of these features are modified if the medium evolution is made more explosive, by introducing pre-equilibrium

flow [133–136], a realistic IQCD EoS with cross-over transition, a more compact initial-density profile and a finite shear viscosity. This resolves the HBT puzzle [137,138], makes the bulk- v_2 saturate close to the hadronization transition, and generates sufficient radial flow to allow multi-strange hadrons to kinetically decouple at chemical freezeout [124]. A “harder” hydro evolution has significant consequences for HF observables. Most notably, the flow bump in the charm-quark (and subsequent D -meson) R_{AA} is shifted to higher p_T , and the pertinent $v_2(p_T)$ tends to be larger for $p_T \gtrsim 2$ GeV, both because the bulk- v_2 is available from earlier times on (giving charm quarks more time to pick it up) and the collectivity of the charm quarks is pushed out to higher p_T . It is interesting to note that an “explosive” medium evolution is an important ingredient to understand the rather large v_2 observed for direct photons at RHIC (and possibly LHC) [139,140]. A harder hydro evolution with improved initial conditions and IQCD-based EoS was also implemented in Refs. [74,89]. Also here the flow bump in the D -meson R_{AA} at RHIC showed a notable shift to higher p_T [141] over previous results with the same HQ transport coefficients [73].

Alternative to macroscopic bulk evolutions based on local thermal equilibrium, semi-classical microscopic transport simulations have been employed [28,38–40,51,75,142,143], or combinations thereof within so-called “hybrid” models [81]. In the BAMPS model [38], for example, the evolution of the partonic system is terminated at the transition temperature, where quarks and gluons are fragmented into hadrons. This model approximately describes the measured bulk-hadron v_2 , suggestive for a rather explosive QGP expansion, but it predicts a much softer flow bump in the D -meson R_{AA} at RHIC than the simulations based on a “hard-hydro” evolution (cf. upper left panel in Fig. 25). In the PHSD transport simulations [40], the D -meson R_{AA} at RHIC turns out to be rather close to the results from “hard-hydro” evolutions.

3. Experimental Results and Comparison to Models

3.1. Experimental Facilities and Techniques

3.1.1. Accelerators

Heavy-ion collisions are a unique way to explore the phase diagram of QCD matter in the laboratory and study the properties of the QGP. The first fixed-target experiments with collisions of light nuclei at ultra-relativistic energies started in 1986 at the BNL AGS and at the CERN SPS. Heavy nuclei (Au and Pb) became available in the 90’s at both facilities. Since the year 2000, heavy-ion colliders are in operation, first at BNL (Relativistic Heavy Ion Collider, RHIC, first Au–Au collisions in 2000) and ten years later at CERN (LHC, first Pb–Pb collisions in 2010).

The AGS and SPS fixed-target programs enabled the study of heavy-ion reactions at center-of-mass (CM) energies of $\sqrt{s_{NN}} = 1$ -20 GeV per nucleon pair. In the heavy-ion program at the CERN SPS, open HF production was not measured directly. Indirect measurements based on the contribution of simultaneous semi-muonic decays of

correlated $D\bar{D}$ pairs to the dimuon invariant-mass spectra were carried out in Pb–Pb and In–In collisions at $\sqrt{s_{\text{NN}}} = 17.2$ GeV by the NA50 and NA60 collaborations [144, 145].

The Relativistic Heavy Ion Collider (RHIC) began operation in 2000 with the capability of colliding nuclei from deuterons to Au at CM energies of up to 200 GeV per nucleon pair. Over the 15 years of data taking to date, several collision systems were studied at different collision energies. The luminosity for full energy Au–Au collisions was increased over the years from the design value of $2 \cdot 10^{26} \text{ cm}^{-2} \text{ s}^{-1}$ to about $5 \cdot 10^{27} \text{ cm}^{-2} \text{ s}^{-1}$ in the 2014 run. During years 2010, 2011 and 2014 a Beam Energy Scan (BES) campaign was conducted, taking data for Au–Au collisions at CM energies per nucleon pair of 62.4, 39, 27, 19.6, 14.5, 11.5 and 7.7 GeV. A summary of the data samples of heavy-ion collisions collected over this period is reported in Tab. 1. Heavy-flavor results were reported by the PHENIX and STAR collaborations for Au–Au collisions at $\sqrt{s_{\text{NN}}}$ of 39, 62.4, 130 and 200 GeV, for Cu–Cu collisions at $\sqrt{s_{\text{NN}}} = 200$ GeV, and for $d\text{Au}$ collisions at $\sqrt{s_{\text{NN}}} = 200$ GeV. Also proton–proton (pp) collisions at $\sqrt{s} = 200$ GeV were studied as a reference for heavy-ion collisions.

The LHC accelerator started operation at the end of year 2009 with pp collisions at $\sqrt{s} = 0.9$ TeV. Subsequently, protons were collided at CM energies of 7 TeV (in years 2010–2011), 8 TeV (in 2012), and 13 TeV (in 2015). Heavy-ion (AA) and proton–nucleus (pA) collisions are an integral part of the LHC physics program. The first two samples of Pb–Pb collisions were collected in years 2010 and 2011 at a CM energy per nucleon–nucleon collision of $\sqrt{s_{\text{NN}}} = 2.76$ TeV. About $10 \mu\text{b}^{-1}$ of integrated luminosity were delivered in 2010 and $166 \mu\text{b}^{-1}$ in 2011 to the three LHC experiments that took part in the heavy-ion program, namely ALICE (a detector dedicated to heavy-ion collisions), ATLAS and CMS. The next LHC run with Pb beams was conducted at the end of 2015 at $\sqrt{s_{\text{NN}}} = 5.02$ TeV. In year 2013, $p\text{Pb}$ collisions were performed at the LHC at $\sqrt{s_{\text{NN}}} = 5.02$ TeV. All four main LHC experiments (ALICE, ATLAS, CMS and LHCb) took data. The delivered integrated luminosity was of about 30 nb^{-1} .

The increase of the CM energy from fixed-target experiments to the colliders RHIC and LHC is reflected in a larger number of produced particles, a higher temperature of the created medium and a longer lifetime of the possible QGP phase. For example, the energy density of the medium estimated with the Bjorken formula for central Au–Au collisions at a nominal formation time of $1 \text{ fm}/c$ increases from about $2 \text{ GeV}/\text{fm}^3$ at $\sqrt{s_{\text{NN}}} = 19$ GeV to about $5 \text{ GeV}/\text{fm}^3$ at $\sqrt{s_{\text{NN}}} = 200$ GeV [156] and reaches about $14 \text{ GeV}/\text{fm}^3$ in central Pb–Pb collisions at the LHC [157]. The decoupling time for hadrons at midrapidity increases by about 40% from top RHIC to top LHC energy, signaling that at higher collision energies the system lives longer and expands to a larger size at freeze-out [42]. Concerning HF hadron production, the cross section for $c\bar{c}$ and $b\bar{b}$ production in nucleon–nucleon collisions increases dramatically with increasing $\sqrt{s_{\text{NN}}}$. A compilation of the measurements of p_{T} -integrated charm and beauty production cross section in pp ($p\bar{p}$) and pA collisions as a function of $\sqrt{s_{\text{NN}}}$ is reported in Fig. 6 (taken from [11, 154]). As will be discussed in the next section, the experimental results are described within uncertainties by calculations within perturbative QCD. The cross

	Year	Collision system	$\sqrt{s_{NN}}$ (GeV)	Delivered int. lumi (nb ⁻¹)
Run-1	2000	Au–Au	130	0.02
Run-2	2001/02	Au–Au	200	0.258
		Au–Au	19.6	$0.4 \cdot 10^{-3}$
Run-3	2002/03	d–Au	200	73
Run-4	2003/04	Au–Au	200	3.53
		Au–Au	62.4	0.067
Run-5	2004/05	Cu–Cu	200	42.1
		Cu–Cu	62.4	1.5
		Cu–Cu	22.4	0.02
Run-7	2006/07	Au–Au	200	7.25
Run-8	2007/08	d–Au	200	437
Run-10	2009/10	Au–Au	200	10.3
		Au–Au	62.4	0.544
		Au–Au	39	0.206
		Au–Au	11.5	$7.8 \cdot 10^{-3}$
		Au–Au	7.7	$4.23 \cdot 10^{-3}$
Run-11	2010/11	Au–Au	200	9.79
		Au–Au	27	0.063
		Au–Au	19.6	0.033
Run-12	2011/12	U–U	193	0.736
		Cu–Au	200	27.0
Run-14	2013/14	Au–Au	200	43.9
		Au–Au	14.5	0.044
		³ He–Au	204	134
Run-15	2014/15	p–Au	200	1270
		p–Al	200	3970

Table 1. Summary of heavy-ion data taking periods at RHIC: collision systems, CM energies and total delivered integrated luminosity (from <http://www.rhichome.bnl.gov/RHIC/Runs/>).

section for charm (beauty) production increases by about a factor of 10 (50) from RHIC to LHC energies.

3.1.2. Open Heavy-Flavor Production Measurement Techniques

Open HF production is measured experimentally in proton–proton, proton–nucleus and nucleus–nucleus collisions exploiting various techniques. Charm and beauty hadrons can be fully reconstructed from their hadronic decays, or, alternatively, they can be studied inclusively by measuring electrons or muons from their semi-leptonic decays.

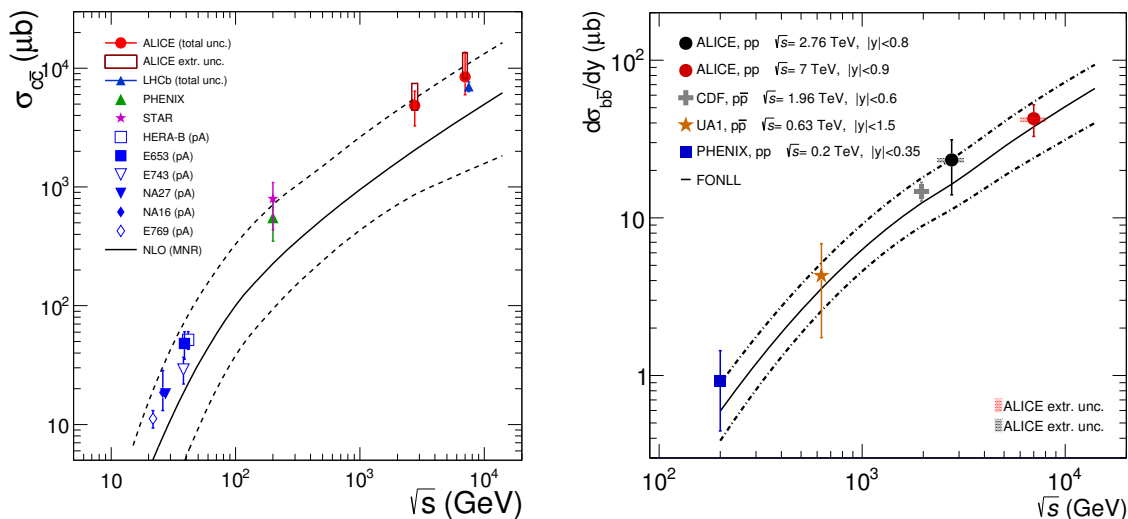


Figure 6. Left: total inclusive charm production cross section as a function of \sqrt{s} [146–150]. Data from pA and deuteron–nucleus (dA) collisions were scaled assuming no nuclear effects (taken from [11]). Right: inclusive beauty production cross section per rapidity unit measured at mid-rapidity as a function of \sqrt{s} in pp and $p\bar{p}$ collisions [151–155] (taken from [154]). Results from perturbative QCD calculations and their uncertainties are shown as solid and dashed lines.

Beauty production is also accessed via the inclusive $B \rightarrow J/\psi + X$ decay mode and by reconstructing jets of hadrons produced in the fragmentation of a beauty quark (b -jets). Experiments featuring vertex detectors with high spatial resolution, which are available at all four main LHC experiments, as well as at STAR and PHENIX at RHIC after their recent upgrades, can exploit the relatively long lifetime of D and B mesons to resolve their decay vertex from the interaction point. D^0 , D^+ and D_s^+ mesons decay weakly with mean proper decay lengths $c\tau$ of approximately 120, 310 and 150 μm , respectively [158]. Beauty mesons have longer lifetimes than charmed hadrons: $c\tau \approx 500 \mu\text{m}$ for B^0 , B^+ and B_s^0 [158], which makes it possible to disentangle the charm and beauty contributions in the sample of HF decay leptons. Most of the beauty-hadron decay channels proceed via $b \rightarrow c$ hadron cascades, giving rise to a topology that contains both a secondary and a tertiary decay vertex. In the remainder of this section the key points of the different experimental approaches to open HF reconstruction are briefly summarized.

Inclusive measurements of heavy-flavor decay leptons. Open HF production is studied inclusively by measuring electrons and muons from semi-leptonic decays of charm and beauty hadrons, which are characterized by branching ratios (BRs) of the order of 5–15% depending on the hadron species [158]. The crucial aspects are the lepton (electron, muon) identification and the subtraction of the background due to leptons not coming from HF hadron decays.

Electrons: For HF decay electrons, the various experimental collaborations have exploited different combinations of identification techniques, which are effective in

different momentum ranges. The STAR [159] and ALICE [160] collaborations used specific energy loss (dE/dx) measurements in combination with time-of-flight information at low momenta and with energy and shower shape from electromagnetic calorimeters at high momenta. In addition, in ALICE the signal from the Transition Radiation Detector was used in pp collisions [160]. In PHENIX, electron identification was performed using a Ring Imaging Cherenkov detector together with the information from an electromagnetic calorimeter [147]. ATLAS performed a measurement of HF decay electrons in pp collisions utilizing clusters in electromagnetic calorimeters matched to charged tracks [161]. The background electrons are dominated by photon conversions in the detector material and by Dalitz decays of π^0 and η mesons. Their contribution can be estimated using different techniques and subtracted statistically. Three main approaches to background estimation have been used: i) low-invariant-mass e^+e^- pairs (invariant-mass method, utilized by the STAR [162] and ALICE [154] collaborations); ii) Monte Carlo simulation of background electrons from hadron decays (cocktail method, used in PHENIX [147] and ALICE [160]); iii) special data taking with additional converter material of well defined thickness (converter method exploited in PHENIX [147]).

Muons: Muons are tracked and identified using spectrometers located downstream of absorbers that stop the majority of the hadrons. The main background contribution is due to the decay in flight of pions and kaons and to hadrons punching through the absorber. It can be estimated via cocktail calculations, as done in PHENIX [163] and ALICE [164]. In ATLAS, the background is discriminated statistically based on a Monte Carlo template fit to the distribution of the difference between the track momentum measured in the muon spectrometer and that measured in the inner tracker, after accounting for energy loss in the calorimeters located in between the inner tracker and the muon spectrometer [161].

Cocktail subtraction methods use as input the yields and momentum/rapidity distributions of all relevant sources of background leptons, which are mainly pions, kaons and η mesons. Ideally, to reduce the uncertainties, this input should be taken from data measured with the same apparatus.

Dilepton invariant-mass analysis. Heavy-flavor production can be studied via the contribution of simultaneous semi-leptonic decays of $D\bar{D}$ and $B\bar{B}$ pairs in the dilepton invariant-mass distribution. In particular, the open HF contribution is extracted from the intermediate-mass region, *i.e.*, the region between the ϕ and the J/ψ peaks, where the main contributions to the dilepton spectrum are expected to be open HF decays, thermal radiation from the QGP and (at SPS energies) Drell-Yan dileptons. This technique was used in Pb–Pb collisions at the SPS with the NA50 [144] and NA60 [145] experiments to measure open-charm and thermal-dimuon production in Pb–Pb and In–In collisions. At RHIC, the PHENIX collaboration measured the di-electron production double differentially in mass and p_T which allowed the separation of regions dominated by charm from those dominated by beauty decays and the extraction of the $c\bar{c}$ and $b\bar{b}$ production cross sections in pp and dAu collisions [165, 166].

Beauty measurements from partially reconstructed decays

Beauty-decay leptons: the beauty contribution to the sample of HF decay leptons can be extracted by exploiting additional information. In particular, charm and beauty decay leptons can be separated based on the longer lifetime of beauty hadrons, which results in a larger separation of the production point of their decay leptons from the interaction vertex [155]. This approach requires high resolution (of the order or better than 100 μm) on the track impact parameter, which is the distance of closest approach of a track (*i.e.*, the reconstructed particle trajectory) to the interaction vertex. Alternatively, the fraction of beauty-decay electrons has been estimated from the azimuthal correlations between HF decay electrons and charged hadrons [153, 154, 167]. This method exploits the fact that the width of the near-side peak is larger for beauty than for charm hadron decays, thus allowing one to disentangle the corresponding relative contribution to the yield of HF decay electrons. The main limitation of the beauty measurement via single electrons (muons) is that the correlation between the measured momentum of the lepton and that of the parent B meson is very broad, especially at low momentum.

Non-prompt J/ψ : the contribution of beauty-hadron decays to the yield of J/ψ mesons can be measured inclusively by decomposing the J/ψ yield into its prompt (*i.e.*, J/ψ produced at the interaction point) and non-prompt (displaced) components. This is achieved via fits to the distribution of the measured distances between the interaction vertex and the J/ψ decay vertex. This approach has been used in pp , $p\text{Pb}$ and Pb-Pb collisions at the LHC by ALICE [168, 169], CMS [170] and LHCb [171, 172]. The branching ratio of inclusive beauty-hadron decays into J/ψ measured at LEP is 1.16% [173–175], lower than that into single leptons. However, as compared to the measurement of beauty-decay leptons, this channel provides a more direct measurement of the beauty-hadron kinematics due to the narrower correlation between the momentum of the J/ψ and that of the parent beauty hadron.

Fully reconstructed decays of charm and beauty hadrons

This approach allows the reconstruction of HF hadrons exploiting hadronic decays of D mesons (and in the future of Λ_c baryons), and J/ψ +hadron (with the J/ψ reconstructed from dileptonic decays) decays of B mesons. The branching ratios are smaller than those in semi-leptonic channels, but this technique has the advantage of providing access to the kinematics of the heavy-flavor hadron.

Charm mesons: D -meson production has been measured down to low transverse momentum by STAR [148] and ALICE [176, 177] in Au–Au and Pb–Pb collisions at RHIC and LHC, respectively. The measurement is based on the invariant-mass analysis of fully reconstructed decay topologies of the following hadronic decay channels: $D^0 \rightarrow K^- \pi^+$ (BR=3.88%), $D^+ \rightarrow K^- \pi^+ \pi^+$ (BR=9.13%), $D^{*+} \rightarrow D^0 \pi^+$ (BR=67.7%), and $D_s^+ \rightarrow \phi \pi^+ \rightarrow K^- K^+ \pi^+$ (BR=2.24%) and their charge conjugates [158]. The huge combinatorial background is reduced by selections on the dE/dx and time-of-flight that provide kaon and pion identification. In addition, the spatial resolution of the ALICE silicon tracker makes it possible to reconstruct the D -meson decay vertex and to apply geometrical selections on its separation from the interaction vertex [176]. A technique

based on geometrical selections on displaced decay-vertex topologies was used also for the preliminary results on D^0 -meson production in Pb–Pb collisions recently reported by CMS [178].

Beauty mesons: CMS Collaboration recently published results of the production of B mesons in p Pb collisions at the LHC in the transverse momentum range $10 < p_T < 60$ GeV/ c [179]. The following decays were reconstructed: $B^+ \rightarrow J/\psi + K^+$, $B^0 \rightarrow J/\psi + K^{*0}(892)$ and $B_s^+ \rightarrow J/\psi + \phi$, all having branching ratios of about 0.1% [158]. Kinematic selections on the displaced decay vertex topologies were applied to reduce the combinatorial background.

b-jets: Reconstructed jets associated with beauty hadrons (“ b -jets”) can be identified based on kinematic variables related to the relatively long lifetime and large mass of beauty hadrons (“ b -tagging”). The first measurement of b -jets in heavy-ion collisions was performed by the CMS collaboration at the LHC [180]. Measurements of b -jets are complementary to those of beauty hadrons, because they are typically performed in a different momentum range and because the reconstructed jet energy is closely related to that of the b quark.

3.1.3. Experimental observables

Interactions of heavy quarks with the constituents of the hot and dense medium created in nucleus–nucleus collisions are expected to modify the momentum and angular distribution of HF hadrons as compared to pp collisions. The main experimental observables used up to now to study these effects are the nuclear modification factor R_{AA} and the elliptic flow v_2 , which is the coefficient of the second harmonic in the Fourier expansion of the particle azimuthal distributions. Further insight into the interaction mechanisms of heavy quarks with the medium and the properties of the medium can be provided by measurements of angular correlations involving HF particles and/or their decay products, and by measuring the higher harmonics in the Fourier expansion of the particle azimuthal distributions. However, with the currently available experimental samples, these more differential observables could only be accessed with limited statistical precision in nucleus–nucleus collisions.

The nuclear modification factor R_{AA} is commonly used to study the modification of the production yield and the momentum distribution of particles originating from hard (*i.e.*, high- Q^2) partonic scattering processes in nucleus–nucleus collisions relative to pp collisions. Since the rate of hard processes is expected to scale with the average number of binary nucleon–nucleon collisions occurring in the nucleus–nucleus collision, $\langle N_{\text{coll}} \rangle$, the nuclear modification factor of the transverse momentum (p_T) distributions is expressed as:

$$R_{AA}(p_T) = \frac{1}{\langle N_{\text{coll}} \rangle} \cdot \frac{dN_{AA}/dp_T}{dN_{pp}/dp_T} = \frac{1}{\langle T_{AA} \rangle} \cdot \frac{dN_{AA}/dp_T}{d\sigma_{pp}/dp_T}, \quad (24)$$

where dN_{AA}/dp_T is the p_T spectrum measured in A–A collisions, dN_{pp}/dp_T ($d\sigma_{pp}/dp_T$) is the p_T -differential yield (cross section) in pp collisions and $\langle T_{AA} \rangle$ is the average nuclear overlap function. The nuclear overlap function is defined as the convolution of the

nuclear density profiles of the colliding ions in the Glauber model [181, 182] and is related to the number of nucleon–nucleon collisions as $N_{\text{coll}} = \sigma_{\text{NN}}^{\text{inel}} \cdot T_{\text{AA}}$, where $\sigma_{\text{NN}}^{\text{inel}}$ is the inelastic nucleon–nucleon cross section at given \sqrt{s} . In absence of nuclear effects, a value of $R_{\text{AA}} = 1$ is expected for HF particles in the whole p_{T} range, because, due to their large mass, charm and beauty quarks are produced predominantly in hard partonic scattering processes. Thermal production in the QGP, which does not scale with N_{coll} , is expected to be negligible at the medium temperatures reached in heavy-ion collisions at RHIC and at the LHC [183, 184]. Parton in-medium energy loss causes a suppression, $R_{\text{AA}} < 1$, of hadrons at high transverse momenta ($p_{\text{T}} \gtrsim 5 \text{ GeV}/c$), and is expected to be the dominant effect in the nuclear modification factor. The R_{AA} can therefore be used to characterize HQ in-medium energy loss and to infer from it the corresponding transport coefficients. At low and intermediate p_{T} ($p_{\text{T}} \lesssim 5 \text{ GeV}/c$), effects other than in-medium energy loss are expected to modify the HF hadron production yield, leading to values of R_{AA} different from unity. These effects are related both to the formation of a hot and dense medium and to nuclear effects in the initial state of the collision. Among the initial-state effects, nuclear modification of the parton distribution functions, k_{T} -broadening and cold-nuclear-matter energy loss due to multiple scatterings of the initial partons could modify the production yield and p_{T} distribution of HF hadrons, as discussed in Section 3.2.2. Final-state effects which could modify the hadron spectra in addition to energy loss are the collective “radial” flow of the medium and the modification of hadronization in the presence of a medium. Low-momentum heavy quarks, including those shifted to low momentum by parton energy loss, could participate in the collective expansion of the system and possibly reach thermalization with the medium as a consequence of multiple interactions with the medium constituents [118, 185]. In elementary collisions heavy quarks are expected to hadronize mainly through fragmentation, while the ample presence of quarks and antiquarks in the medium makes the coalescence of charm and beauty quarks with light quarks a plausible hadronization mechanism (as discussed in Sec. 2.2.6). This will impart (part of) the large radial and elliptic flow of the quarks from the medium on the heavy quarks and introduce a p_{T} -dependent modification to the observed charmed hadron spectrum compared to a pure fragmentation scenario (even in the limit where heavy quarks do not take part in the collective expansion of the medium) [73, 76, 118, 122]. Furthermore, hadronization via coalescence may lead to a modification of the relative abundance of the different HF hadron species. In particular, a baryon-to-meson and strange-to-non-strange enhancement for charmed hadrons, similar to that observed for light-flavor hadrons, is predicted [106, 126, 186–189].

An observable complementary to the nuclear modification factor R_{AA} to study the interaction of heavy quarks with the medium is the anisotropy in the azimuthal distribution of HF hadrons. Anisotropy in particle momentum distributions originates from the initial anisotropy in the spatial distribution of the nucleons participating in the collision. The anisotropy of the azimuthal distribution of the particles produced in

the collision is usually characterized with the Fourier coefficients:

$$v_n = \langle \cos[n(\varphi - \Psi_n)] \rangle, \quad (25)$$

where φ is the azimuthal angle of the particle, and Ψ_n is the azimuthal angle of the initial state symmetry plane for the n -th harmonic. If nuclei were spherically symmetric with a matter density depending only on the distance from the centre of the nucleus, the symmetry planes Ψ_n for all harmonics would coincide with the reaction plane, *i.e.*, the plane defined by the beam direction and the impact parameter of the two colliding nuclei. For non-central collisions the overlap region of the colliding nuclei has an “almond” shape, and the largest contribution to the anisotropy is given by the second coefficient v_2 , which is called elliptic flow. At RHIC and LHC energies, a positive v_2 is observed for many different hadron species [190–192] and is commonly ascribed to the combination of two mechanisms. The first one, which is dominant at low and intermediate momenta ($p_T < 6$ GeV/ c), is the build-up of a collective expansion through interactions among the medium constituents, which convert the initial-state geometrical anisotropy into a momentum anisotropy of the final-state particles [193]. The second mechanism is the path length dependence of in-medium parton energy loss, which is predicted to give rise to a positive v_2 for hadrons up to large p_T [194, 195]. This path length dependence is expected to be different for the different energy-loss mechanisms: linear for collisional processes [47, 196] and close to quadratic for radiative processes [197]. Hence, the measurement of v_2 at high p_T can constrain the path length dependence of parton energy loss. At low p_T , HF hadron v_2 offers a unique opportunity to test whether also heavy quarks take part in the collective expansion and possibly thermalize in the medium. In addition, at low and intermediate p_T , the D and B meson elliptic flow (as well as that of their decay leptons) is expected to be sensitive to the role of hadronization via recombination, which is predicted to augment the v_2 of HF hadrons with respect to that of charm and beauty quarks [118, 198].

The measurement of higher-order flow coefficients of HF hadrons was proposed in Ref. [199] as a sensitive probe of the degree of charm- and beauty-quark thermalization. In particular, in this model, the triangular-flow coefficient v_3 is likely to show an incomplete coupling of the heavy quarks to the bulk medium as well as the expected mass hierarchy.

The study of angular correlations between HF hadrons could further constrain the models of interactions of heavy quarks with the medium, possibly providing valuable information on the path length dependence of energy loss and on the relative contributions of collisional and radiative processes [89, 122, 200–202]. The medium effects on the angular (de)correlation and momentum imbalance of heavy quark-antiquark pairs can be studied via the correlations of two HF hadrons, $D\bar{D}$ and $B\bar{B}$. However, this measurement is extremely challenging because of the huge data samples required to cope with the small branching ratios of the hadronic channels through which D and B mesons can be fully reconstructed. In the beauty sector, angular correlations and energy imbalance of b -jets, the latter quantified, *e.g.*, by measuring the asymmetry

$A_J = (E_{T1} - E_{T2})/(E_{T1} + E_{T2})$ of di-jets emitted in opposite hemispheres [203, 204], could become accessible in Pb–Pb collisions with the integrated luminosities that will be recorded during the LHC Run-2, *i.e.*, the 2015–2018 data taking period. As an alternative, correlations involving electrons and muons from HF hadron decays can be studied, such as $D - e$, $e^+ - e^-$, $\mu^+ - \mu^-$, $e - \mu$. The interpretation of the results from these observables is, however, less straightforward than that of $D\bar{D}$ or b -jet correlations, because they contain also angular decorrelation effects due to the HF hadron decay kinematics, and because the lepton carries only a fraction of the parent-hadron momentum. With the currently available data samples, a measurement of $e - \mu$ correlations could be carried out in d Au collisions [205]. In addition, two-particle correlations involving heavy flavors were measured utilizing a D meson or a HF decay lepton as trigger particle and the hadrons produced in the collision as associated particles. Such observables have also sensitivity to the HQ production and fragmentation process, as well as to the presence of collective effects that induce correlations between the HF particles and the bulk of hadrons produced in the collision. Measurements of e -hadron correlations in Au–Au collisions at RHIC were published by PHENIX [206], but with the current level of statistical uncertainties no quantitative conclusion can be drawn on the modification of the azimuthal-correlation shape as compared to pp collisions. Preliminary results for e -hadron correlations were also reported by STAR for Au–Au collisions at RHIC [207] and by ALICE for Pb–Pb collisions at the LHC [208]. The larger data samples of Au–Au and Pb–Pb collisions that will be collected in the coming years at RHIC and at the LHC will make it possible to fully exploit the potential of e -hadron and D -hadron correlations, to provide further constraints for the characterization of HQ interactions with the medium.

3.2. Open Heavy-Flavor Data in pp and p -A (d -A) Collisions

3.2.1. Production in pp and Comparison to pQCD Calculations

In the context of the study of HQ production in heavy-ion collisions, measurements in pp reactions provide a crucial reference to establish a baseline that allows the identification of modifications in AA reactions, which can be related to the formation of a hot and dense medium. In particular, a pp reference is needed to quantify the modification of the momentum distribution of HF particles in AA collisions through the nuclear modification factor R_{AA} . Also in the studies of two-particle angular correlations, comparisons to pp results are mandatory to interpret the measurements in heavy-ion collisions.

A key aspect of open HF studies is that their production in elementary hadronic collisions can be calculated in the framework of perturbative QCD (pQCD) down to low p_T with the HQ mass, m_Q , acting as a long distance cutoff [209, 210]. The differential cross section for the inclusive production of HF hadrons in nucleon–nucleon collisions can be computed using the collinear factorization approach as a convolution of three factors: (i) the parton distribution functions of the incoming nucleons, (ii) the

partonic hard scattering cross section calculated as a perturbative series in the strong coupling constant, and (iii) the fragmentation process describing the non-perturbative transition of a charm (beauty) quark into a heavy hadron. The latter is modeled by a fragmentation function, which parametrizes the fraction of quark energy transferred to the produced hadron, as discussed in Sec. 2.2.6. This formalism is implemented at next-to-leading order (NLO) accuracy in the general-mass variable-flavor-number scheme, GM-VFNS [211, 212] and in the fixed order next-to-leading-log (FONLL) resummation approach [111]. Both of these frameworks are based on the matching of “massive” NLO calculations in the Fixed-Flavor Number Scheme (FFNS, valid at low p_T), where heavy quarks are not active partons in the nucleon appearing only in the partonic hard scattering process, with “massless” calculations in the Zero-Mass Variable Flavor Number Scheme (ZM-VFNS, valid for $p_T \gg m_Q$), where charm and beauty quarks appear also as active partons in the nucleon PDFs and their mass can be neglected in the partonic hard scattering cross section.

Calculations of inclusive production cross section of HF hadrons in hadronic collisions are also performed in the leading order (LO) approximation within the framework of k_T -factorization with unintegrated gluon distribution functions (UGDFs) to account for the transverse momenta of the initial partons [213–215].

These theoretical frameworks allow for a mostly analytic calculation of inclusive p_T and y differential cross section of heavy quarks, HF hadrons and their decay leptons at NLO+NLL (or LO) accuracy. However, for some particular studies, such as those of HF jets or correlations of HF hadrons with other particles produced in the interaction, a more complete description of the hadronic final state is needed, which can be obtained using Monte Carlo (MC) generators. General-purpose MC generators, such as PYTHIA [123, 216] or HERWIG [217], can serve this purpose, but are limited to LO accuracy. A more versatile description of hard processes can be achieved with the MC@NLO [218] and POWHEG [219] generators, where a consistent matching of NLO pQCD calculations with parton showers is implemented, thus combining the strength of MC generators (*i.e.*, a complete modelling of the hadronic final state) with NLO accuracy in the hard scattering process and leading-logarithm resummation in the soft/collinear regimes.

These pQCD-based approaches are used in the models of HQ production and in-medium energy loss to compute the initial HQ distributions in heavy-ion collisions. In particular, HQ distributions calculated with FONLL are used in WHDG [84, 220], MC@sHQ+EPOS [89], TAMU [65], Djordjevic *et al.* [221], and CUJET 3.0 [222, 223]. Other models make use of MC generators, *e.g.*, MC@NLO in BAMPS [75], POWHEG in POWLANG [36], and PYTHIA (tuned to fit FONLL predictions for heavy quarks) in PHSD [40, 51]. In the model of Cao *et al.*, a LO pQCD calculation was originally used to compute the initial HQ distributions [82], while in recent studies of angular correlations an improved initialization based on MC@NLO was adopted [201].

Since the above-mentioned pQCD calculations and MC generators provide a fundamental input for the studies of HQ interactions in the QGP, it is crucial to verify

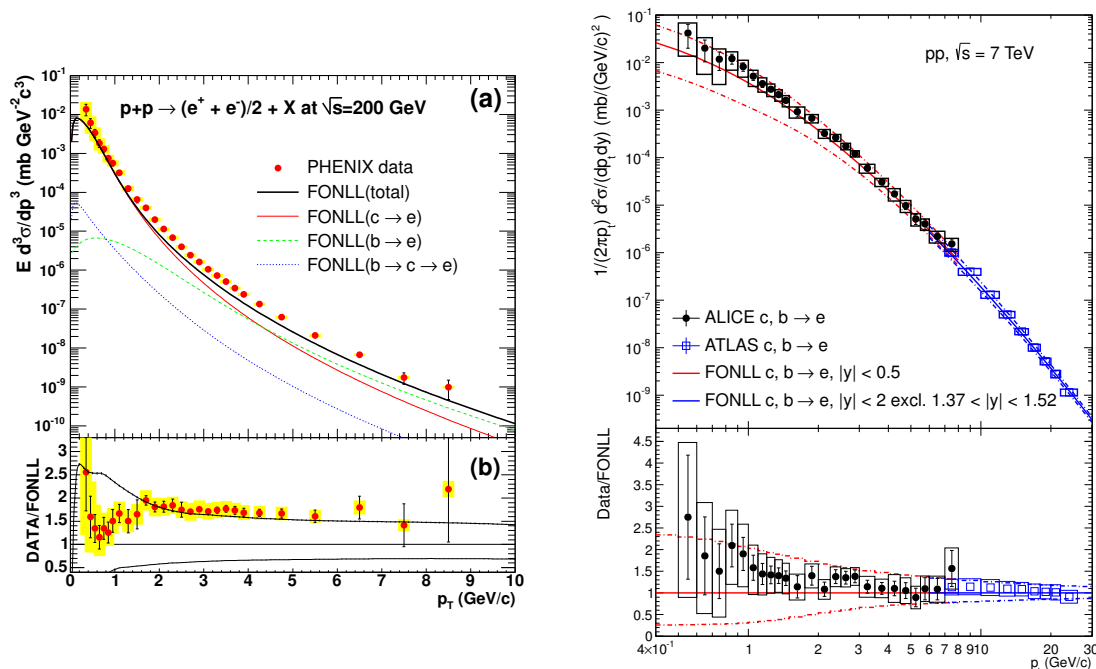


Figure 7. Transverse-momentum differential production cross sections of HF decay electrons at mid-rapidity. Left: results at $\sqrt{s} = 200$ GeV from PHENIX [226]. Right: results at $\sqrt{s} = 7$ TeV from ALICE [160] and ATLAS [161]. Data are compared to FONLL calculations [111, 227].

that they can describe the data from pp collisions at RHIC and LHC energies. This data-to-theory comparison consists also an important test of our understanding of QCD in its perturbative regime. Furthermore, a solid understanding of open-charm production is important also for cosmic-ray and neutrino astrophysics, because ‘prompt’ neutrino flux from charm decays is the dominant background for astrophysical neutrinos at energies of the order of 1 PeV [224, 225]. In the following, a selection of measurements of p_T and y differential inclusive production cross sections of open HF in pp collisions at RHIC and at the LHC will be presented and compared to the results of the pQCD calculations and MC generators presented above. Note that HF production was also measured at the Tevatron collider [152] at CM energies in between the RHIC and LHC ones. They are not reported in this review, which focuses on the accelerators and energies at which heavy-ion collisions have been studied.

In Fig. 7 the p_T -differential production cross section of electrons from HF hadron decays at mid-rapidity measured by the PHENIX collaboration in pp collisions at $\sqrt{s} = 200$ GeV (left panel) [226] and by the ALICE [160] and ATLAS [161] collaborations at $\sqrt{s} = 7$ TeV (right panel) is shown. The data are compared to FONLL pQCD calculations [227], which at both energies can describe the measurements within uncertainties. The central values of FONLL calculations are obtained using CTEQ-6.6 parton distribution functions [228], $m_c = 1.5$ GeV/ c^2 and $m_b = 4.75$ GeV/ c^2 for the

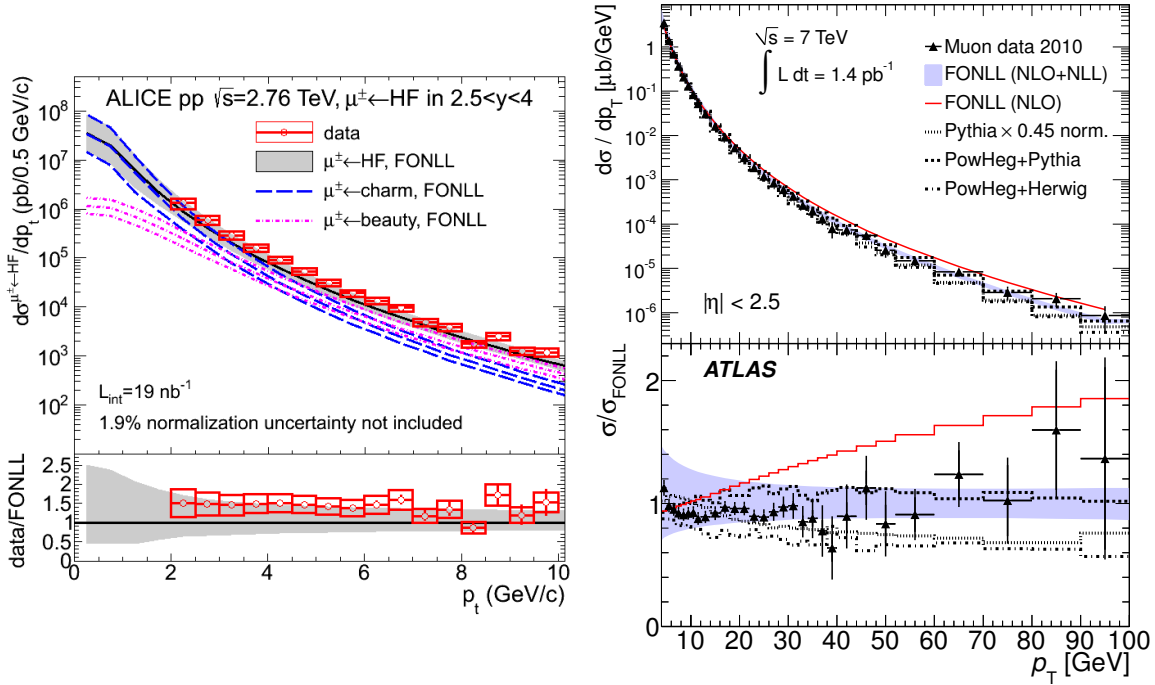


Figure 8. Transverse-momentum differential production cross section of heavy-flavor decay muons. Left: results at $\sqrt{s} = 2.76$ TeV at forward rapidity from ALICE [164]. Right: results at $\sqrt{s} = 7$ TeV at mid-rapidity from ATLAS [161]. Data are compared to FONLL [111, 227], POWHEG [219] and PYTHIA [123] predictions.

charm and beauty quark masses, and QCD renormalization (μ_R) and factorization (μ_F) scales of $\mu_R = \mu_F = \sqrt{p_T^2 + m_q^2}$. The theoretical uncertainty band is defined by varying the charm and beauty quark masses in the ranges $1.3 < m_c < 1.7$ GeV/ c^2 and $4.5 < m_b < 5.0$ GeV/ c^2 , and the QCD scales in the ranges $0.5 < \mu_R/\mu_0 < 2$ and $0.5 < \mu_F/\mu_0 < 2$ with the constraint $0.5 < \mu_F/\mu_R < 2$. The outcomes of GM-VFNS and POWHEG, not shown in this figure, agree with the FONLL predictions within uncertainties (see Ref. [229] for a systematic comparison of FONLL, GM-VFNS and FONLL at LHC energies). A similar agreement between HF decay electron measurements and pQCD-based calculations is found for pp collisions at $\sqrt{s} = 2.76$ TeV [230].

Heavy-flavor decay muon production has been measured in pp collisions at the LHC by the ATLAS collaboration at mid-rapidity at $\sqrt{s} = 7$ TeV [161] and by the ALICE collaboration at forward rapidity ($2.5 < y < 4$) at $\sqrt{s} = 2.76$ and 7 TeV [164, 231]. The measured p_T -differential cross sections at forward rapidity at $\sqrt{s} = 2.76$ TeV and at mid-rapidity at $\sqrt{s} = 7$ TeV are shown in the left and right panels of Fig. 8, respectively. In both rapidity intervals, the predictions from FONLL calculations are compatible within uncertainties with the measured cross sections. In the forward-rapidity interval, the results of FONLL calculations are also shown separately for muons from charm and beauty decays. The predictions for beauty-decay muons include the contributions of muons coming directly from beauty-hadron decays ($B \rightarrow \mu$) and of muons from decays of charmed hadrons produced in beauty-hadron decays ($B \rightarrow D \rightarrow \mu$). According to

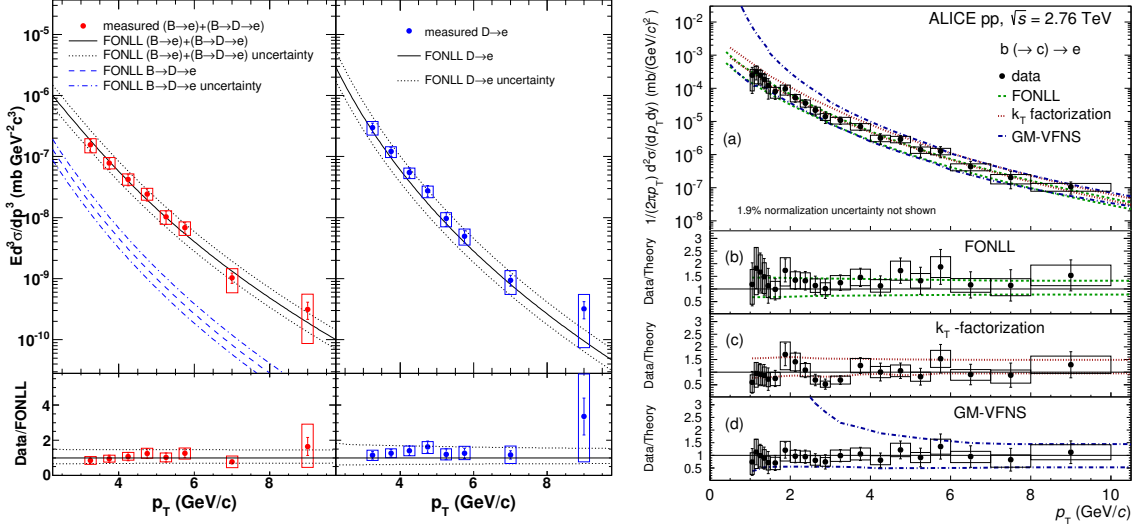


Figure 9. Transverse-momentum differential production cross section of beauty-decay electrons in pp collisions. Left: results at $\sqrt{s} = 200$ GeV from STAR [162]. Right: results at $\sqrt{s} = 2.76$ TeV from ALICE [154]. Data are compared to FONLL [111, 227], GM-VFNS [232] and LO k_T -factorization [214] calculations.

FONLL, the yield of HF decay muons is dominated by muons from charm decays for $p_T < 4 - 5$ GeV/ c , while at higher p_T the main contribution is from beauty decays. The mid-rapidity results in the right panel of Fig. 8 are also compared to predictions obtained with the POWHEG Monte Carlo generator, interfaced to either PYTHIA or HERWIG for the parton shower simulation. POWHEG+PYTHIA agrees well with the FONLL calculations, while POWHEG+HERWIG predicts a significantly lower total cross-section. As pointed out in Ref. [161], less than half of this difference may be accounted for by the different HF hadron decay models implemented in PYTHIA and HERWIG. Also shown in the right panel of Fig. 8 is the outcome of the PYTHIA event generator (LO plus parton shower), which describes well the measured p_T dependence, but overestimates the total cross section by a factor of about two. The FONLL(NLO) curve displayed in Fig. 8 is the central value of a FONLL calculation in which the next-to-leading-log resummation part was disabled in the pQCD calculation. Such a NLO calculation deviates significantly from the measured cross section, showing sensitivity to the NLL resummation term in the pQCD calculation. A very good description of the data is also provided by GM-VFNS, as can be seen in Fig. 3 of Ref [232].

Electrons from open-charm and -beauty decays could be statistically separated at RHIC using the ratio $e_B/(e_B + e_D)$ measured from e -hadron azimuthal correlations [167] and the measured HF decay electron cross section. The invariant cross section of electrons from beauty and charm decays measured by the STAR Collaboration in pp collisions at $\sqrt{s} = 200$ GeV is shown in the left panel of Fig. 9 [162], together with FONLL predictions, which describe the data within uncertainties. At the LHC, in addition to the studies of azimuthal correlations, a selection on the electron impact

parameter was applied to disentangle charm and beauty contributions to the measured HF decay electrons [154, 155]. The ALICE results for beauty-decay electron p_T -differential cross section at $\sqrt{s} = 2.76$ GeV [154] are reported in the right panel of Fig. 9. They are compared to the predictions from FONLL, GM-VFNS [232] and LO k_T -factorization [214] calculations. The data and the pQCD calculations are consistent within the experimental and theoretical uncertainties.

Open-charm production was measured at RHIC and at the LHC by reconstructing hadronic D -meson decays. A selection of results on D -meson p_T -differential cross sections in pp collisions is presented in Fig. 10. In the top left panel, Fig. 10(a), the D^0 and D^{*+} cross sections (scaled by the respective branching fractions $f(c \rightarrow D^0)$ and $f(c \rightarrow D^{*+})$) measured in pp collisions at $\sqrt{s} = 200$ GeV at mid-rapidity by the STAR collaboration [148] are shown along with FONLL predictions. This production cross section is measured for “inclusive” D -meson yields, including both the “prompt” contribution coming from charm-quark fragmentation and decays of excited charmed-hadron states and the feeddown contribution due to beauty-hadron decays. The LHCb results on prompt D^0 production at forward rapidity at $\sqrt{s} = 7$ TeV [150] are shown in Fig. 10(b). The differential cross section is reported as a function of p_T for different rapidity intervals and is compared to pQCD calculations with the FONLL and GM-VFNS [233] approaches. Also shown is the outcome of GM-VFNS calculations using the the CTEQ-6.5c2 parton densities with intrinsic charm [234], showing that the effect of intrinsic charm is expected to be small in the phase space region of the LHCb measurement. The LHCb collaboration recently reported results on the p_T -differential production cross section of D mesons at $\sqrt{s} = 13$ TeV and found them to be in agreement with NLO predictions from FONLL, POWHEG, and GM-VFNS [235]. The measured ratios of the cross sections at 13 and 7 TeV are also found to be described within uncertainties by FONLL and POWHEG, even though the data are consistently above the central values of the ratios of pQCD predictions in all the considered p_T and y intervals. As argued in Refs. [225, 236, 237], ratios of cross sections at different CM energies can be predicted through pQCD calculations with an accuracy of a few percent because some theoretical parameters (factorization and renormalization scales, quark mass, fragmentation fractions) are correlated at different energies and their uncertainties cancel almost completely in the ratio. On the other hand, PDF uncertainties do not cancel completely, because of the different Bjorken- x range of initial-state partons covered by the measurements at the two CM energies, making these ratios sensitive to the PDFs, and in particular to gluon PDFs at small x , where they are not yet well constrained by data. In the bottom panels, (c) and (d), of Fig. 10 the ALICE results on D^+ and D_s^+ p_T -differential cross sections at mid-rapidity at $\sqrt{s} = 7$ TeV are reported together with predictions from FONLL, GM-VFNS and LO k_T -factorization. The NLO pQCD calculations provide also a good description of the D^+ , D^{*+} , and D_s^+ cross sections measured by the ATLAS collaboration in pp collisions at $\sqrt{s} = 7$ TeV in the intervals $3.5 < p_T < 100$ GeV/ c and $|\eta| < 2.1$ [238]. A similar conclusion about the ability of pQCD calculations to describe the measurements at LHC energies is

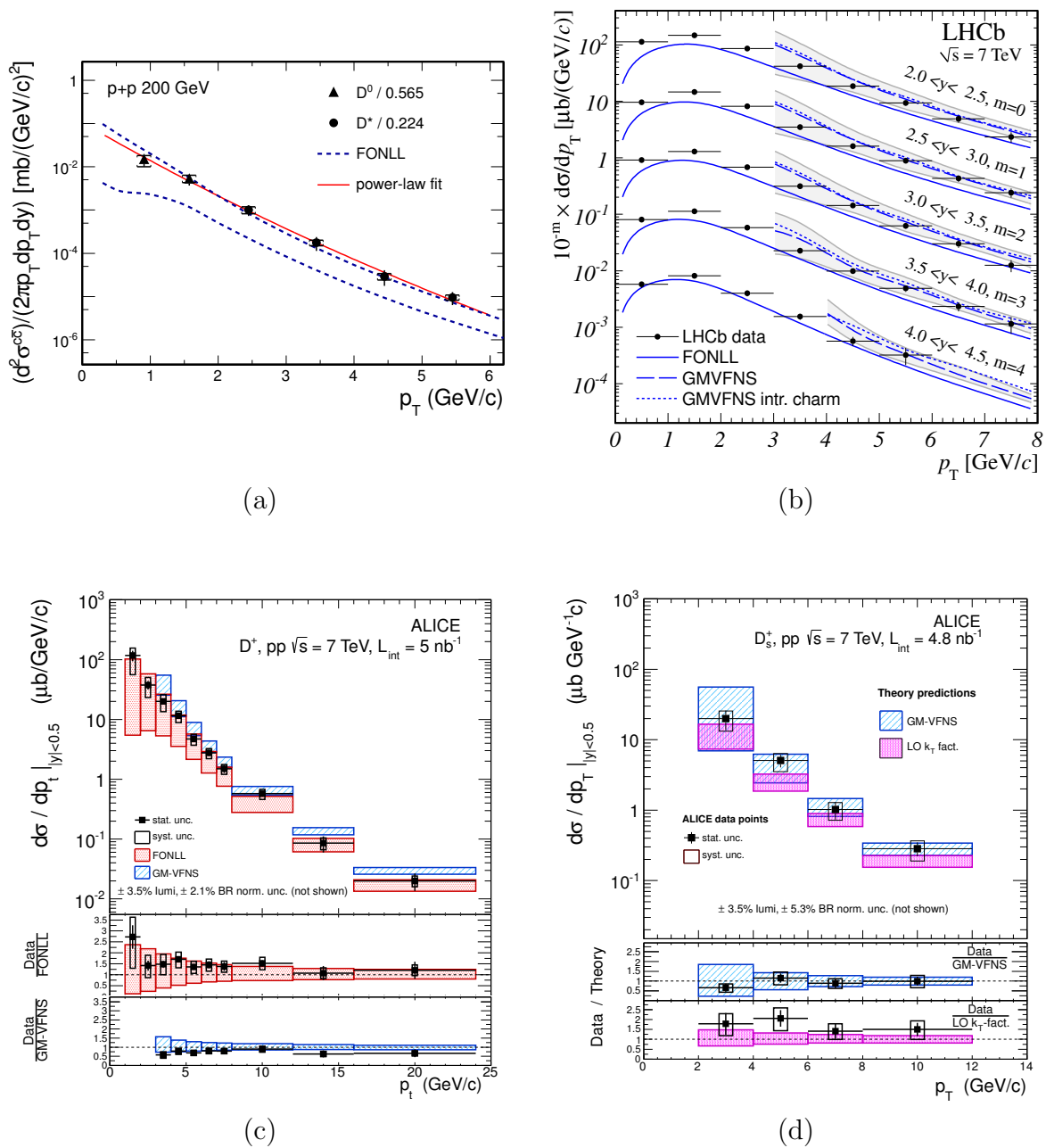


Figure 10. Transverse-momentum differential production cross section of prompt D mesons in pp collisions. (a) D^0 and D^{*+} at $\sqrt{s} = 200$ GeV at mid-rapidity from STAR [148]; (b) D^0 at $\sqrt{s} = 7$ TeV at forward rapidity from LHCb [150]; (c) D^+ at $\sqrt{s} = 7$ TeV at mid-rapidity from ALICE [176]; (d) D_s^+ at $\sqrt{s} = 7$ TeV at mid-rapidity from ALICE [177]. Data are compared to FONLL [111, 227], GM-VFNS [233] and LO k_T -factorization [214] calculations.

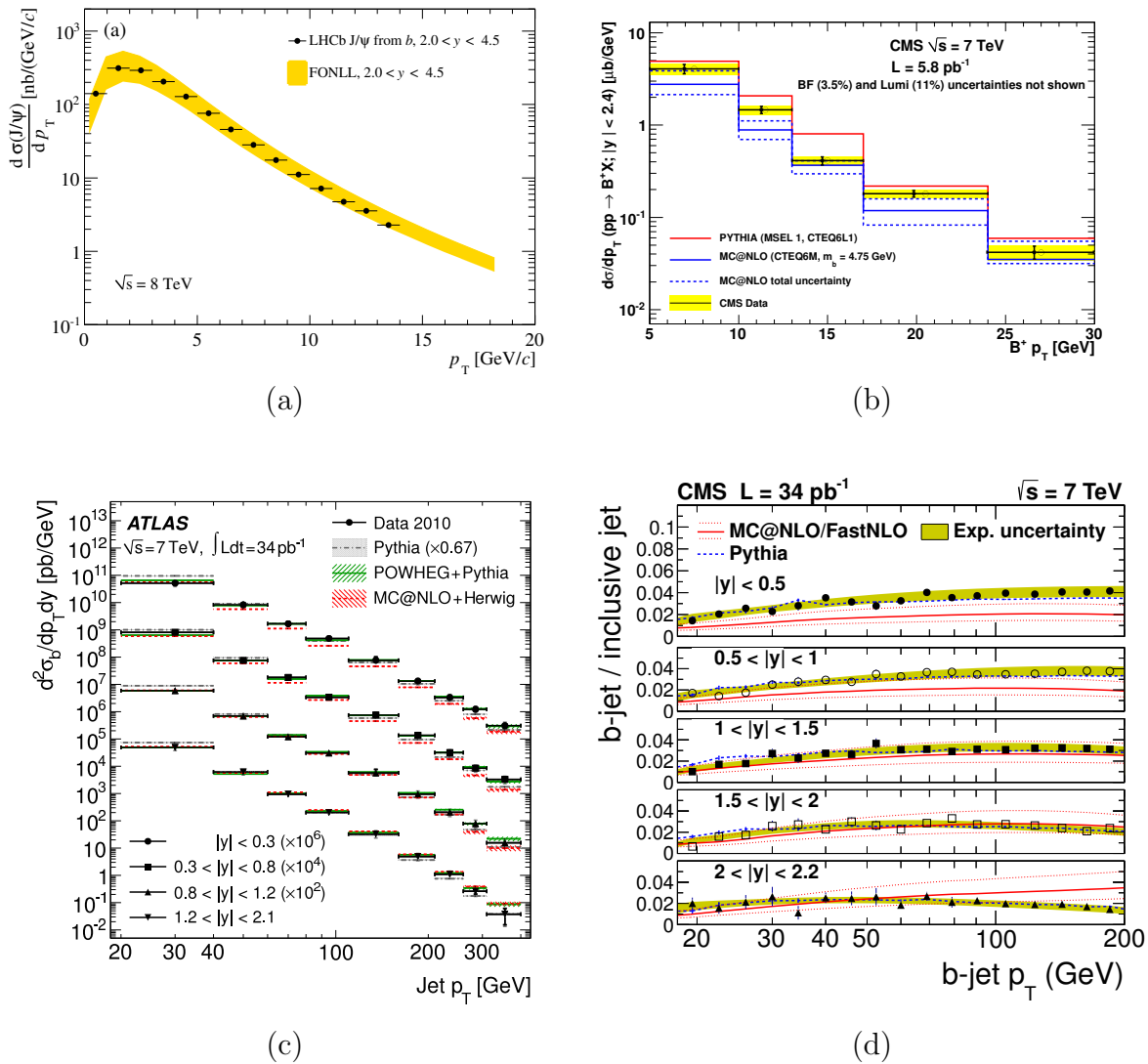


Figure 11. Transverse-momentum differential measurements of beauty production at the LHC. (a) non-prompt J/ψ at $\sqrt{s} = 8$ TeV at forward rapidity from LHCb [240]; (b) B^+ meson at $\sqrt{s} = 7$ TeV at mid-rapidity from CMS [241]; (c) b -jets at $\sqrt{s} = 7$ TeV in four rapidity intervals from ATLAS [242]; (d) ratio of b -jet to inclusive-jet cross section in four rapidity intervals from CMS [243]. Data are compared to FONLL [111,227] calculations and to MC@NLO [218], POWHEG [219] and PYTHIA [123] MC generators.

obtained. At all energies and rapidities the pQCD calculations agree with the measured cross sections within uncertainties. Yet, the FONLL predictions obtained with the central values of the calculation parameters tend to underestimate the data, with the measured cross sections lying close to the upper edge of the theoretical uncertainty band. The tendency of FONLL to underestimate the charm data was also observed at the Tevatron [239]. On the other hand, the central value of the GM-VFNS predictions lies systematically above the data.

Figure 11 displays a selection of results on beauty production as a function of

p_T at the LHC. In particular, the non-prompt J/ψ cross section at forward rapidity, measured by the LHCb collaboration at $\sqrt{s} = 8$ TeV [240] is shown in panel (a); the B^+ -meson cross section at mid-rapidity measured by CMS at $\sqrt{s} = 7$ TeV [241] is shown in panel (b); and panel (c) depicts the cross section of b -jets measured by ATLAS at $\sqrt{s} = 7$ TeV in different rapidity intervals [242]. Furthermore, in Fig. 11(d), the ratios of b -jet to inclusive-jet cross sections measured by CMS [243] in different rapidity intervals are shown as a function of p_T . The data are compared to different theoretical predictions. FONLL provides a good description of the non-prompt J/ψ data. A similar agreement with FONLL is observed for the recent measurements of non-prompt J/ψ cross section at $\sqrt{s} = 13$ TeV [244]. However, the measured ratios of the production cross sections of J/ψ from beauty-hadron decays at CM energies of 13 and 8 TeV are found to lie systematically above the predictions from FONLL calculations. As pointed out above, in the calculations of ratios of cross sections at different energies, the sensitivity to the pQCD scale variation is substantially reduced, thus providing some sensitivity to the (mostly gluon) PDFs in regions where they are not yet well constrained by data [225, 237]. PYTHIA, which has LO+LL accuracy, does not provide a good description of the measured B -meson cross section, which is instead correctly predicted by MC@NLO. The measurements of b -jet cross section can be compared to predictions from MC event generators featuring a complete description of the hadronic final state. The NLO generators POWHEG (matched to PYTHIA parton shower) and MC@NLO (interfaced to HERWIG for the parton shower) are found to describe the data reasonably well, with POWHEG+PYTHIA providing a slightly better agreement with the data across the different rapidity regions (see [242] for details). The LO+LL predictions from PYTHIA do not predict the correct normalization, overestimating the measured integrated cross section by a factor of about 1.5, but they can describe reasonably well the p_T dependence of the b -jet production cross section.

Additional insight into HQ production and fragmentation can be obtained from measurements of HF azimuthal correlations, which help to constrain MC models and to disentangle different production processes for HF particles. For example, measurements of azimuthal correlations between B and \bar{B} hadrons from CMS show a substantial contribution from production at small opening angles ($\Delta\varphi \approx 0$), which is not reproduced by PYTHIA [245]. This result points to the importance of the “near” production (via the gluon splitting mechanism) in addition to the “back-to-back” production (mostly via flavor creation). Preliminary results of D -hadron azimuthal correlations from ALICE [246] show that PYTHIA and POWHEG+PYTHIA provide a reasonable description of the data for this observable, which is sensitive to charm-quark fragmentation and jet structure. The production of D mesons, prompt and non-prompt J/ψ , and Υ was also measured by ALICE and CMS as a function of the multiplicity of particles produced in the collision [247–249]. The per-event yields of open charm and beauty hadrons and quarkonia are found to increase with increasing multiplicity. This trend can be described by models including multiple parton interactions (MPI), thus providing sensitivity to the role of MPIs at the hard momentum scales relevant for $c\bar{c}$

and $b\bar{b}$ pair production.

3.2.2. Results from p - A (d - A) collisions and Cold-Nuclear-Matter Effects

The study of the properties of the hot and dense medium created in heavy-ion reactions requires a quantitative understanding of the effects induced by the presence of nuclei in the initial-state of the collisions, as well as, possibly, by the relatively high multiplicities of particles in the final state. Such effects are commonly referred to as cold-nuclear-matter (CNM) effects and are assessed experimentally by studying particle production in proton–nucleus (pA) or deuteron–nucleus (dA) collisions.

Heavy-flavor production can be affected by a variety of CNM effects, which include the following.

- *Modification of the Parton Distribution Functions.* The nuclear environment affects the quark and gluon distributions, which are modified in bound nucleons compared to those of free nucleons. The modification depends on the fractional parton momentum (x), on the scale of the parton–parton interaction (Q^2), and on the atomic mass number (A) of the nucleus [250, 251]. This effect is commonly studied experimentally via the ratio between the PDF of nucleons in nuclei (nPDF) and those of the proton (deuteron), $R_i^A(x, Q^2)$, where i is the parton flavor. Four regions, depending on the value of x , are usually identified: (i) *Shadowing*, which is a depletion ($R_i^A < 1$) at small x ($x < 10^{-2}$); (ii) *Anti-shadowing*, an enhancement ($R_i^A > 1$) at intermediate x ($10^{-2} < x < 10^{-1}$); (iii) *EMC effect*, a depletion ($R_i^A < 1$) in the valence quark region ($x \sim 10^{-1}$); and (iv) an enhancement ($R_i^A > 1$) at large x ($0.8 < x < 1$) associated with the *Fermi motion* of nucleons inside the nucleus. There is no comprehensive theoretical understanding of the observed pattern over the entire x range. The $R_i^A(x, Q^2)$ values can be calculated using phenomenological parameterizations based on global fit analyses of lepton–nucleus and proton–nucleus data, such as EPS09 [252], HKN07 [253] and nDS [254]. The depletion in the low- x region (shadowing) can be understood as due to gluon phase-space saturation, and it can be described within the Colour Glass Condensate (CGC) effective theory, where an initial high-energy nucleus is treated as a coherent and dense (saturated) gluonic system [255]. The modification of the PDFs results in a modification of the effective partonic luminosity (and consequently of the HQ production cross section) in collisions involving nuclei relative to pp collisions.
- *Multiple scattering of partons* in the nucleus before and/or after the hard scattering affects the kinematic distribution of the produced heavy quarks and/or hadrons. These multiple collisions lead to transverse-momentum broadening (usually denoted Cronin effect) [256–258] and parton energy loss [259–262].
- On top of initial-state CNM effects, also effects in the final state, due to the high multiplicity of particles produced in pA (dA) collisions, may be responsible for a

modification of the HF hadron yields and momentum distributions. The presence of final-state effects in small collision systems is suggested by measurements of long-range correlations of charged hadrons in p Pb collisions at the LHC [263–266]. These observations can be described by hydrodynamic calculations assuming the formation of a medium with some degree of collectivity. It is still highly debated if such a collective flow is established, and alternative explanations, based, *e.g.*, on the CGC effective theory [267] have been proposed. It should be pointed out that if a collective motion of the final-state particles is established, the medium could also impart a flow on HF particles. Additional indications for the importance of final-state effects in small collision systems are provided by the larger suppression of the $\psi(2S)$ meson with respect to the J/ψ in d Au collisions at RHIC [268] and p Pb collisions at the LHC [269], see, *e.g.*, Refs. [270,271] for pertinent model calculations.

Heavy-flavor production was studied at RHIC and at the LHC in d Au and p Pb collisions at $\sqrt{s_{\text{NN}}} = 200$ GeV and 5.02 TeV, respectively. At RHIC, the measurements were carried out by STAR [159] and PHENIX [272,273] in the semi-leptonic channel. In particular, HF decay electrons were measured at mid-rapidity ($|\eta| < 0.35$ for PHENIX and $0 < \eta < 7$ for STAR) and HF decay muons at forward (deuteron-going direction) and backward (Au-going) rapidity with PHENIX. The PHENIX collaboration also reported results for peripheral and central collisions. The resulting nuclear modification factor, $R_{d\text{Au}}$, of HF decay leptons is shown in Fig. 12 as a function of p_{T} for multiplicity integrated (bottom panels), central (middle panels) and peripheral (top panels) collisions. The mid-rapidity results (left panels) show a slight enhancement of the production with respect to binary-scaled pp collisions, with a mild dependence on collision centrality. The data can be described in terms of nuclear PDFs (anti-shadowing) and k_{T} -broadening (Cronin enhancement). The possible development of a collective flow in the HQ sector is also expected to lead to values of $R_{d\text{Au}}$ larger than unity in the p_{T} range covered by the measurements. An approximate description of the measured values of nuclear modification factor can be obtained employing a blast-wave function, with parameters extracted from fits to the light-hadron spectra, to determine the momentum distribution of HF hadrons in d Au collisions [275]. Recently, the outcome of calculations in the POWLANG transport setup at RHIC energies were published [276]. In this model, it is assumed that in p A and d A collisions a hot and deconfined medium is formed. The relativistic Langevin equation is used to follow the propagation of charm and beauty quarks in the hydrodynamically expanding medium until hadronization, which is modeled by combining each heavy quark with a light parton from the medium to form color-singlet objects (strings), which are fragmented with PYTHIA to produce the final-state hadrons. The model can describe the midrapidity data within uncertainties, suggesting that, within such a framework, the enhancement of $R_{d\text{Au}}$ of HF decay electrons observed at RHIC reflects the radial flow acquired by the parent- D and $-B$ mesons.

In the right panels of Fig. 12 the results on the HF muon $R_{d\text{Au}}$ at forward and

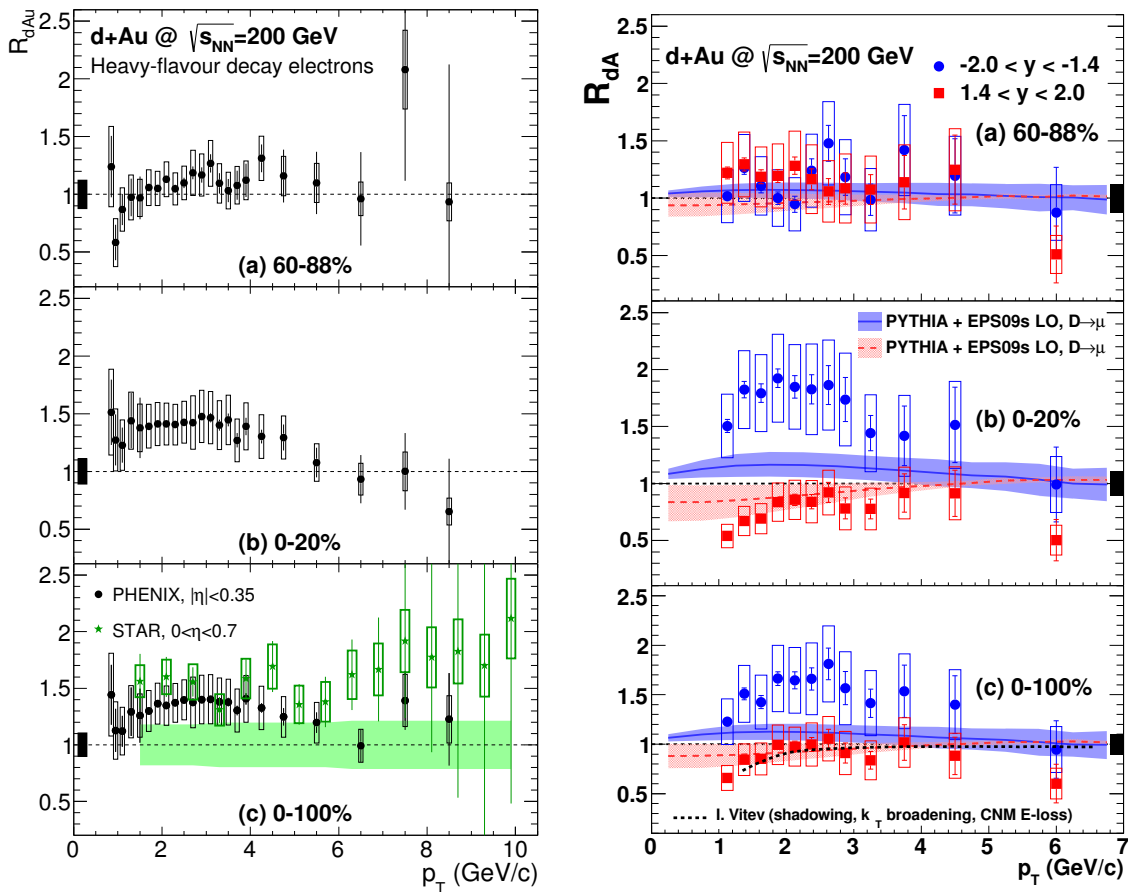


Figure 12. Nuclear modification factor of heavy-flavor decay leptons as a function of p_T in dAu collisions at $\sqrt{s_{NN}} = 200$ GeV. Left: heavy-flavor decay electrons at mid-rapidity from PHENIX [272] and STAR [159]. Right: heavy-flavor decay muons at backward (Au-going side) and forward (d -going side) rapidity from PHENIX [273]. PHENIX results are shown for the centrality-integrated sample (0–100%) and for peripheral (60–88%) and central (0–20%) collisions separately. Muon data are compared to predictions based on nuclear modification of the PDF (EPS09s nPDF [274]); and to a theoretical calculation including shadowing, k_T -broadening and cold-nuclear-matter energy loss effects [261].

backward rapidities are reported. They show a pronounced centrality dependence, with similar R_{dAu} values in peripheral collisions at forward and backward rapidity, but significant differences in central collisions, namely a suppression at forward rapidity (d -going direction) and an enhancement at backward rapidity (Au-going direction). The data at forward rapidity are described both by the model of Vitev *et al.* [261], which includes shadowing, k_T broadening and CNM energy loss, and by pQCD calculations including EPS09 nPDFs [274]. The results at backward rapidity cannot be described by only considering nPDF effects, suggesting that other mechanisms are at work.

The $b\bar{b}$ production cross section was determined at mid-rapidity by the PHENIX collaboration from the invariant-mass and p_T distributions of e^+e^- pairs. The result, $\sigma_{b\bar{b}}^{dAu} = 1.37 \pm 0.28(\text{stat}) \pm 0.46(\text{syst})$ mb, is consistent with binary scaling of the

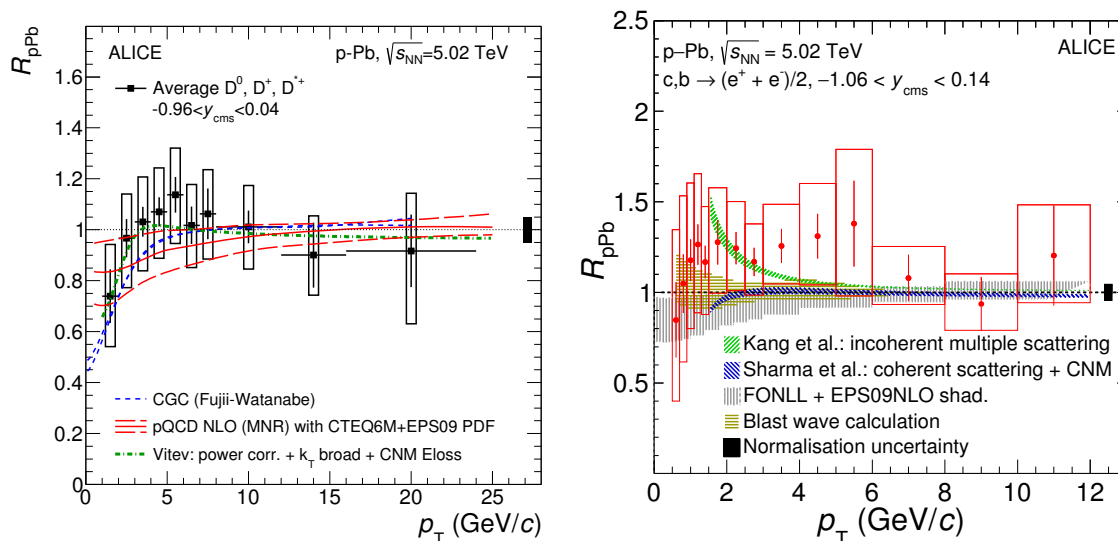


Figure 13. Nuclear modification factor of D mesons [278] (left) and HF decay electrons [277] (right) as a function of p_T in pPb collisions at $\sqrt{s_{NN}} = 5.02$ TeV. Data are compared to calculations including CNM effects: NLO pQCD calculations with EPS09 nPDF [252], Color Glass Condensate [281], shadowing, k_T -broadening and CNM energy loss [72], incoherent multiple scatterings [282] and a blast-wave ansatz for a collectively expanding medium [275].

cross section measured in pp collisions [166]. The modification due to CNM effects on HF production at mid-rapidity is expected to be small as compared to the quoted uncertainties of the measurement.

At LHC energies, charm and beauty production was studied by measuring HF decay electrons (ALICE [277]), D mesons (ALICE [278]), B mesons (CMS [179]), and b -jets (CMS [279]) at mid-rapidity; at forward (p -going side) and backward (Pb-going) rapidity, beauty was studied via measurements of non-prompt J/ψ by the LHCb collaboration [172]. Preliminary results were also reported by the ALICE collaboration for HF decay muons at forward and backward rapidity [280] and beauty-decay electrons at mid-rapidity [280].

The nuclear modification factor R_{pPb} of prompt D mesons [278] and HF decay electrons [277] measured by the ALICE collaboration as a function of p_T at mid-rapidity is shown in Fig. 13. The reference pp cross sections at $\sqrt{s} = 5.02$ TeV were obtained with a pQCD-based energy scaling of the p_T -differential cross sections measured at $\sqrt{s} = 7$ TeV [283]. No significant difference among different D -meson species (D^0 , D^+ , D^{*+} and D_s^+) is observed [278]. The average R_{pPb} of D^0 , D^+ and D^{*+} mesons is reported in the left panel of Fig. 13. Within uncertainties, the measured D -meson R_{pPb} is compatible with unity, indicating small ($< 10 - 20\%$) CNM effects for $p_T > 2$ GeV/c. The D -meson R_{pPb} is compared to model calculations including CNM effects, namely NLO pQCD calculations with EPS09 nPDF [252], calculations based on CGC effective theory [281] and predictions including shadowing, k_T broadening and CNM energy

loss [72]. The data are fairly well described by the above mentioned models, which consider only initial-state effects. The effect of the possible formation of a collectively expanding medium, as calculated with the blast-wave approach of [275], is expected to be small for D mesons in multiplicity-integrated collisions. The first results from two different transport models assuming the formation of a hot and deconfined medium in p Pb collisions at the LHC, which modifies the propagation and hadronization of heavy quarks, were recently published [276, 284]. In these frameworks, a small bump in the $R_{p\text{Pb}}$ at low/intermediate p_T due to radial flow is predicted, possibly accompanied by a moderate ($< 20 - 30\%$) suppression at high p_T , due to in-medium energy loss. The models describe the data within uncertainties, even though the measured $R_{p\text{Pb}}$ disfavors a suppression larger than 15–20% in the transverse momentum interval $5 < p_T < 10$ GeV/ c . However, the current uncertainties on the experimental and theoretical side do not allow us to discriminate between scenarios with only CNM effects or with CNM and hot medium effects.

The HF decay electron result, shown in the right panel of Fig. 13, is also consistent with unity within uncertainties over the whole p_T range of the measurement. Given the large systematic uncertainties, the measured $R_{p\text{Pb}}$ is also compatible with an enhancement in the transverse-momentum interval $1 < p_T < 6$ GeV/ c , as observed at midrapidity in d Au collisions at $\sqrt{s_{\text{NN}}} = 200$ GeV (see Fig. 12). Similarly to what is observed for D mesons, the data are described within uncertainties by pQCD calculations with nPDFs [252], and by a model including shadowing, k_T broadening and CNM energy loss [72], both of them predicting a small suppression at low p_T . Calculations based on incoherent multiple scatterings [282] or on a blast-wave modeling of the possible establishment of collective flow [275] predict an enhancement in the nuclear modification factor at low p_T . The uncertainties of the current measurements do not allow a discrimination among these different theoretical approaches.

Results on D -meson production as a function of the p Pb collision centrality were recently published [285]. In Fig. 14, the nuclear modification factor, $Q_{p\text{Pb}}$, of prompt D mesons (average of D^0 , D^+ and D^{*+}) is shown as a function of p_T for four different centrality classes, defined from the energy deposited in the neutron zero-degree calorimeters. This selection provides the least biased estimation of the collision geometry, as discussed in detail in Ref. [286]. The results indicate that charm-hadron production is compatible with binary scaling of the pp reference in all the considered centrality classes. In particular, no evidence of a substantial modification of D -meson production with respect to pp collisions is observed in the 20% most central collisions, in which the multiplicity of produced particles is comparable to that in peripheral nucleus-nucleus collisions at RHIC/LHC energies. Nevertheless, considering the current statistical and systematic uncertainties, centrality-dependent effects of the order of 10% cannot be excluded.

The production of beauty mesons, namely B^0 , B^+ and B_s^0 , was measured by the CMS collaboration [179] in p Pb collisions as a function of transverse momentum in the range $10 < p_T < 60$ GeV/ c . The production of B^+ mesons was also studied as

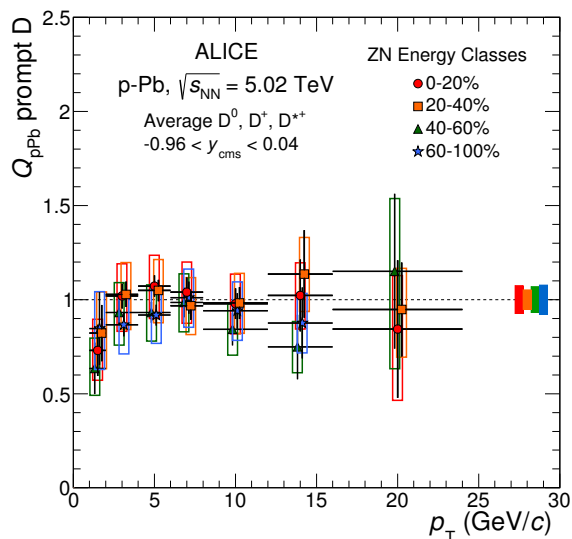


Figure 14. Nuclear modification factor of D mesons (average of D^0 , D^+ and D^{*+}) as a function of p_T in different centrality classes for p Pb collisions at $\sqrt{s_{NN}} = 5.02$ TeV [285]. The notation Q_{pPb} is used for the nuclear modification factor in centrality classes to emphasize the possible presence of potential biases in the centrality estimation (see Ref. [286])

a function of rapidity. The B^+ nuclear modification factor, computed using FONLL pQCD calculations as the pp reference, is shown in Fig. 15 as a function of p_T (left panel) and rapidity (right panel). No significant modification of B -meson production is observed in p Pb collisions compared to the binary-scaled FONLL reference over the measured p_T range.

The CMS collaboration recently reported measurements of b -jet p_T -differential cross section and nuclear modification factor in p Pb collisions at $\sqrt{s_{NN}} = 5.02$ TeV in the jet transverse-momentum and pseudorapidity intervals $55 < p_T < 400$ GeV/ c and $2.5 < \eta_{CMS} < 1.5$ [279]. As there are no pp data available at the CM energy of p Pb collisions, the pp reference for the R_{pPb} calculation was obtained from PYTHIA simulations. The discrepancies between PYTHIA and data observed at $\sqrt{s} = 2.76$ and 7 TeV were accounted for in the systematic uncertainty. The resulting R_{pPb}^{PYTHIA} as a function of p_T is shown in the left panel of Fig. 16; it is compatible with unity within uncertainties, especially considering the 22% uncertainty on the PYTHIA reference. The data are described within uncertainties by a pQCD model that includes modest initial-state energy-loss effects [287]. Overall, the conclusions from the b -jet studies agree with those drawn from the measurements of B meson production reported above. Future measurements of B mesons and b -jets in pp collisions at $\sqrt{s} = 5.02$ TeV are expected to provide a substantial reduction of the uncertainties on the pp reference, thus enabling a more definite assessment of possible modifications of beauty production in p Pb collisions.

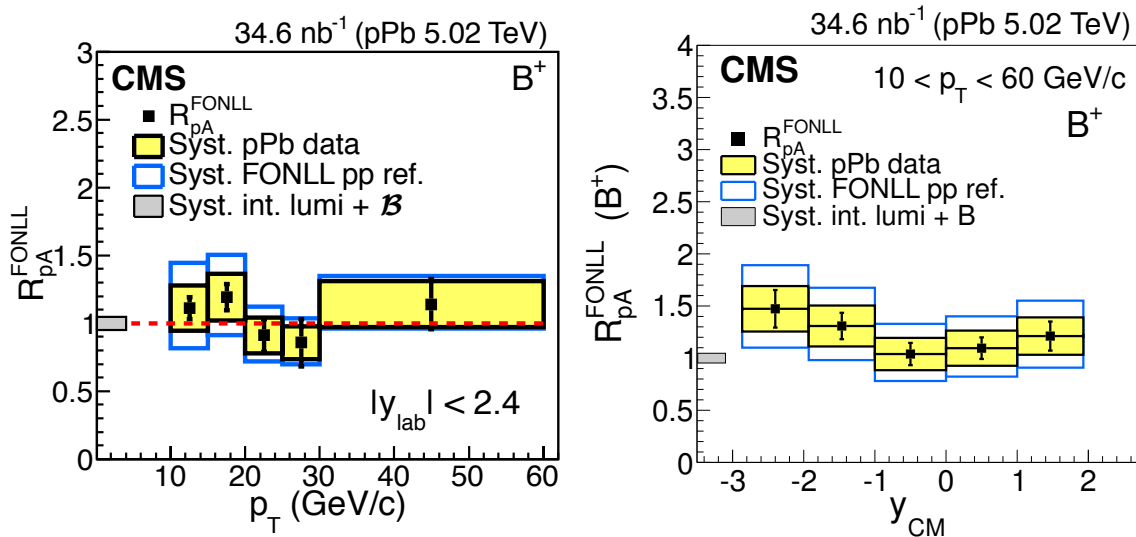


Figure 15. Nuclear modification factor of B^+ mesons as a function of p_T (left) and rapidity (right) in $p\text{Pb}$ collisions at $\sqrt{s_{\text{NN}}} = 5.02$ TeV [179]. The pp reference is taken from FONLL pQCD calculations.

Beauty production in $p\text{Pb}$ collisions at the LHC was also studied by the LHCb collaboration by measuring non-prompt J/ψ at large rapidities ($2 < y_{\text{lab}} < 4.5$) down to $p_T = 0$ [172]. The pp reference at $\sqrt{s} = 5.02$ TeV was obtained via an interpolation of the measurements at \sqrt{s} values of 2.76, 7 and 8 TeV. The p_T -integrated $R_{p\text{Pb}}$ as a function of rapidity is shown in the right panel of Fig. 16 together with theoretical calculations. The nuclear modification factor is compatible with unity at backward rapidity (Pb-going side). In the forward rapidity region the data show a modest suppression relative to the binary-scaled pp reference. Perturbative QCD calculations at LO including EPS09 or nDSg nPDF parameterizations [288] describe the data well at forward rapidity, while in the backward region the agreement is not as good.

As pointed out in Ref. [289], the nuclear modification of the PDFs at small x can be better constrained by means of a data-to-theory comparison of the p_T -differential D -meson forward-to-backward ratio, *i.e.*, the ratio of the D -meson cross sections in symmetric intervals at backward and forward rapidity, in the kinematical region accessible with the LHCb apparatus. In this ratio, the theoretical uncertainties due to pQCD scales and quark mass partially cancel, as well as some of the contributions to the experimental systematic uncertainties, thus providing improved sensitivity to CNM effects on the PDFs.

Further insight into possible modifications of HF production in $d\text{Au}$ and $p\text{Pb}$ collisions can be obtained from measurements of azimuthal correlations. The angular correlation between HF hadrons reflects the correlation between HQ pairs and is therefore sensitive to their production mechanisms. In proton(deuteron)–nucleus collisions, the CGC effective theory predicts, in addition to a reduction of the overall particle yield, a broadening and suppression of the away-side peak (at $\Delta\varphi = \pi$) in the

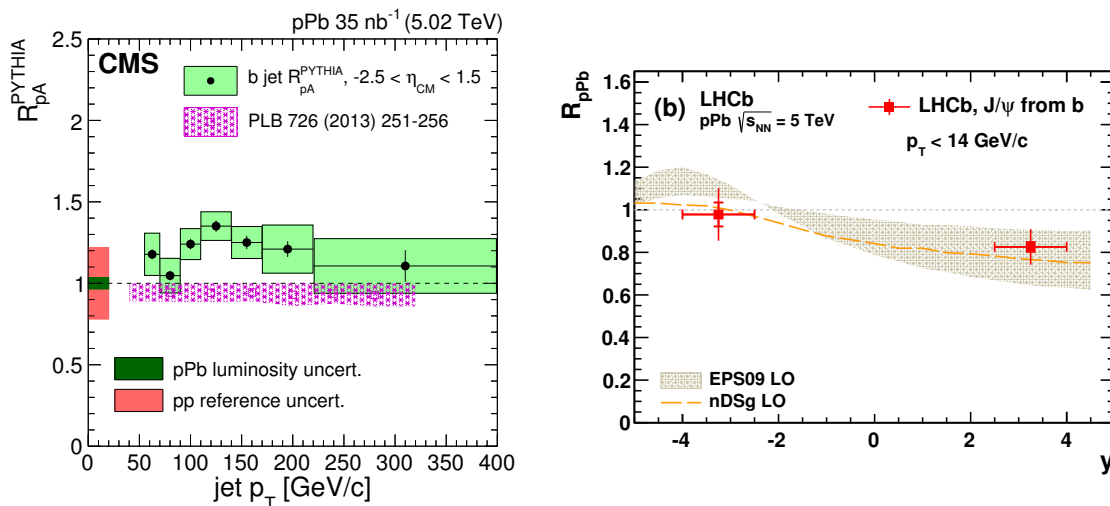


Figure 16. Nuclear modification of beauty production in pPb collisions at $\sqrt{s_{NN}} = 5.02$ TeV. Left: R_{pPb} of b -jets as a function of p_T measured by CMS [279], compared to predictions of a model including initial-state energy loss [287]. Right: R_{pPb} of J/ψ from beauty-hadron decays as a function of y measured by LHCb [172], compared to predictions of models with nuclear modification of the PDFs [288].

two-particle azimuthal correlations [255, 290, 291]. A depletion of the away-side yields in two-particle azimuthal correlations is also expected to be induced by CNM energy loss and multiple scattering processes in the initial and final state [292]. These effects could also affect HF angular correlations. The azimuthal correlation between HF decay electrons at mid-rapidity ($p_T > 0.5$ GeV/ c , $|\eta| < 0.35$) and HF decay muons at forward rapidity ($p_T > 1$ GeV/ c , $1.4 < \eta < 2.1$) were measured by the PHENIX collaboration in pp and dAu collisions at $\sqrt{s} = 200$ GeV [205]. The selection of a muon at forward rapidity allows to probe a low- x range in the Au nucleus, where saturation effects are predicted to occur. A suppression of the away-side peak ($\Delta\varphi = \pi$) is observed in dAu collisions compared to pp , indicating that the charm-quark pair kinematics is modified in the cold nuclear medium. Preliminary results of D -hadron azimuthal correlations in pPb collisions at the LHC were reported by the ALICE collaboration [246]. With the current level of uncertainties, no conclusion can be drawn on a possible modification of D -hadron correlations with respect to pp collisions.

Measurements of two-particle angular correlations in pA collisions can also be exploited to study whether also charm and beauty show v_2 -like double-ridge long-range angular correlations in “small systems”, as observed for light hadrons [263–266]. An intriguing possible hint for a non-zero HF v_2 in high-multiplicity pPb collisions is provided by the ALICE measurements of angular correlations between a muon at forward rapidity and hadrons at midrapidity [293]. A positive v_2 is observed in the 20% highest-multiplicity pPb interactions for muon tracks up to $p_T \approx 4$ GeV/ c . Therefore, in the transverse momentum interval $p_T > 2$ GeV/ c , where the inclusive muon yield is expected to be dominated by HF hadron decays, the data may support a finite value of

HF v_2 .

In summary of this section, the measurements in proton(deuteron)–nucleus collisions show small to moderate modifications of HF production as compared to the binary-scaled pp references. The magnitude of this modification depends on rapidity, p_T , and (at least at RHIC energy) collision centrality. The measured values of charm and beauty nuclear modification factors can be described by models including CNM effects: nuclear modification of the PDFs, (gluon) saturation, transverse-momentum broadening, and initial-parton energy loss. The uncertainties on the current experimental results, together with the large uncertainties on the parameterized nuclear PDFs at small Bjorken- x prevent a more conclusive theoretical interpretation of the data, making it difficult to address in a more quantitative way the role of the various CNM effects in the initial and final state.

3.3. Results from A-A Collisions and Model Comparisons

Charm and beauty quarks are sensitive probes of the properties of the hot and dense medium created in heavy-ion collisions at ultra-relativistic energies. They are predominantly produced in hard-scattering processes occurring in the early stages of the collision, characterized by time scales shorter than the expected formation times of the QGP medium. Thermal production in the medium is expected to be small or negligible at the temperatures attained in heavy-ion collisions at RHIC and at the LHC [183,184]. Their total yield is therefore essentially set by the yield in pp collisions, which, as discussed in Section 3.2.1, is described by pQCD calculations within current uncertainties, further modified by nuclear corrections to the PDFs (see Section 3.2.2) and scaled by the number of binary nucleon–nucleon collisions (N_{coll}) occurring in the nucleus–nucleus interaction. The initially produced heavy quarks interact with the constituents of the medium through the exchange of energy and momentum. At sufficiently high p_T ($p_T \gtrsim 5(15)$ GeV/ c for charm (bottom)), the main effect is that heavy quarks lose energy while traversing the medium (although the precise characterization of the transition to the energy-loss regime is still an open question and is expected to depend on collision energy, centrality, quark flavor, etc.). The energy loss can occur via both inelastic (radiative) and elastic (collisional) processes, resulting in a suppression of the yield of HF hadrons (and their decay leptons) at high p_T as compared to the binary-scaled pp reference (recall Secs. 2.2.1 and 2.2.2). The interest in HF studies in the high- p_T regime is mostly related to the predicted color-charge and quark-mass dependence of in-medium parton energy loss, expected to lead to a hierarchy where beauty quarks lose less energy than charm quarks, and the latter less energy than light quarks and gluons. At lower p_T ($p_T \lesssim 5(15)$ GeV/ c for charm (bottom)), measurements of HF particles are sensitive to other aspects of the interactions of charm and beauty quarks with the medium. Low-momentum heavy quarks, including those shifted to low momentum by energy loss, are expected to couple to the collective expansion (flow) of the system and approach local thermal equilibrium with the medium [118, 185]. It

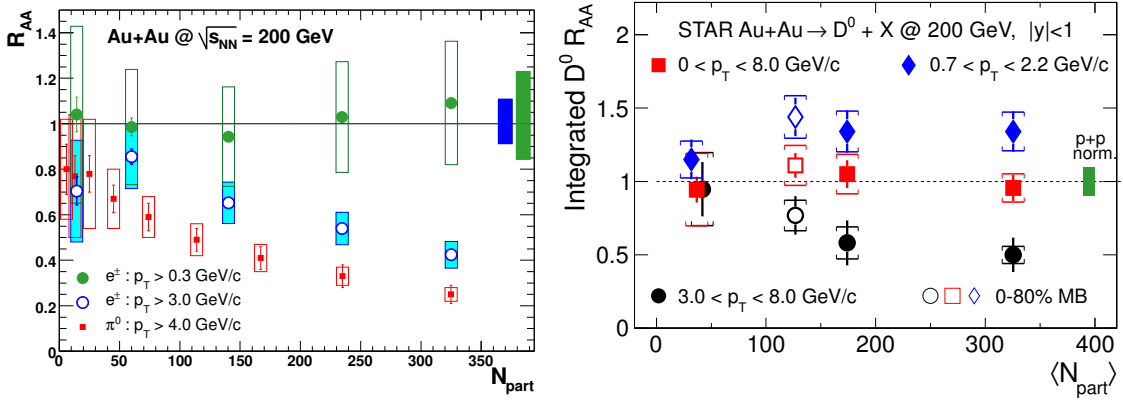


Figure 17. Centrality dependence of the nuclear modification factor R_{AA} of HF decay electrons (left, from PHENIX [44]) and D^0 mesons (right, from STAR [294]) at mid-rapidity in different p_T intervals. Also shown in the left panel is the R_{AA} of π^0 with $p_T > 4$ GeV/ c .

is also predicted that a significant fraction of low- and intermediate-momentum heavy quarks hadronizes via recombination with other quarks from the medium [118, 186] (as discussed in Sec. 2.2.6). These questions can be addressed via the study of the nuclear modification factor, R_{AA} , and of the azimuthal anisotropy, in particular the elliptic flow v_2 , of HF hadrons and their decay leptons at low and intermediate p_T (smaller than roughly five times the HQ mass).

All final-state effects described above, which are a consequence of the interactions of the heavy quarks with the hot and dense medium, influence the momentum distribution of charm (beauty) quarks, but they have little or no effect on the total yield of HF hadrons. For this reason, the p_T -integrated yield is expected to be consistent with N_{coll} scaling of the yield measured in pp reactions, apart from effects due to nuclear modifications of the PDFs affecting the production process. This is confirmed by the results shown in Fig. 17 where the nuclear modification factor of HF decay electrons [44] and D^0 mesons [294] measured in Au–Au collisions at a CM energy of $\sqrt{s_{NN}} = 200$ GeV per nucleon pair, are shown as a function of the collision centrality, expressed in terms of the number of participant nucleons N_{part} , for different p_T intervals. The production of HF decay electrons with $p_T > 0.3$ GeV/ c , which measures a large part of the total charm production yield, and of D^0 mesons with $0 < p_T < 8$ GeV/ c , are consistent with a scaling with the number of binary collisions (corresponding to $R_{AA} = 1$) within experimental uncertainties, as expected for initial HQ production from hard-scattering processes. In contrast, the yield at high p_T shows a clear suppression ($R_{AA} < 1$), which increases from peripheral to central collisions, following the qualitative expectation from in-medium charm (and beauty) quark energy loss.

At present, HF production has not been measured down to $p_T = 0$ in Pb–Pb collisions at the LHC. Hence, no results of total charm (beauty) production in heavy-ion collisions at LHC energies are currently available to check the binary scaling. It is

worth to point out that the nuclear modification of the PDF, which has a small effect on the total charm production at RHIC energies, is expected to induce a $\sim 20\%$ reduction of initial charm production at $\sqrt{s_{\text{NN}}} = 2.76$ TeV, according to NLO calculations [210] with the EPS09 parameterization of nPDFs [252]. This is due to the smaller values of Bjorken- x probed at the LHC, *i.e.*, a larger expected shadowing, as compared to lower collision energies. Hence, the p_{T} -integrated R_{AA} of charm hadrons is expected to be lower than unity at LHC energies.

In the remainder of this section, the results from measurements at RHIC and at the LHC will be briefly summarized, focusing on the p_{T} dependence of the nuclear modification factor R_{AA} and the elliptic flow v_2 . The overview of the experimental results is organized as follows. In the first subsection, the results from measurements of HF decay leptons at different collision energies are reviewed. Then, the D -meson measurements at RHIC and at the LHC are discussed and compared to results for light-flavor hadrons. Finally, the experimental results in the beauty sector from the LHC experiments are reported together with a comparison of the nuclear modification factors of charm and beauty hadrons. The presentation of the experimental results is accompanied by a discussion of their consequences for the characterization of the produced QCD matter and the estimation of its transport coefficients. The main ingredients of the different theoretical model calculations utilized in this discussion are summarized in Table 3.3.

3.3.1. Heavy-flavor decay leptons

Measurements of HF decay leptons in heavy-ion collisions have been carried out at RHIC and at the LHC by the STAR, PHENIX, ALICE and ATLAS collaborations at mid- and forward rapidity, exploiting both semi-electronic and the semi-muonic decay modes.

The first measurements of HF decay electron spectra in Au–Au reactions at RHIC were performed by PHENIX on the data sample recorded during the first RHIC run at a CM energy of $\sqrt{s_{\text{NN}}} = 130$ GeV per nucleon pair [300]. The limited precision of the measurement prevented from drawing conclusions about possible modifications of charm production in heavy-ion collisions relative to a binary-scaled pp reference. The larger data sample of Au–Au collisions at $\sqrt{s_{\text{NN}}} = 200$ GeV collected in year 2001 allowed the measurement of the centrality and p_{T} dependence of the yield of electrons from HF hadron decays at mid-rapidity [43, 301]. The measurements of the nuclear modification factor of HF decay electrons, reported in [43], showed a substantial suppression for $p_{\text{T}} > 2\text{GeV}/c$ in central Au–Au collisions relative to the expectation based on binary scaling of the yields measured in pp collisions. The magnitude of the observed suppression turned out to be compatible with that measured for neutral pions and was larger than expected in radiative-energy loss calculations, posing a challenge to this class of models. More precise measurements were carried out by the PHENIX [44, 147] and STAR [159] collaborations utilizing the larger data samples of Au–Au collisions at $\sqrt{s_{\text{NN}}} = 200$ GeV collected during the RHIC run-4. In addition,

Model	Heavy-quark production	nPDFs	Medium modelling	Quark-medium interactions	Hadronization	Hadron phase
Transport models						
BAMPS [28, 38, 75]	MC@NLO	No	Boltzmann parton 3+1D	Boltzmann pQCD coll+rad	frag	no
Cao <i>et al.</i> /Duke [82, 83, 201]	MC@NLO	EPS09	Hydro 2+1D viscous	Langevin coll+pQCD rad	frag+ reco	yes
MC@sHQ+EPOS [46, 73, 74]	FONLL	EPS09	Hydro 3+1D (EPOS)	Boltzmann pQCD coll+rad	frag+ reco	no
PHSD [40, 51]	PYTHIA	EPS09	off-shell parton transport	off-shell trans pQCD coll	frag+ reco	yes
POWLANG [36, 48, 122]	POWHEG	EPS09	Hydro 2+1D viscous	Langevin pQCD coll	string-reco	no
TAMU [65, 76, 124]	FONLL	EPS09	Hydro 2+1D ideal	Langevin T-mat coll	frag+ reco	yes
Energy-loss models						
AdS/CFT (HG) [295, 296]	FONLL	No	Glauber no hydro	AdS/CFT drag	frag	no
CUJET 3.0 [222, 223]	FONLL	No	Hydro 2+1D viscous	rad+coll	frag	no
Djordjevic <i>et al.</i> [297, 298]	FONLL	No	Glauber no hydro	rad+coll+ magn. mass	frag	no
Vitev <i>et al.</i> [72, 299]	non-zero mass VFNS	No	Glauber+ 1D Bjorken exp	rad+ in-med dissoc	frag	no
WHDG [84, 220]	FONLL	No	Glauber no hydro	rad+coll	frag	no

Table 2. Overview of the main features of models of heavy-quark in-medium energy loss and transport; see Sec. 2 for more details. The non-standard acronyms are: coll=collisional, rad=radiative, frag=fragmentation, reco=recombination, dissoc=dissociation, exp=expansion.

PHENIX published results from a sample of Cu–Cu collisions at $\sqrt{s_{NN}} = 200$ GeV collected in run-5 [163] and in Au–Au collisions at $\sqrt{s_{NN}} = 62.4$ GeV from run-10 [302]. The STAR collaboration published a study of v_2 in Au–Au collisions at different energies utilizing the run-10 data samples. Recently, the PHENIX collaboration reported first results of separated yields of single electrons from charm- and beauty-hadron decays from the sample of Au–Au collisions at $\sqrt{s_{NN}} = 200$ GeV collected in run-11 after the installation and commissioning of the vertex detector [303]. During the first run at the LHC (years 2009-2013), HF decay muon R_{AA} and v_2 were measured at forward rapidity by the ALICE collaboration [164, 304]. Preliminary results for HF decay electrons and muons at mid-rapidity were reported by ALICE [305] and ATLAS [306].

A selection of results on the p_T dependence of the nuclear modification factor of HF decay leptons for different colliding systems and collision energies and centralities is collected in Fig. 18. In the top-left panel, the results on HF decay electron R_{AA} at midrapidity in central Au–Au, Cu–Cu and d Au collisions at $\sqrt{s_{NN}} = 200$ GeV are

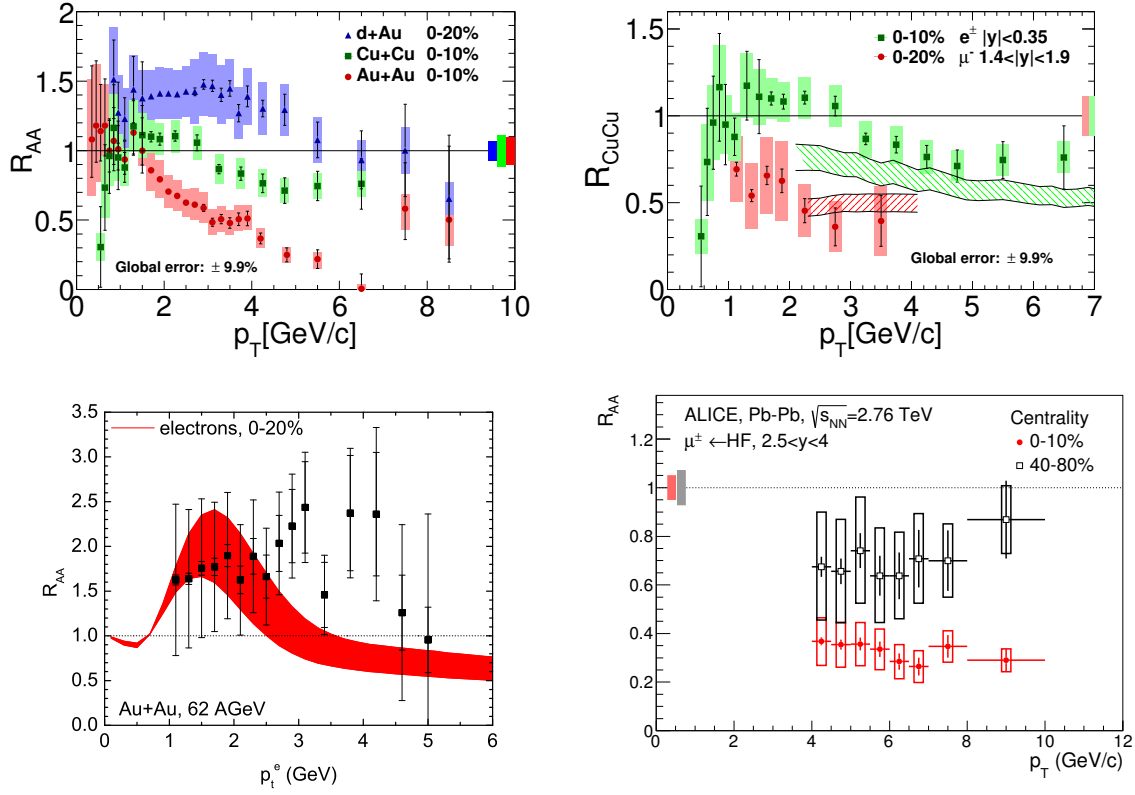


Figure 18. Nuclear modification factor of HF decay leptons as a function of p_T at RHIC and at the LHC. Top left: Heavy-flavor decay electrons at mid-rapidity in central d Au [272], Cu–Cu [307] and Au–Au collisions [147] at $\sqrt{s_{NN}} = 200$ GeV. Top right: Heavy-flavor decay leptons at mid- (electrons) and forward (muons) rapidity in central Cu–Cu collisions at $\sqrt{s_{NN}} = 200$ GeV [163] compared to model calculations [72]. Bottom left: Heavy-flavor decay electrons at mid-rapidity in central Au–Au collisions at $\sqrt{s_{NN}} = 62.4$ GeV [302], compared to the TAMU model calculation [308]. Bottom right: Heavy-flavor decay muons at forward rapidity in central and peripheral Pb–Pb collisions at $\sqrt{s_{NN}} = 2.76$ TeV [164].

compared [307]. A substantial suppression of the yield of electrons with $p_T > 1.5$ GeV/ c is observed in the 10% most central Au–Au collisions [147]. The suppression increases with increasing p_T , reaching a factor of about four at $p_T = 4$ GeV/ c . The results from d Au collisions [272], showing a nuclear modification factor consistent or larger than unity, provide clear evidence that the high- p_T suppression observed in central Au–Au collisions is a final-state effect due to the formation of a hot and dense medium. In the 10% most central Cu–Cu collisions a moderate suppression of the HF decay electron yield is observed for $p_T > 3$ GeV/ c . The magnitude of the suppression is smaller than that observed in central Au–Au collisions, as expected from the smaller size of the system created in the collisions of the lighter Cu nuclei.

In Cu–Cu collisions at $\sqrt{s_{NN}} = 200$ GeV, HF decay muons were measured at forward rapidity ($1.4 < y < 1.9$) [163]. The results are reported in the top-right panel of

Fig. 18 and compared to the mid-rapidity results. Open HF production is found to be significantly more suppressed at forward rapidity than at midrapidity. The magnitude of the suppression observed in Cu–Cu collisions at forward rapidity is comparable to that in central Au–Au collisions at midrapidity. This observation suggests that in-medium energy loss is not the only mechanism responsible for the observed suppression, as the medium size and density are larger in Au–Au than in Cu–Cu collisions. Other nuclear effects, such as gluon shadowing at small Bjorken- x or partonic energy loss in cold nuclear matter, can be relevant for the description of the forward-rapidity results. The gross features of the data are caught by the Vitev *et al.* model calculations [72], shown in the top-right panel of Fig. 18, which includes in-medium energy loss due to gluon radiation and in-medium hadron formation and dissociation, as well as cold-nuclear matter effects such as shadowing and k_T -broadening.

The HF decay electron R_{AA} in the 20% most central Au–Au collisions at $\sqrt{s_{NN}} = 62.4$ GeV is shown in the bottom-left panel of Fig. 18 [302]. Since a sample of pp collisions at RHIC is not available for this CM energy, the pp reference was taken from ISR data. The R_{AA} is found to be consistently larger than unity and no suppression is observed in the measurement p_T range. In contrast to the HF results, the π^0 measurements at this lower collision energy show a suppression that increases with centrality [309]. Measurements at this lower collision energy offer the possibility to study HF production in a situation in which the initial temperature of the medium is reduced as compared to top RHIC energy, while still encompassing the transition region. This could shed light on the question whether the HQ coupling to the medium is primarily driven by an increasing temperature (or energy density), or by an increase in coupling strength in the pseudo-critical region of the chiral/deconfinement transition [308]. The measured HF decay electron nuclear modification factor can be described within uncertainties by the TAMU model [308], shown as a red band in the bottom-left panel of Fig. 18. In this approach, the R_{AA} pattern at $\sqrt{s_{NN}} = 62.4$ GeV emerges from the interplay of initial- and final-state effects, in particular the partial thermalization of heavy quarks in the hot medium (starting from a softer initial-production spectrum than at $\sqrt{s_{NN}} = 200$ GeV) and a Cronin enhancement, which is known to become more pronounced toward lower collision energies.

In the bottom-right panel of Fig. 18, the R_{AA} of HF decay muons at forward rapidity ($2.5 < y < 4$) is shown for central and peripheral Pb–Pb collisions at the LHC energy of $\sqrt{s_{NN}} = 2.76$ TeV. A strong suppression, by a factor of 3-4, is observed in the 10% most central collisions in the measurement p_T range ($4 < p_T < 10$ GeV/ c), without a significant p_T dependence within uncertainties. A smaller suppression is observed for peripheral (40–80%) collisions. The higher collision energy allowed a precise determination of the nuclear modification factor in the momentum interval $p_T > 6$ GeV/ c , which was accessible with limited statistical precision at RHIC energies. In this high- p_T interval, according to the central value of FONLL pQCD calculations, the dominant contribution to the HF muon yield is due to beauty-hadron decays.

The system size dependence of the nuclear modification factor can be investigated

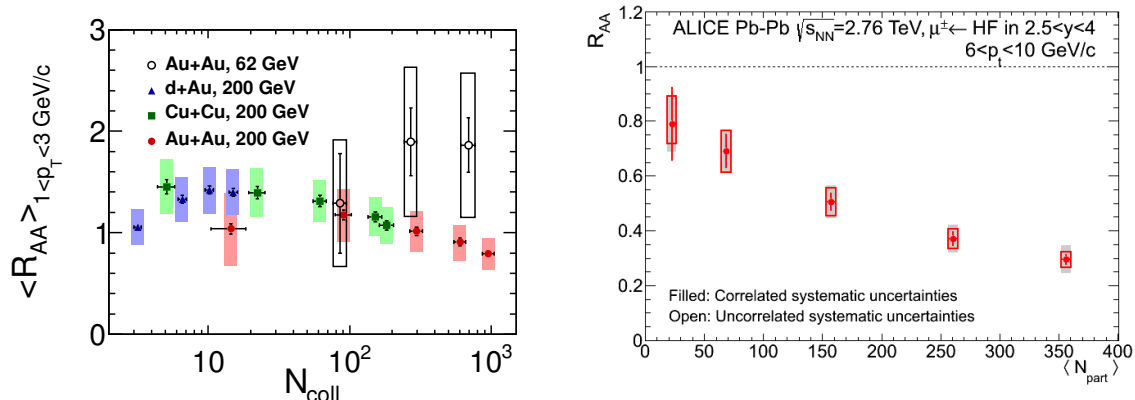


Figure 19. System size dependence of HF decay lepton R_{AA} . Left: Heavy-flavor decay electrons in $1 < p_T < 3 \text{ GeV}/c$ in $d\text{Au}$, Cu-Cu and Au-Au collisions at RHIC energies as a function of the average number of nucleon–nucleon collisions [302,307]. Right: Heavy-flavor decay muons in $6 < p_T < 10 \text{ GeV}/c$ in Pb-Pb collisions at the LHC as a function of the average number of participant nucleons [164].

by comparing results at different centralities and in different colliding systems. It was observed in Ref. [307] that when results from $d\text{Au}$, Cu-Cu and Au-Au collisions are compared in centrality intervals of comparable system size (*i.e.*, similar average number of participant nucleons or binary collisions), similar trends and magnitudes are found for the R_{AA} as a function of p_T . This is illustrated in the left panel of Fig. 19, where the HF decay electron R_{AA} in the range $1 < p_T < 3 \text{ GeV}/c$ from $d\text{Au}$, Cu-Cu and Au-Au collisions is compiled as a function of $\langle N_{\text{coll}} \rangle$. The data at $\sqrt{s_{NN}} = 200 \text{ GeV}$ indicate a common trend among the three different systems, showing an enhancement which increases with increasing system size at low $\langle N_{\text{coll}} \rangle$, followed by suppression for larger system sizes. This common trend suggests that the enhancement and suppression effects are dependent on the size of the colliding system and the produced medium and are the result of the interplay between CNM (nPDF, Cronin enhancement) and hot-medium (energy-loss, radial flow) effects. The results at $\sqrt{s_{NN}} = 62.4 \text{ GeV}$, also shown in the left panel of Fig. 19, suggest that at this lower collision energy the competition among different effects (Cronin enhancement, flow and energy loss) favors HF enhancement over suppression, consistently with previous observations of an increased Cronin enhancement with decreasing collision energy [310]. Studies of the system size dependence in Pb-Pb collisions at the LHC are shown in the right panel of Fig. 19, which reports the R_{AA} of HF decay muons for $2.5 < y < 4$ and $6 < p_T < 10 \text{ GeV}/c$, where, according to FONLL calculations, the beauty contribution is expected to be dominant. A trend of increasing suppression with increasing centrality is observed, qualitatively similar to that found in Au-Au collisions at RHIC, suggesting that HQ in-medium energy loss dominates over other cold and hot medium effects.

The nuclear modification factor of electrons from HF hadron decays cannot be compared directly to that of light hadrons at the same p_T , because of the kinematics of

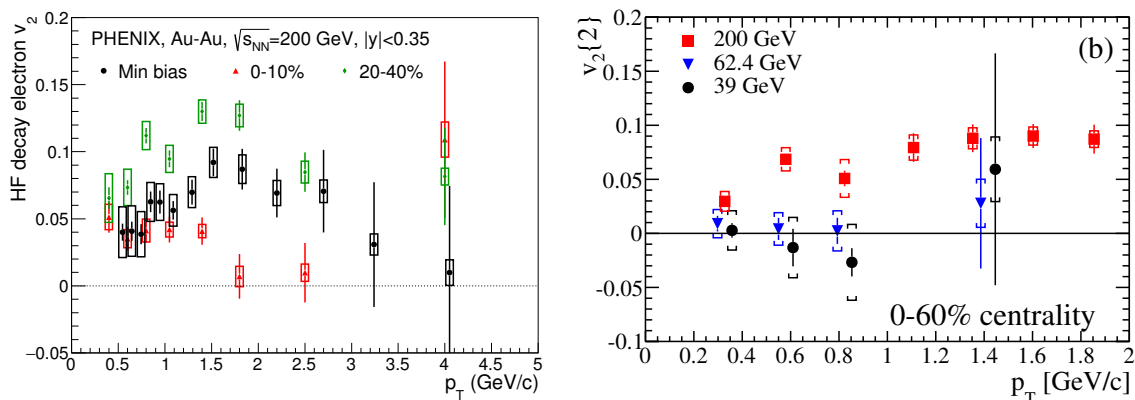


Figure 20. Heavy-flavor decay electron v_2 in Au–Au collisions as function of p_T . Left: PHENIX results for different centrality intervals at $\sqrt{s_{NN}} = 200$ GeV [147]. Right: STAR results at three different collision energies [311].

the semi-leptonic decay. According to PYTHIA simulations [123], HF decay electrons with $p_T > 3$ GeV/ c originate to a large extent from the decay of D mesons with $p_T > 4$ GeV/ c , with the beauty contribution expected to be small at low p_T according to FONLL calculations. For this reason, in the left panel of Fig. 17, the R_{AA} of HF decay electrons with $p_T > 3$ GeV/ c is compared to that of π^0 for $p_T > 4$ GeV/ c . In this intermediate p_T range, the data suggest a smaller suppression of HF hadrons as compared to light-flavor mesons. In addition, in order to draw conclusions on the parton energy loss starting from the measurements of charm and light-flavor hadron R_{AA} , one should also consider the effects of the different momentum distributions of the initially produced charm quarks as compared to light quarks and gluons, their different fragmentation functions into hadrons, as well as the different initial-state effects on light and heavy quarks (*e.g.*, the different Cronin enhancement of hadrons with different mass [272,310]). This will be discussed in more detail in the next sub-section where the D -meson measurements are presented and discussed.

Further insight into the interaction of heavy quarks with the medium is provided by the measurements of elliptic flow and their comparison to model calculations. The results of the measurements of HF decay electron v_2 at mid-rapidity as a function of p_T in Au–Au collisions at RHIC are shown in Fig. 20. The left panel reports the results of the PHENIX collaboration for collisions at $\sqrt{s_{NN}} = 200$ GeV in different centrality intervals [147]. The largest v_2 is observed in semi-peripheral collisions (20–40% shown in the plot and 40–60% not shown in the plot), for which the initial geometrical anisotropy is largest. The elliptic flow is found to be larger than zero in the interval $0.5 < p_T < 2.5$ GeV/ c , with a maximum value of about 0.1 at $p_T \approx 1.5$ GeV/ c . Note that a non-zero v_2 of HF decay electrons does not necessarily imply a non-zero v_2 of charm (beauty) quarks usually associated with heavy quarks taking part in the collective expansion of the medium. A significant contribution to HF electrons at low and intermediate p_T may arise from the decays of charm (and beauty) hadrons produced

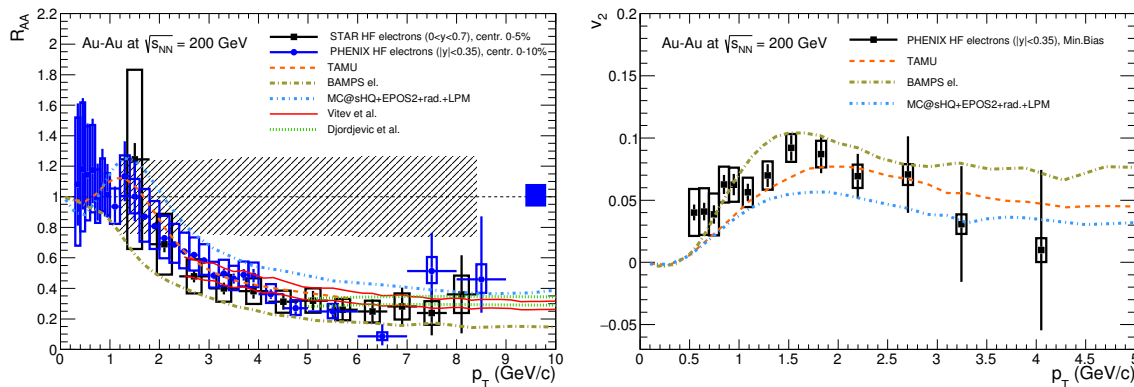


Figure 21. Heavy-flavor decay electron R_{AA} in central and v_2 in minimum-bias Au–Au collisions at RHIC from PHENIX [147] and STAR [147, 159] compared to model predictions: MC@sHQ+EPOS [46, 74], TAMU [65, 76], BAMPS [28, 38, 75], Vitev et al [72] and Djordjevic et al. [298] (taken from [11]).

via the recombination of a heavy quark with a light quark from the medium. Due to the light-quark collective flow, HF hadrons produced with this recombination mechanism can acquire a non-zero v_2 also in the case in which charm quarks have vanishing elliptic flow [118]§. In the right panel of Fig. 20 the STAR measurements of HF decay electron v_2 at three different collision energies are compared for the 0–60% centrality class [311]. The results at $\sqrt{s_{NN}} = 200$ GeV are compatible with the measurement by the PHENIX collaboration in the same centrality class (see Ref. [311] for the comparison). At lower collision energies, $\sqrt{s_{NN}} = 39$ and 62.4 GeV, the v_2 values are smaller and consistent with zero within uncertainties. Also the PHENIX collaboration reported a measurement of HF decay electron v_2 at $\sqrt{s_{NN}} = 62.4$ GeV in the interval $1 < p_T < 4$ GeV/c. The central values are non-zero but lower than at 200 GeV, and consistent with the STAR results at lower p_T . However, the large uncertainties prevent from drawing firm conclusions on the dependence of v_2 on the collision energy.

A number of theoretical model calculations are available for the elliptic flow coefficient and the nuclear modification factor of HF decay electrons at RHIC energies. In Fig. 21, taken from [11], a comprehensive comparison of the outcome of model calculations to the measurements is shown. Overall, the HF decay electron R_{AA} in central Au–Au collisions measured by the PHENIX [147] and STAR [159] collaborations and the v_2 measured by PHENIX [147] in minimum-bias (MB) collisions are fairly well described by available model calculations. In some of the models the quark-medium coupling (represented by the medium density/temperature and interaction cross section) is tuned to describe the R_{AA} of pions (Djordjevic et al., WHDG, Vitev et al.) or electrons (BAMPS) at RHIC energies.

The ALICE Collaboration recently published results on the elliptic flow of HF decay

§ Recall, however, that a sharp separation between diffusion and coalescence effects is somewhat academic since hadronization should smoothly emerge from the interactions that a heavy quark undergoes when approaching T_{pc} from above (cf. the discussion in Sec. 2.2.6).

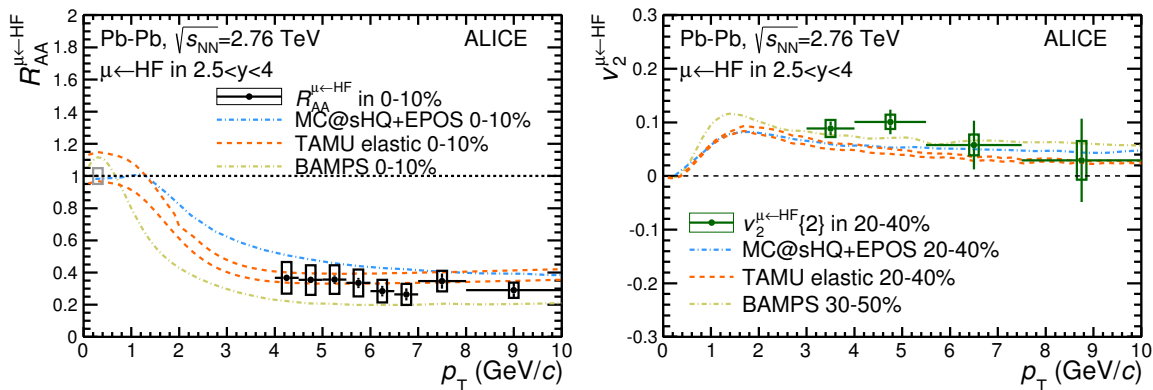


Figure 22. Heavy-flavor decay muon R_{AA} in central and v_2 in semi-central Pb–Pb collisions at the LHC [304] as a function of p_T compared to transport model predictions: MC@sHQ+EPOS [74], TAMU [65] and BAMPS [28, 38, 75].

muons at forward rapidity in the interval $3 < p_T < 10$ GeV/ c for three different centrality classes of Pb–Pb collisions at the LHC [304]. The p_T dependence of v_2 in the 20–40% class is shown in the right panel of Fig. 22. A positive v_2 is observed with a significance larger than 3σ . The data are compared to the predictions of the MC@sHQ+EPOS [74], TAMU [65] and BAMPS [38, 75] models. All the three models predict a substantial suppression of the high- p_T yield (left panel of Fig. 22) and a positive v_2 (right panel of Fig. 22), approximately consistent with what is observed in the data. However, the BAMPS and MC@sHQ+EPOS models, which give a good description of the measured v_2 , tend to underestimate and overestimate the R_{AA} , respectively, while the TAMU model describes the R_{AA} , but slightly underestimates the elliptic flow. This indicates that it is challenging to simultaneously describe the strong suppression of HF decay muons at high- p_T in central collisions and their azimuthal anisotropy in semi-central collisions.

A major progress in the HF decay lepton studies can be provided by the separation of the contributions of charm and beauty hadron decays. The PHENIX collaboration recently published the measurements performed on a sample of MB Au–Au collisions at $\sqrt{s_{NN}} = 200$ GeV/ c recorded in 2011 with their new vertex detectors (VTX) [303]. The enhanced vertexing capabilities allow the separation of beauty and charm decay electrons based on the shape of the measured distributions of the distance of closest approach (DCA) of the tracks to the interaction vertex. An unfolding procedure was utilized to infer the parent charm- and beauty-hadron yields as a function of p_T starting from the measured electron yield as a function of p_T and DCA. The extracted fraction of beauty-decay electrons in the HF electron yield ($\frac{b \rightarrow e}{c \rightarrow e + b \rightarrow e}$) as a function of p_T is shown as a red band in Fig. 23 and compared to the expectation from theoretical calculations. In particular, predictions from FONLL pQCD calculations (corresponding to no medium effects) and from three transport models, namely POWLANG [122], Duke (also denoted as Cao, Qin, Bass or Cao *et al.*) for two different values of the $D_s(2\pi T)$ parameter

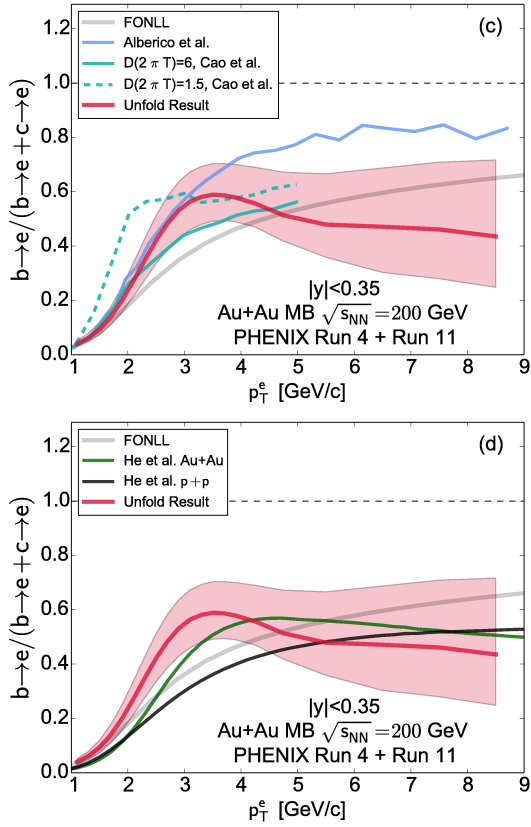


Figure 23. Fraction of electrons from beauty-hadron decays in MB Au–Au collisions as a function of p_T from the DCA-based unfolding analysis by the PHENIX collaboration [303] compared to model calculations.

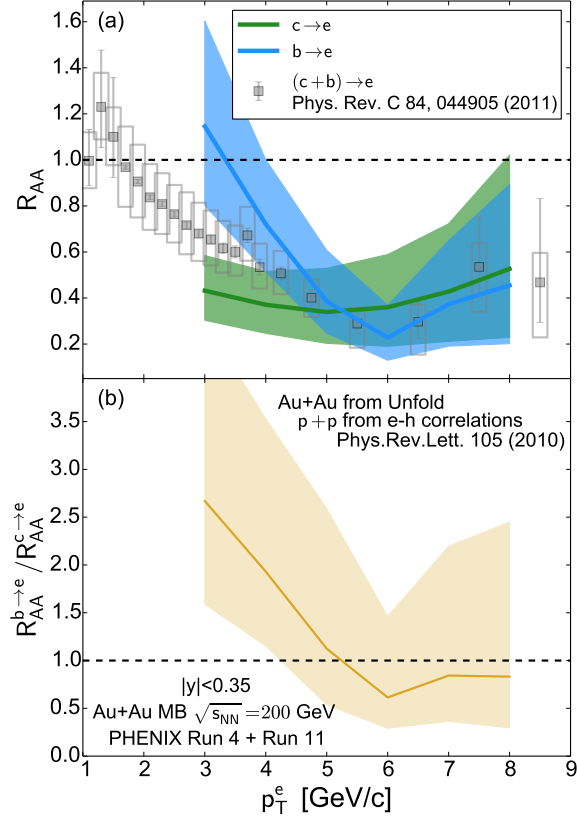


Figure 24. Nuclear modification factor of electrons from charm and beauty hadron decays in MB Au–Au collisions from the DCA-based unfolding analysis by the PHENIX collaboration [303]

governing the HQ-medium coupling [312], and TAMU [65] are displayed. Comparisons to other model calculations, not shown in Fig. 23, can be found in Ref. [303]. The models are in reasonable agreement with the extracted bottom electron fraction within the relatively large uncertainties. From these results on the beauty-fraction in Au–Au collisions, the nuclear modification factors of electrons from charm and beauty hadron decays were disentangled using (i) the additional information on the beauty-electron fraction in pp collisions extracted from the the angular correlation analysis performed by the STAR collaboration [167] and (ii) the measured R_{AA} of HF decay electrons in Au–Au collisions. The resulting R_{AA} 's are reported in Fig. 24 together with the ratio $R_{AA}^{b \rightarrow e} / R_{AA}^{c \rightarrow e}$. The electrons from beauty-hadron decays are found to be less suppressed than those from charm-hadron decays at a 1σ level in the range $3 < p_T < 4$ GeV/ c .

Preliminary results on beauty-decay electron R_{AA} in central Pb–Pb collisions at the LHC, also exploiting the different DCA shapes of charm and beauty decay electrons,

were reported by the ALICE Collaboration [313]. A suppression of the yield relative to the binary-scaled pp cross section ($R_{AA} < 1$), albeit with sizeable uncertainties, is observed for $p_T > 3$ GeV/ c , consistent with in-medium energy loss of beauty quarks.

3.3.2. Charm hadrons

The production of D mesons was measured p_T differentially in Au–Au collisions at RHIC by the STAR collaboration [294] and in Pb–Pb collisions at the LHC with ALICE [314–319]. Preliminary results on D^0 -meson nuclear modification factor in Pb–Pb collisions at the LHC were recently reported by CMS [178] and they are consistent with the ALICE results. All these measurements were carried out at midrapidity ($|y| < 1$ in the case of STAR and CMS and $|\eta| < 0.8$ for ALICE). The STAR collaboration measured the D^0 -meson yield in the transverse-momentum range $0 < p_T < 8$ GeV/ c using a data sample of $\sim 8.2 \cdot 10^8$ MB-triggered events and $\sim 2.4 \cdot 10^8$ events in the 0–10% centrality interval recorded during run-10 and run-11 [294]. Preliminary results were reported on D^0 production in U–U collisions at $\sqrt{s_{NN}} = 193$ GeV [320]. Recently, STAR reported preliminary results on D_s^+ -meson R_{AA} and v_2 in Au–Au collisions at top RHIC energy [344], which, although limited by statistics, show similar features as the ALICE measurements at the LHC [319]. ALICE obtained the first results on D^0 -, D^+ - and D^{*+} -meson nuclear modification factors in Pb–Pb collisions at $\sqrt{s_{NN}} = 2.76$ TeV by analyzing a sample of 13×10^6 collisions in the centrality range of 0–80% collected in 2010 [314]. This sample allowed the measurement of the D -meson R_{AA} in the momentum interval $2 < p_T < 16$ GeV/ c in the 0–20% and 40–80% centrality classes. Using the larger data sample of $16.4 \cdot 10^6$ central (0–10%) and $9.0 \cdot 10^6$ semi-peripheral (30–50%) Pb–Pb collisions recorded in year 2011, the R_{AA} of D^0 , D^+ , and D^{*+} mesons could be measured with improved precision in a wider transverse-momentum interval ($1 < p_T < 36$ GeV/ c for the 10% most central collisions) [317,318]. In addition, the D -meson elliptic flow [315,316] and the D_s^+ -meson nuclear modification factor [319] were measured for the first time. Due to the small size of the data sample of pp collisions collected at $\sqrt{s} = 2.76$ TeV, the pp reference for the R_{AA} at the LHC was obtained via a \sqrt{s} -scaling of the measurements at $\sqrt{s} = 7$ TeV. The scaling factor and its uncertainty were obtained from FONLL calculations of the D -meson p_T differential cross section at $\sqrt{s} = 2.76$ and 7 TeV [283].

A selection of results on the D -meson nuclear modification factor and elliptic flow is shown in Fig. 25. In the top-left panel, the transverse-momentum dependence of the R_{AA} of D^0 mesons in the 10% most central Au–Au collisions at $\sqrt{s_{NN}} = 200$ GeV from the STAR experiment [294] is compared to the outcome of various model calculations [28, 72, 73, 76, 82, 122]. The data show a structure in transverse-momentum which is characterized by an increase of R_{AA} with increasing p_T for $p_T < 1.5$ GeV/ c , a maximum at p_T around 1.5 GeV/ c , where a value $R_{AA} > 1$ is measured, followed by a decrease. For $p_T > 3$ GeV/ c , a clear suppression relative to the binary-scaled pp cross section is observed. A similar trend is observed in the preliminary results from U–U collisions [320]. The R_{AA} measured by the STAR collaboration in the interval

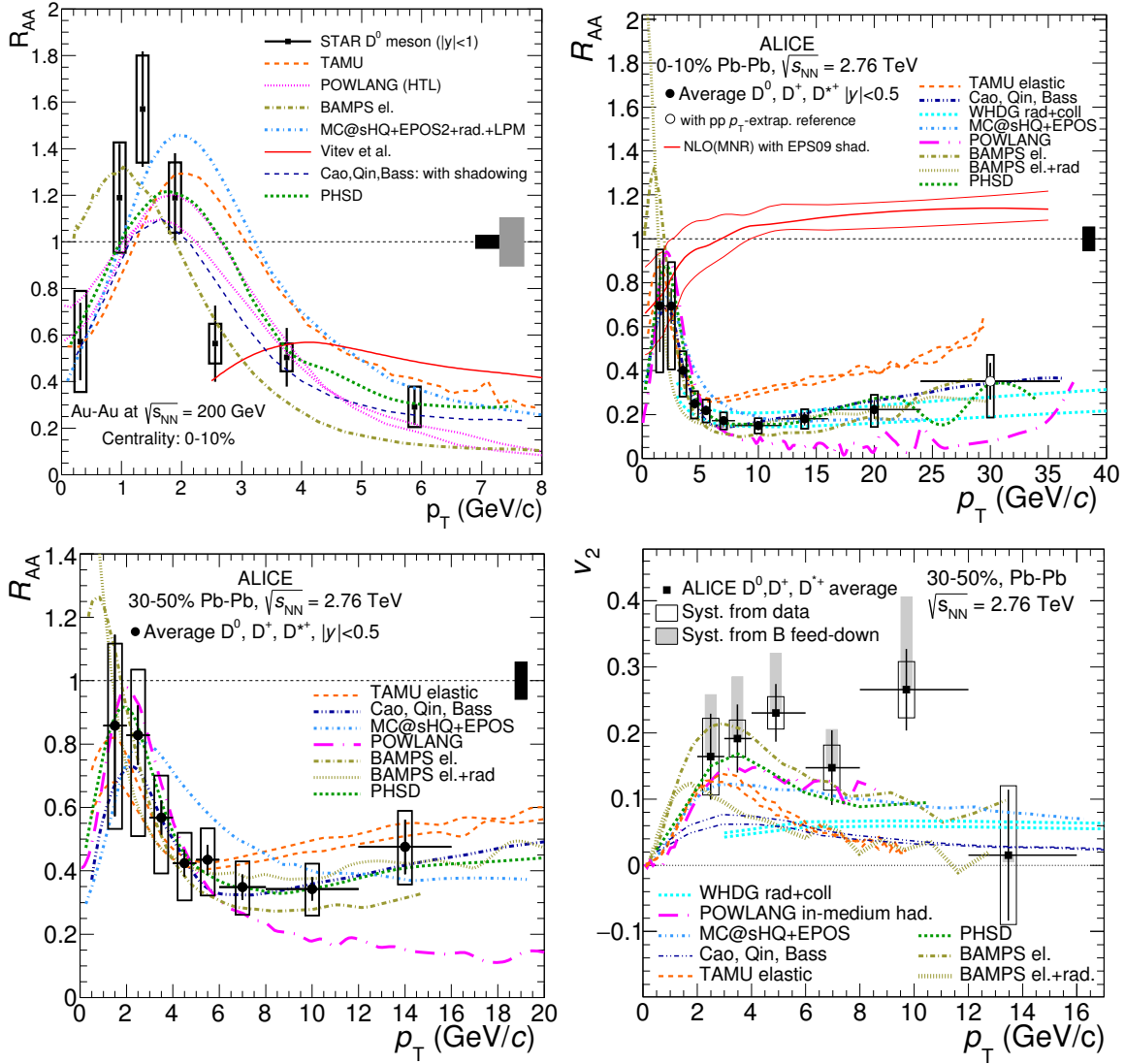


Figure 25. D -meson nuclear modification factor and elliptic flow as a function of p_T compared to model calculations [28, 40, 51, 65, 72–74, 76, 82, 122, 220, 296, 321] Top left: D^0 -meson R_{AA} in central Au–Au collisions at $\sqrt{s_{NN}} = 200$ GeV [294] (taken from Ref. [11]). Top Right: D -meson (average of D^0 , D^+ and D^{*+}) R_{AA} in the 10% most central Pb–Pb collisions at $\sqrt{s_{NN}} = 2.76$ TeV [318] (taken from Ref. [322]). Bottom left: D -meson R_{AA} in semi-central (30–50%) Pb–Pb collisions at $\sqrt{s_{NN}} = 2.76$ TeV [318]. Bottom right: D -meson v_2 in semi-central (30–50%) Pb–Pb collisions at $\sqrt{s_{NN}} = 2.76$ TeV [315, 316] (taken from Ref. [322]).

$0 < p_T < 3$ GeV/ c is described qualitatively, and to some extent also quantitatively, by the models that include interactions in an expanding fluid-dynamical medium, causing energy loss and radial flow (TAMU [76], BAMPS [28], Cao *et al.* [82], MC@sHQ [73], POWLANG [122], and PHSD [40]). In these models, the R_{AA} shape at low p_T is the effect of the collective flow on the light and charm quarks and of the contribution of the recombination mechanism to charm-quark hadronization. In some of these models, *e.g.*, TAMU [76], POWLANG [122] and Duke [83], the effect of hadronization via recombination, which converts low- and intermediate- p_T charm quarks into D mesons, is rather crucial to describe the data at low and intermediate p_T . In the TAMU [124] and PHSD models [40] the contribution to the v_2 due to D -meson rescattering in the hadronic phase is found to be significant (also for the R_{AA} in the PHSD model). The model by Vitev *et al.* [72], which includes CNM and hot QGP (in-medium energy loss and meson dissociation) effects, is consistent with the data in the region of its applicability, $p_T > 3$ GeV/ c (since the medium's transverse collective expansion is neglected).

The prompt D -meson R_{AA} (average of D^0 , D^+ , and D^{*+} nuclear modification factors) measured with ALICE [318] in central (0–10%) Pb–Pb collisions at $\sqrt{s_{NN}} = 2.76$ TeV is shown in the top-right panel of Fig. 25 together with a selection of model predictions [28, 65, 74, 82, 122, 220, 296, 321]. In particular, only models for which simultaneous predictions for v_2 are available were included in this plot (other predictions compared to data are deferred to the left panel of Fig. 28). The prompt D -meson yield at high p_T is found to be strongly suppressed with respect to the binary-scaled pp reference. In the interval $3 < p_T < 10$ GeV/ c , the suppression increases (R_{AA} decreases) with increasing p_T . The maximal suppression is observed around $p_T = 10$ GeV/ c , where the yields are reduced by a factor of 5–6 relative to the binary-scaling expectation value. For $p_T > 10$ GeV/ c , the R_{AA} appears to increase (decreasing suppression) with increasing p_T , even though the large uncertainties prevent a conclusion on the trend of the nuclear modification factor at high p_T . A significant suppression, $R_{AA} < 0.5$, is observed for D mesons with $p_T > 25$ GeV/ c . Since no significant modification of the D -meson production is observed in p Pb collisions for $p_T > 2$ GeV/ c , the strong suppression of the D -meson yields observed for $p_T > 3$ GeV/ c cannot be explained in terms of CNM effects and therefore is predominantly due to final-state effects induced by the hot and dense medium created in the collisions. This is also supported by the fact that the data cannot be described by the the outcome of a NLO pQCD calculation [210] including only the initial-state effects related to the nuclear modification of the PDF [252] (“NLO with EPS09” curve in Fig. 25), which instead was able to reproduce the measured D -meson nuclear modification factor in p Pb collisions (see Fig. 13). On the other hand, all the models including interactions of charm quarks with an hot and dense partonic medium provide in general a reasonable description of the observed R_{AA} .

To illustrate the evolution of the nuclear modification factor with \sqrt{s} , the D -meson R_{AA} measured in the 10% most central Au–Au and Pb–Pb collisions at $\sqrt{s_{NN}} = 200$ and 2.76 TeV are compared in the left panel of Fig. 26. At high p_T ($p_T > 3$ GeV/ c), where the nuclear modification factor is expected to be dominated by the effect of in-medium

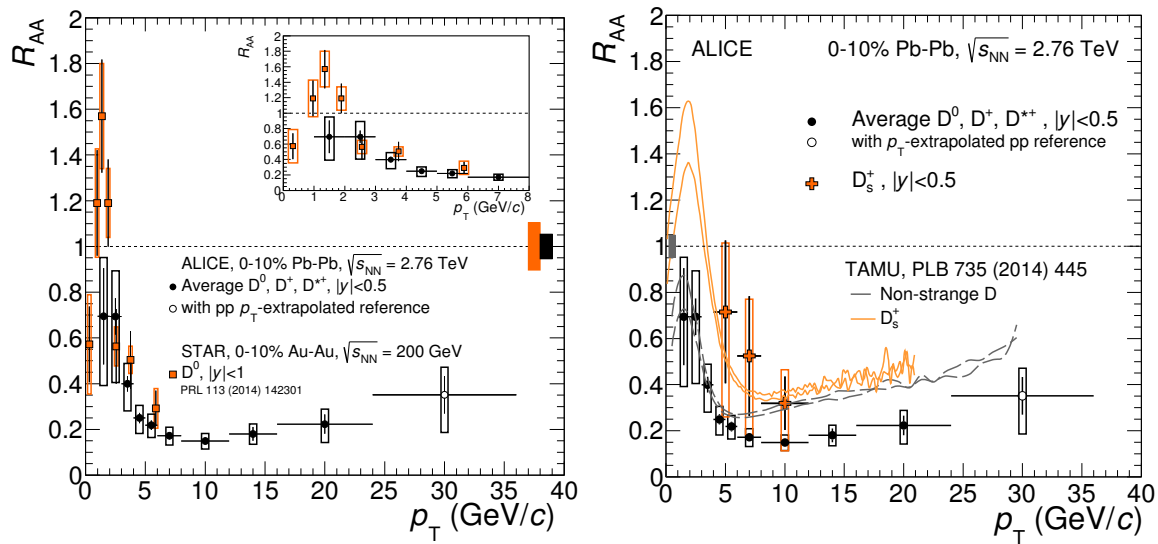


Figure 26. Left: comparison between the R_{AA} of D^0 mesons in central (0–10%) Au–Au collisions at $\sqrt{s_{NN}} = 200$ GeV [294] and of D mesons (average of D^0 , D^+ and D^{*+}) in central Pb–Pb collisions at $\sqrt{s_{NN}} = 2.76$ TeV [318]. Right: D_s^+ [319] and average D -meson [318] R_{AA} in central Pb–Pb collisions at $\sqrt{s_{NN}} = 2.76$ TeV compared to predictions from the TAMU model [65].

parton energy loss, the R_{AA} values measured at the two energies are compatible within uncertainties. However, as pointed out in [318], this does not necessarily imply a similar charm-quark energy loss and medium density at the two collision energies, since the nuclear modification factor is also sensitive to the slope of the p_T spectra of the hard-scattered partons. Therefore, the combined effect of a denser medium and harder initial p_T spectra at the LHC could result in similar values of R_{AA} as at RHIC energies (see, *e.g.*, Ref. [323]). At lower p_T , the R_{AA} measured at $\sqrt{s_{NN}} = 2.76$ TeV is lower than the one at $\sqrt{s_{NN}} = 200$ GeV and does not show a ‘bump-like’ trend with a rise, a maximum and a successive decrease with increasing p_T . However, due to the large uncertainties and the coarser binning at low p_T , no firm conclusion can be drawn. In this comparison, it has to be considered that the R_{AA} at low and intermediate p_T is the result of the interplay of different effects occurring in the initial and final state. Therefore, a different R_{AA} trend at different CM energies could arise from a different role of initial-state effects and radial flow. As far as initial-state effects are concerned, with increasing $\sqrt{s_{NN}}$ one expects a stronger reduction of the HQ production yields at low p_T due to nuclear shadowing (due to the smaller values of Bjorken- x being probed [252]) and a less pronounced Cronin peak at intermediate p_T [257, 324]. On the other hand, the radial flow of the medium at LHC energies is about 10–20% larger than at RHIC [4, 5]. However, this does not necessarily imply that the bump-like structure observed in the R_{AA} trend at low p_T at RHIC energy should become more pronounced with increasing collision energy. The stronger radial flow effect could be counter-balanced in the R_{AA} by the different shape of the reference spectra in pp collisions at different \sqrt{s} . In this respect, is interesting to notice in the

top-left and top-right panels of Fig. 25 that a reasonable description of the low and intermediate p_T data at both the collision energies is obtained with the models that include nuclear modification of the PDF, charm-quark interactions with the medium constituents, hydrodynamical medium expansion and hadronization via recombination, such as TAMU [65,76], POWLANG [122], Duke [82] and MC@sHQ+EPOS [73,74]. The BAMPS model [28], which does not include nuclear modification of the PDFs, predicts for LHC energies at low p_T (where shadowing is relevant) a value of R_{AA} larger than that observed in the data.

In the bottom panels of Fig. 25 the R_{AA} (left) and v_2 (right) of prompt D mesons (average of D^0 , D^+ , and D^{*+}) in semi-central (30–50%) Pb–Pb collisions at $\sqrt{s_{NN}} = 2.76$ TeV are shown and compared to model predictions. The nuclear modification factor indicates that the D -meson yield is suppressed in the 30–50% centrality class in the measured p_T range with respect to the binary-scaled pp reference [318]. This reduction of the yield in Pb–Pb collisions is smaller, by a factor of about two, than in the 10% most central collisions, as expected due to the decreasing medium density, size and lifetime from central to peripheral collisions. A positive elliptic flow is measured for prompt D mesons in the centrality class 30–50% [315]. In particular, in the interval $2 < p_T < 6$ GeV/ c the measured v_2 is found to be larger than zero with 5.7σ significance. A positive v_2 of D^0 mesons was also observed in the 10–30% centrality class [316]. These results indicate that the interactions with the medium constituents transfer information on the azimuthal anisotropy of the system to the charmed particles [315]. It also suggests that low-momentum charm quarks take part in the collective expansion of the medium, even though, with the current uncertainties, the possibility that the observed D -meson v_2 is completely due to the light-quark contribution in a scenario with hadronization via recombination cannot be ruled out. A positive v_2 is also observed for $p_T > 6$ GeV/ c , which is likely to originate from the path-length dependence of the partonic energy loss, although the large uncertainties do not allow for a firm conclusion.

As already pointed out in the discussion of the HF decay lepton results, the simultaneous comparison of the measured R_{AA} and v_2 to theoretical model calculations constrains the description of the interactions of heavy quarks with the medium, possibly providing sensitivity to the relative contributions of elastic (collisional) and inelastic (radiative) processes, and to the path length dependence of in-medium parton energy loss. Overall, the observed elliptic flow is qualitatively described by the models that include both charm-quark energy loss in a spatially anisotropic medium and momentum gain processes transferring elliptic flow produced through the system expansion to charmed particles. The WHDG model does not include a hydrodynamical description of the medium expansion, so that the anisotropy results only from path length dependent energy loss (the models of Djordjevic *et al.* and Vitev *et al.* do not provide a calculation for v_2 ; their R_{AA} is compared to the data in Fig. 28 below). The models that include only collisional energy loss (TAMU, POWLANG, BAMPS-elastic and PHSD) provide in general a good description of the v_2 , but tend to overestimate (TAMU) or underestimate (POWLANG, BAMPS-elastic) the R_{AA} in central and/or semi-peripheral collisions.

On the other hand, models including both radiative and collisional energy loss (Cao *et al.*, BAMPS rad+el and WHDG) describe the R_{AA} in central collisions well, but tend to underestimate the elliptic flow at low p_T . This may be a consequence of the fact that the inclusion of radiative processes reduces the weight of elastic interactions, which are more effective in building up the azimuthal momentum anisotropy. The MC@sHQ+EPOS model, which also includes both collisional and radiative processes, can describe the measured R_{AA} and v_2 within uncertainties at low ($p_T < 2$ GeV/ c) and high ($p_T > 6-8$ GeV/ c) transverse momenta at different collision energies and centrality, but it tends to overestimate R_{AA} and underestimate v_2 in the intermediate p_T region. From this discussion, it emerges that the role of the different interaction mechanisms, in particular radiative and collisional energy loss, is not yet completely clarified, even though the data-to-theory comparison suggests that both of these contributions are relevant. Finally, models including hadronization of charm quarks from recombination with light quarks from the medium (TAMU, Cao *et al.*, MC@sHQ+EPOS, POWLANG and PHSD) predict a more pronounced radial flow peak in the low- p_T R_{AA} and a larger v_2 , due to the light-quark contribution, thus providing a better description of the data at low p_T (see, *e.g.*, the discussion in Ref. [122]). In summary, this comprehensive data-to-theory comparison reiterates the challenges for theoretical models to simultaneously describe the measured D -meson R_{AA} and v_2 at different collision energies and centralities. This indicates that the current data from RHIC and LHC have the potential to better constrain the description of the interactions of charm quarks with the medium constituents and their hadronization mechanism.

In the right panel of Fig. 26, the nuclear modification factor of D mesons (average of D^0 , D^+ and D^{*+}) in central (0–10%) Pb–Pb collisions at $\sqrt{s_{NN}} = 2.76$ TeV is compared to that of D_s^+ mesons [319] and to the corresponding predictions from the TAMU model [65,106]. This comparison is meant to address the expected effect of hadronization via quark recombination in the partonic medium on the relative abundances of strange and non-strange D -meson species. An enhancement of the D_s^+ yield relative to that of non-strange D mesons at low and intermediate momenta is expected in nucleus–nucleus collisions as compared to pp interactions, if the dominant process for D -meson formation is in-medium hadronization of charm quarks via recombination with light quarks, due to the large abundance of strange quarks in the QGP [106,186,187,325,326]. In particular, the p_T dependence of this comparison has been suggested as a tool to map out the relative importance of recombination processes [106]. In the three p_T intervals, in which the D_s^+ yield could be measured in Pb–Pb collisions, the central values of its R_{AA} are found to be higher than those of non-strange D mesons, although compatible within uncertainties. Even though part of the systematic uncertainty is correlated between strange and non-strange D mesons [319], the current uncertainties prevent a conclusion on the expected modification of the relative abundance of charm-hadron species due to hadronization via recombination. Among the various models of open-charm production in heavy-ion collisions, TAMU is the only one providing a quantitative prediction for the D_s^+ -meson nuclear modification factor. The measured R_{AA} is described within

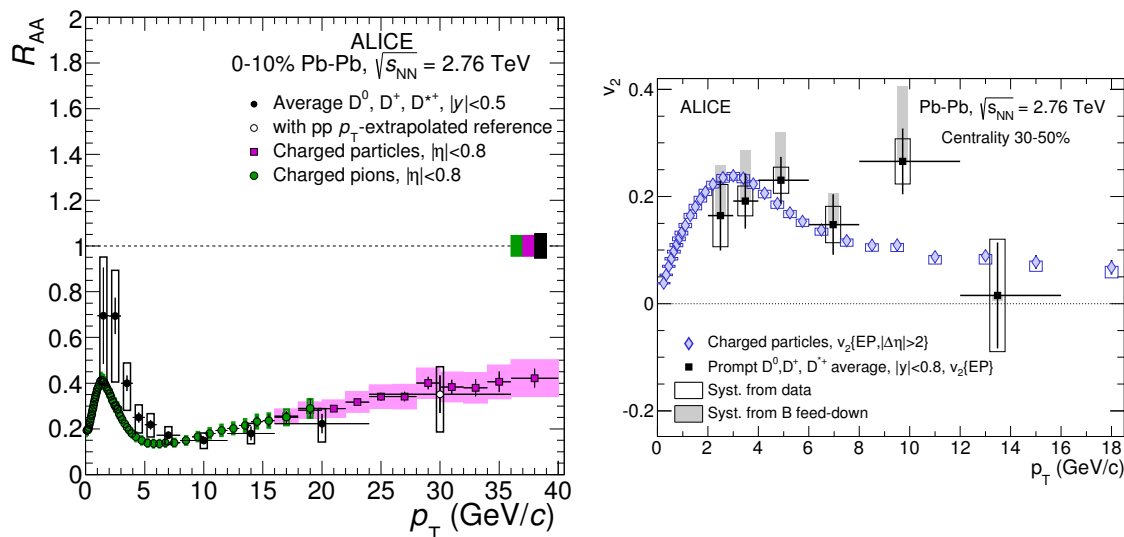


Figure 27. D -meson R_{AA} in central [318] and v_2 in semi-peripheral [315] Pb–Pb collisions at $\sqrt{s_{NN}} = 2.76$ TeV compared to results for charged pions [327] and charged particles [328, 329].

uncertainties by this prediction, where the p_T dependent enhancement of D_s^+ mesons relative to that of non-strange D mesons is a consequence of the recombination of charm quarks with thermally equilibrated strange quarks in the QGP. As discussed in Sec. 2.2.6, an enhanced production of D_s^+ mesons (as well as Λ_c baryons, etc.) in heavy-ion collisions due to recombination entails a reduction of charm quarks available for hadronization into non-strange meson species. This “chemistry effect” should therefore be considered in the interpretation of the comparison of the nuclear modification factors of non-strange D mesons and light-flavor hadrons (*e.g.*, pions), which is discussed in the next paragraphs.

It is interesting to compare both the nuclear modification factor and the elliptic flow of D mesons with those of light-flavor particles, as done in Fig. 27. This could provide some additional insight into the interactions of partons with the medium constituents and on the degree of equilibration of charm quarks in the collectively expanding system. In the right panel of Fig. 27, the elliptic flow coefficients of D mesons [315] and charged particles [329] measured in Pb–Pb collisions at $\sqrt{s_{NN}} = 2.76$ TeV in the 30–50% centrality class are compared. The magnitude and p_T trend of v_2 are observed to be similar (within uncertainties of about 30%) for charmed and light-flavor hadrons, which dominate the charged-particle sample. A similar observation was made for the D^0 -meson and charged-particle v_2 in the 0–10% and 10–30% centrality classes [316]. The current uncertainties do not allow a conclusion on whether the D -meson elliptic flow follows the mass dependence predicted by hydrodynamical calculations, which would suggest a full thermalization of charm quarks with the medium. The comparison of the nuclear modification factor of D mesons and light-flavor particles (pions), mostly originating from gluon fragmentation at LHC energies, was long proposed as a test

for the expected color-charge and quark mass dependence of in-medium parton energy loss [77, 78, 197, 330]. This comparison is shown in the left panel of Fig. 27 for the 10% most central Pb–Pb collisions at $\sqrt{s_{\text{NN}}} = 2.76$ TeV, where the R_{AA} of D mesons, pions (in the interval $1 < p_{\text{T}} < 20$ GeV/ c) [327] and charged particles (in $16 < p_{\text{T}} < 40$ GeV/ c) [328] are collected. At high p_{T} ($p_{\text{T}} > 8 - 10$ GeV/ c) all light-flavor hadron species are found to be equally suppressed in Pb–Pb collisions and the particle ratios are compatible with those in vacuum [327], so that the charged particle R_{AA} can be used in this comparison in place of the pion R_{AA} at high p_{T} . The nuclear modification factors of D mesons and light-flavor hadrons are found to be consistent for $p_{\text{T}} > 6$ GeV/ c . At lower p_{T} ($p_{\text{T}} < 6$ GeV/ c), the R_{AA} of D mesons tends to be slightly higher than that of pions. Since, as pointed out in [318], the systematic uncertainties of D -meson yields are mainly correlated across p_{T} intervals, the current data provide a hint for $R_{\text{AA}}^{\text{D}} > R_{\text{AA}}^{\pi}$ (at about a 1σ level) at intermediate and low p_{T} . An interpretation of this potential difference between the D -meson and pion R_{AA} in terms of different in-medium parton energy loss of charm quarks, light quarks and gluons is, however, not straightforward because in this p_{T} range the R_{AA} is sensitive to other initial- and final-state effects, which could have rather different weights in the light and charm sectors. As pointed out in Ref. [297], similar values of the D -meson and pion R_{AA} could originate from the interplay of the color-charge and quark-mass dependent energy loss with the different p_{T} distributions in the pp reference and different fragmentation functions of charm quarks as compared to light quarks and gluons. In addition, at LHC energies the pion yield at $p_{\text{T}} \sim 3 - 4$ GeV/ c could still have a significant component from soft production (due to the strong radial flow) which does not scale with the number of binary nucleon–nucleon collisions (contrary to the D -meson yield, modulo shadowing). A priori, initial-state effects, radial flow and hadronization via recombination (see the above remark about the hadro-chemistry in the charm sector) can affect the R_{AA} of D mesons and pions quite differently.

Four models provide a calculation for the nuclear modification factors of D mesons and pions (charged particles) namely Djordjevic *et al.* [298], CUJET3.0 [222, 223], WHDG [220, 296, 321] and Vitev *et al.* [72]. In Fig. 28, the outcome of these model calculations is compared to the measured R_{AA} of D mesons (left) and pions/charged particles (right) in central Pb–Pb collisions at the LHC. The models Djordjevic *et al.*, WHDG and CUJET3.0 include both radiative and collisional energy loss. The WHDG calculations tend to overpredict the measured suppression of the pion R_{AA} while describing the D -meson one within experimental and theoretical uncertainties. For the Vitev *et al.* model, two different implementations are considered: the first one (labelled as ‘Vitev rad’) includes only radiative energy loss; the second one (‘rad+dissoc’) considers in addition the effect of in-medium formation and dissociation of HF hadrons. The in-medium formation and dissociation process is not considered as being relevant for pions due to their much longer formation time. These model calculations can describe the measured light-flavor R_{AA} within uncertainties, while for D mesons a better agreement with the data is obtained when the in-medium dissociation mechanism is

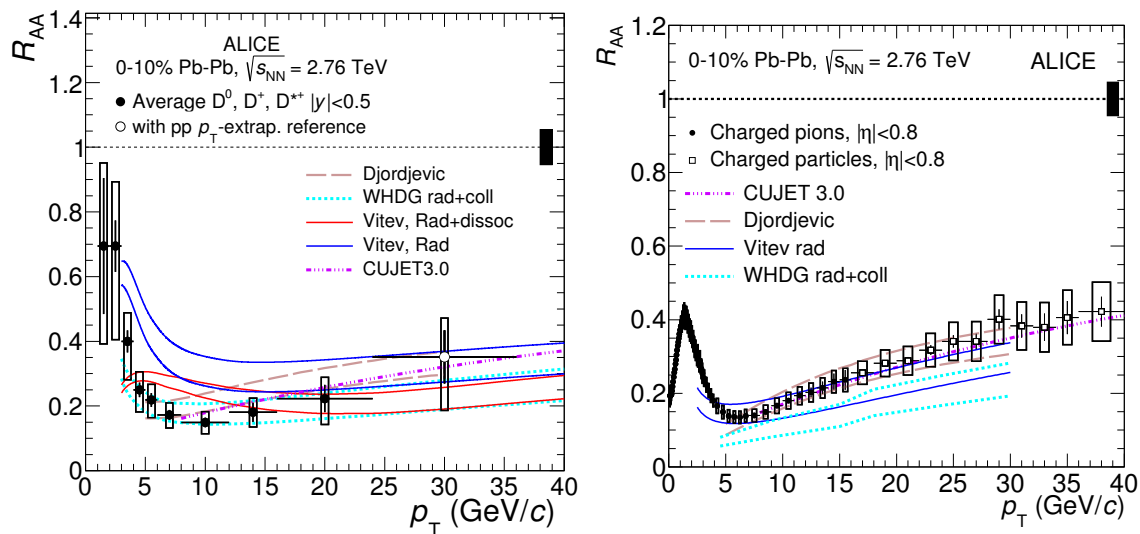


Figure 28. D -meson [318], pion [327] and charged-particle [328] R_{AA} as a function of p_T in the 10% most central Pb–Pb collisions at $\sqrt{s_{NN}} = 2.76$ TeV, compared to predictions from pQCD energy loss models: Djordjevic [298], CUJET 3.0 [222, 223], WHDG with radiative and collisional energy loss [220, 296, 321] and Vitev with radiative and dissociation processes [72].

included in the calculation, indicating the relevance of this effect in the Vitev *et al.* approach. However, within this model an overestimation of the measured D -meson R_{AA} toward lower momenta, $p_T \lesssim 12$ GeV/ c , persists. The Djordjevic *et al.* and CUJET3.0 models can describe both the pion and D -meson R_{AA} results (as well as their ratio, see Ref. [318]) over the full p_T interval of the calculations ($p_T > 5$ and 8 GeV/ c , respectively). In these models, which include collisional and radiative energy loss, the nuclear modification factors of D mesons and light-flavor hadrons turn out to be similar as a consequence of the interplay among (i) the larger energy loss of gluons with respect to that of charm quarks (mainly due to the larger color coupling factor), (ii) the different amount of gluon and light-quark contributions to the observed pion yield in pp and Pb–Pb collisions, and (iii) the harder p_T distribution and fragmentation of charm quarks with respect to those of gluons and light quarks.

3.3.3. Beauty production

Besides the measurements of leptons from beauty-hadron decays described above, beauty production in Pb–Pb collisions at the LHC was studied at mid-rapidity through the measurements of non-prompt J/ψ carried out by the ALICE [169] and CMS [331] collaborations. These measurements cover the low- and intermediate- p_T regions, $1.5 < p_T^{J/\psi} < 30$ GeV/ c , although with large uncertainties at low p_T . At higher momenta, $p_T > 80$ GeV/ c , beauty production could be studied by CMS via the measurement of b -jets [180].

The R_{AA} of non-prompt J/ψ in Pb–Pb collisions at $\sqrt{s_{NN}} = 2.76$ TeV is shown in

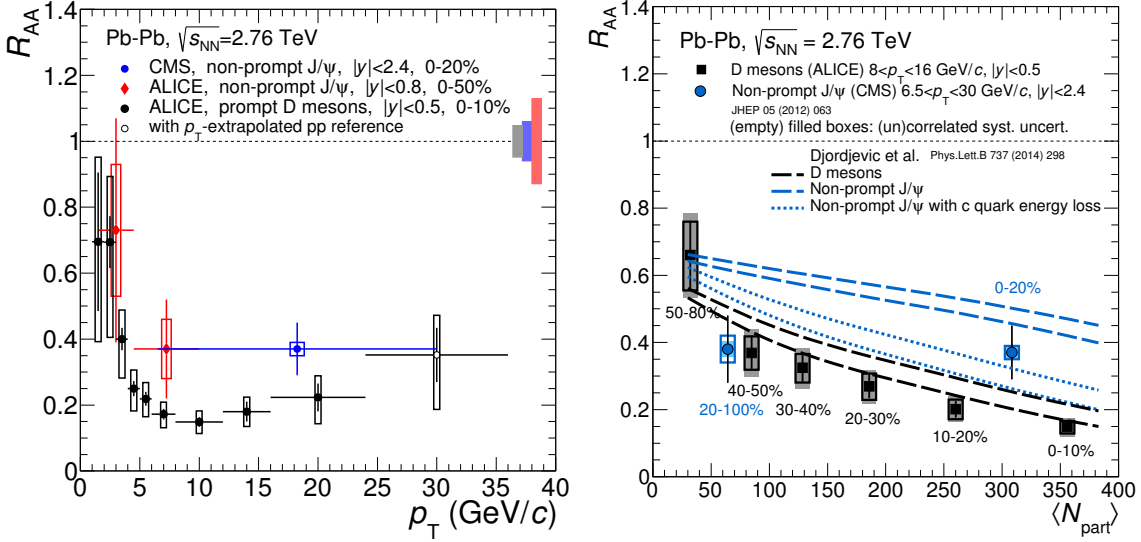


Figure 29. Left: non-prompt J/ψ R_{AA} as a function of p_T at mid-rapidity in Pb–Pb collisions at $\sqrt{s_{NN}} = 2.76$ TeV compared to the prompt D -meson R_{AA} [318]. Results from ALICE [169] at low p_T in the 0–50% centrality class and CMS [331] at high p_T in the 0–20% centrality class are reported. Right: non-prompt J/ψ [331] and prompt D -meson [317] R_{AA} as a function of centrality compared to model predictions including radiative and collisional energy loss [298]. For non-prompt J/ψ additional model calculations are shown in which the beauty-quark interactions are calculated using the charm-quark mass [11].

the left panel of Fig. 29 as a function of p_T . The ALICE results (at low p_T , $1.5 < p_T^{J/\psi} < 10$ GeV/c) are obtained for the centrality class 0–50% [169], while the CMS results at higher p_T ($6.5 < p_T^{J/\psi} < 30$ GeV/c) are for the 20% most central collisions [331]. A clear suppression as compared to the binary-scaled pp reference is observed in central collisions for $p_T^{J/\psi} > 6.5$ GeV/c, with $R_{AA} = 0.37 \pm 0.08(\text{stat}) \pm 0.02(\text{syst})$. A suppression is also observed in the intermediate p_T interval, covering the range $4.5 < p_T^{J/\psi} < 10$ GeV/c, albeit with larger uncertainties. A larger data sample is needed at lower p_T , where the uncertainties on the current result do not allow to draw any conclusion. Nevertheless, the results at intermediate and high p_T indicate that the beauty quarks are substantially affected by interactions with the constituents of the hot and dense medium, which induce a significant modification of their momentum distributions in heavy-ion collisions as compared to those observed in pp interactions. The nuclear modification factor of non-prompt J/ψ is compared to that measured for prompt D mesons (average of D^0 , D^+ and D^{*+}) in central (0–10%) Pb–Pb collisions [318]. This comparison is meant to test the expected quark-mass dependence of in-medium energy loss [77–79]. The suppression of non-prompt J/ψ seems to be weaker than that of D mesons at high and intermediate p_T , although the uncertainties on the measurements reported in Fig. 29 prevent from drawing strong conclusions. In the discussion of this comparison of R_{AA} magnitudes, it is worth noting that the p_T of the J/ψ is shifted to lower momenta with

respect to that of the parent B meson, due to the decay kinematics. The average p_T of the parent B mesons in the highest J/ψ transverse momentum interval measured by CMS is about 11 GeV/ c . For a more direct comparison of D and B nuclear modification, the D -meson R_{AA} was measured by the ALICE Collaboration [317] in the interval $8 < p_T < 16$ GeV/ c , which provides a significant overlap with the p_T distribution of B mesons decaying to J/ψ particles with $6.5 < p_T^{J/\psi} < 30$ GeV/ c (for which 70% of the parent B mesons are estimated to have transverse momenta in the range $8 < p_T < 16$ GeV/ c). In the right panel of Fig. 29, the centrality dependence of the nuclear modification factors of D mesons and non-prompt J/ψ in the chosen p_T intervals are compared. The D -meson R_{AA} values in the centrality classes 0–10% and 10–20% are lower than that of non-prompt J/ψ mesons in the centrality class 0–20%. The significance of this difference is, however, smaller than 3σ considering the statistical and systematic uncertainties [317]. A preliminary measurement of non-prompt J/ψ production performed on the larger data sample of Pb–Pb collisions recorded in 2011 was reported by the CMS Collaboration [332]. The non-prompt J/ψ nuclear modification factor in $|y| < 1.2$ is measured as a function of centrality using finer centrality intervals and the same p_T interval ($6.5 < p_T^{J/\psi} < 30$ GeV/ c) of the published result. Considering this measurement, the R_{AA} of non-prompt J/ψ is larger than that of D mesons in the 0–10% and 10–20% centrality classes with a significance of about 3.5σ [317].

The experimental observation of $R_{AA}^D < R_{AA}^{J/\psi \leftarrow B}$ alone does not allow to conclude on the predicted difference between the in-medium energy loss of charm and beauty quarks. In analogy to the comparison of charm and light-flavor hadron nuclear modifications discussed above, effects other than quark-mass dependent parton energy loss could contribute to differences in the R_{AA} : (i) the different p_T distributions of the initially produced charm and beauty quarks (which are steeper for charm than for beauty), and (ii) the different shapes of the fragmentation functions (which is harder for beauty than for charm quarks) as well as (iii) recombination contributions. Therefore, for a proper interpretation of the experimental results, the measured R_{AA} of D and B mesons (via non-prompt J/ψ) should be compared with the outcome of model calculations including HQ production, in-medium propagation and hadronization. Essentially all available models predict $R_{AA}^D < R_{AA}^B$ in the momentum range $p_T < 20$ GeV/ c , where the quark masses are not negligible with respect to their momenta [38, 48, 65, 72, 79, 81, 82, 220, 296, 299, 321, 333–335]. In the right panel of Fig. 29, the data are compared to the calculations by Djordjevic *et al.* [298], which include both radiative and collisional processes and consider dynamical scattering centers in the medium. Note that, as discussed above, this model can describe the similarity of the D -meson and pion R_{AA} . The model describes well the centrality dependence of the D -meson nuclear modification factor in the high- p_T range considered in Fig. 29 and predicts a smaller suppression of non-prompt J/ψ mesons as compared to D mesons, in qualitative agreement with the CMS result for the most central collisions. Care has to be taken in the data-to-model comparison for the 20–100% class, as the centrality interval is very broad. The preliminary CMS results in finer centrality intervals from

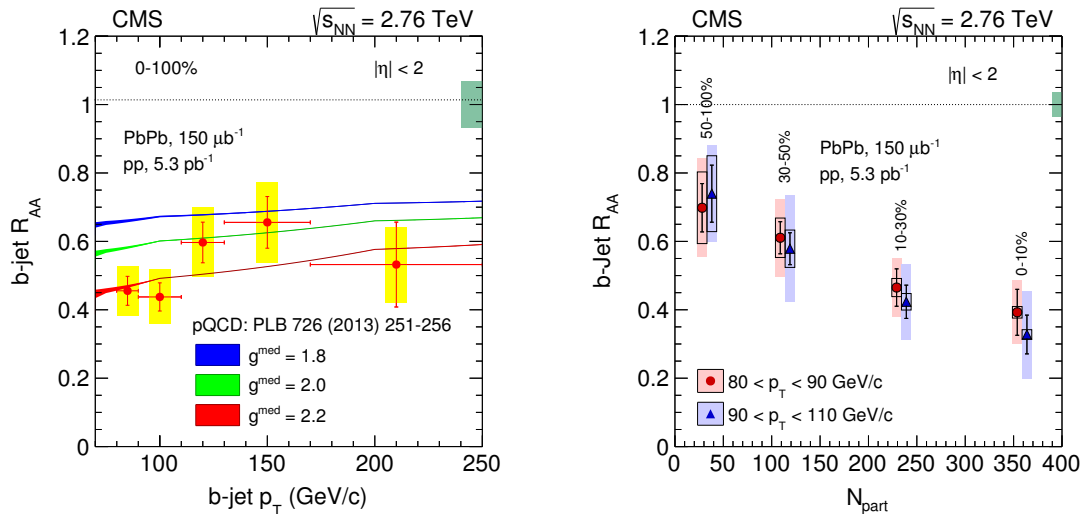


Figure 30. Nuclear modification factor of b -jets in Pb–Pb collisions at $\sqrt{s_{NN}} = 2.76$ TeV [180]. Left: centrality-integrated R_{AA} as a function of jet p_T compared to pQCD energy-loss calculations [287]. Right: R_{AA} as a function of centrality for two different jet p_T intervals.

the 2011 Pb–Pb sample [332], are well described by the calculations of Djordjevic *et al.* (see Fig. 4 in Ref. [298]). In order to study the origin of the difference in the nuclear modification factors of D and B mesons in this model, the R_{AA} of non-prompt J/ψ was also computed using the charm-quark mass value in the calculation of the in-medium interactions of beauty quarks. The outcome of this test case, depicted as dotted lines in the right panel of Fig. 29, shows a substantially lower R_{AA} of non-prompt J/ψ , close to that of D mesons, as compared to the case in which the beauty-quark mass is used in the calculation (dotted lines in Fig. 29). This indicates that, in this model, the large difference in the R_{AA} of D mesons and non-prompt J/ψ arises predominantly from the mass dependence of quark-medium interactions and is only moderately affected by the different production and fragmentation kinematics of charm and beauty quarks. Similar conclusions are derived by performing the same test with the MC@sHQ+EPOS and TAMU models (see Refs. [11, 317]).

A complementary approach to study beauty-quark interactions with the medium is provided by measurements of b -jets. Assuming that the quark hadronizes outside the medium, the jet energy should be, in first approximation, the sum of the energy of the beauty quark after its interaction with the medium and of the energy transferred by the quark to the medium that remains inside the jet cone. The nuclear modification factor of b -jets is shown in Fig. 30. In the left panel, the centrality-integrated R_{AA} is displayed as a function of p_T and compared to the pQCD-based calculations by Vitev *et al.* including radiative and collisional energy loss [287]. The data show a significant suppression, almost independent of p_T in the measured range, of the b -jet yield relative to the pp expectation, indicating parton energy loss in the hot and dense

medium. The measured R_{AA} is described by the Vitev *et al.* model using values of the jet-medium coupling parameter in the range $g^{\text{med}} = 1.8 - 2$, similar to the value found for inclusive jets. In the right panel of Fig. 30, the b -jet R_{AA} is shown as a function of centrality, expressed in terms of the number of participant nucleons, N_{part} , for two p_T intervals. A smooth decrease of R_{AA} with increasing centrality is observed, reaching a suppression of a factor of about 2.5 in the most central collisions. In the p_T range covered by these measurements the nuclear modification of the b -jet yield is found to be compatible, within the sizeable systematic uncertainties, with that of inclusive jets [336, 337]. This observation challenges models based on the strong-coupling limit, *e.g.*, within the AdS/CFT correspondence [295], in which quark-mass dependent effects persist up to large p_T . On the other hand, in pQCD-based models the quark mass effects are expected to be small at large p_T [287]. Nevertheless, even though quark mass related effects may not play a role in the high-momentum interval where the measurement was carried out, a difference between the R_{AA} 's of b -jets and inclusive jets could have been expected due to the color charge dependence of energy loss, since inclusive jets at LHC energies should be dominated by gluon jets up to very large p_T . In this respect, it should be considered that at LHC energies a sizeable fraction of beauty quarks are produced by splitting of gluons into $b\bar{b}$ pairs (gluon splitting) [338]. As pointed out in Ref. [11], in the case of b -jets at very high p_T , a significant part of the in-medium path length is likely to be covered by the parent gluon. For example, the formation (coherence) time of beauty quarks with an energy of 150 GeV is of about 1 fm/ c , implicating that the very early (hot and dense) stages of the medium evolution are probed by the parent gluon, and not by the beauty quark. Note that, following the arguments of coherence time for HQ pairs from gluon splitting [11], the fact that the medium could be probed by the parent gluon is relevant only for beauty quarks at high p_T . In the case of charm (for which the contribution of gluon splitting is smaller, $\approx 10\text{-}20\%$, than for beauty [339, 340]), and for beauty at not-too-high p_T ($p_T \lesssim 50$ GeV/ c , for which the coherence time is small because it is not increased by a large Lorentz boost) it is reasonable to assume that HF hadrons (and jets) probe the interactions of the heavy quarks with the medium.

3.4. Summary of Model-to-Data Comparisons and Implications for HF Transport

In this section we summarize and discuss the current experimental results in light of their theoretical interpretations, organized into two regimes of high and low transverse momentum following the expectation of different prevailing processes. We augment this discussion with an attempt to identify a transverse-momentum scale which possibly delineates the predominantly elastic and radiative interaction regimes, accompanied by schematic estimates of the pertinent HF transport coefficients. Since theoretical calculations of HF transport predict appreciable momentum dependencies of the coefficients (recall Fig. 2), a separation into regions of “low” and “high” p_T may be considered a minimal accounting procedure of this aspect, while keeping in mind that the dominant effects may also arise from rather different temperatures (*e.g.*, around T_{pc}

vs. the early hottest phases).

At high p_T , the initial HQ spectra are far above the equilibrium limit of the medium in heavy-ion collisions, and thus the interactions chiefly probe energy *loss* mechanisms of charm and beauty particles. This can also be gleaned from the Langevin process, eq. (16), where the dominant mechanism becomes a momentum degradation by a force $dp_j/dt = -\Gamma(p, T)p_j$. In a simplified form, the friction coefficient, $\Gamma \simeq A \sim n_p \sigma_{Qp}^{\text{trans}}$, is a product of medium density and HQ-parton transport cross section, where the latter is expected to be in the perturbative regime with a mild temperature dependence. Since $n_p \propto T^3$, the energy loss is presumably dominated by the hottest phases in a heavy-ion collision. The RHIC and LHC data on the nuclear modification factor of D mesons, non-prompt J/ψ and HF decay leptons all show a strong suppression of the high- p_T HF yield in semi-/central heavy-ion collisions relative to binary scaled pp cross sections, clearly associated with final-state effects. For high- p_T D -mesons in central Pb–Pb collisions at the LHC, the BAMPS, Duke and MC@sHQ+EPOS models describe the ALICE data well, while the elastic approaches of POWLANG and TAMU over- and under-predict the suppression, respectively. Taking Fig. 2 around $p \simeq 10$ GeV and for $T \simeq 0.3\text{--}0.4$ GeV as guidance (with MC@sHQ+EPOS typically requiring a moderate K factor for elastic-only calculations), we estimate an “average” high- p_T friction coefficient of $A \simeq 0.2 \pm 0.08/\text{fm}$ to describe the data (this probably includes part of the systematic uncertainty due to, *e.g.*, the different medium evolutions employed in the transport models). The POWLANG and TAMU coefficients with $A(p=10 \text{ GeV}) \simeq 0.25\text{--}0.3/\text{fm}$ and $0.07\text{--}0.1/\text{fm}$, respectively, roughly bracket the estimated uncertainty. A conversion of the HQ transport coefficients into a jet-quenching parameter, \hat{q} , as commonly adopted for light-parton energy loss, has been suggested in Ref. [341] in terms of the transverse-momentum broadening per unit path length, leading to $\hat{q} \equiv \hat{q}_\perp = 4TE_p^2 A/p$ (E_p : HQ energy). This translates into an estimate of $\hat{q} \simeq 2.8 \pm 1.1 \text{ GeV}^2/\text{fm}$ at $T \simeq 0.35$ GeV, or $\hat{q}/T^3 \simeq 13 \pm 5$, which is more stable in temperature. This result tends to be larger than the values extracted from light-parton jet quenching [342], possibly indicative of non-perturbative physics (and/or larger contributions from elastic interactions) which could still play a role for a charm quark at $p_T \simeq 10$ GeV.

The measurements of the azimuthal momentum anisotropy suggest a positive v_2 at high p_T , but they do not have enough precision yet to yield meaningful constraints on transport coefficients or the path length dependence of parton energy loss.

The beauty sector, currently accessed via non-prompt J/ψ mesons and b -jets at the LHC, shows less suppression in the R_{AA} than charm in a p_T interval around 10 GeV/ c . This observation is consistent with the expectation of quark-mass dependent energy loss (gluon Bremsstrahlung off the heavier beauty quarks is suppressed). However, the measured R_{AA} and v_2 of HF decay leptons at both RHIC and the LHC also show fair agreement with the BAMPS, MC@sHQ+EPOS and TAMU transport calculations, up to $p_t \simeq 10$ GeV. Since TAMU does not include radiative contributions, this suggests that the $p_T \simeq 10$ GeV regime for beauty is still in the realm of elastically dominated

interactions. The generic expectation for the transition from elastic to radiative regimes is a scaling with mass. Thus, based on an estimate for the transition regime around $p_T^{\text{trans}} \simeq 15$ GeV for beauty, one would deduce $p_T^{\text{trans}} \simeq 5$ GeV for charm. The latter value is supported in the discussion of the low- p_T regime below.

The color-charge dependence of parton energy loss has been one of the original motivations for high- p_T HF measurements. The measured R_{AA} 's of D mesons and pions, which are expected to be sensitive to the different coupling of gluons and quarks with the medium, agree within current uncertainties at RHIC and LHC energies. The R_{AA} 's of b -jets and inclusive jets are also observed to be compatible within uncertainties at very high momenta, $p_T > 80$ GeV. Hence, an experimental evidence of the color-charge dependence of energy loss remains elusive from the current data. According to model calculations, the similarity of the R_{AA} 's for D mesons and pions could result from the combined effect of a color-charge dependent energy loss and the softer p_T distribution and fragmentation function of gluons relative to charm quarks. To scrutinize this question, comparisons of B -, D - and π -meson data over a larger range in p_T will be needed, at both RHIC and the LHC. However, care has to be taken when going down to p_T 's where effects of radial flow and/or recombination set in. In the beauty sector these could become relevant at transverse momenta as high as 15 GeV. Likewise, at very high p_T , the gluon splitting contribution to b -quarks is expected to become sizable (implying that part of the energy loss is suffered by the parent gluon).

The low- p_T region is particularly interesting because of its sensitivity to a low-momentum transport coefficient of the QCD medium, *i.e.*, the HF diffusion coefficient D_s . In addition, the approach toward equilibrium does not merely induce a suppression of the spectra, but is expected to produce non-monotonic structures (like a “flow bump” in the HF hadron R_{AA} 's) whose quantitative features (such as the flow bump's height and location in p_T) are especially revealing for both medium evolution and the transport properties of the embedded HF particles. Measurements of R_{AA} and v_2 of different HF hadron species are expected to quantify the degree to which charm and beauty particles participate in the collective expansion of the system, thus directly reflecting their coupling strength to the medium. This includes the effects of in-medium hadronization, which is a manifestation of the HQ-medium coupling in the vicinity of T_{pc} (through hadronic pre-/resonant states). Experimentally, the D -meson R_{AA} at RHIC energy shows a pronounced maximum around $p_T \simeq 1-2$ GeV, which was predicted by models including strong elastic interactions of charm quarks in an expanding QGP, together with hadronization via in-medium heavy-light quark recombination. The same models also describe the low- p_T D -meson R_{AA} measured at the LHC, where the “radial-flow bump” is less pronounced (*e.g.*, due to the harder initial spectra and stronger shadowing) and/or not yet resolved. The approximate agreement of these models extends to the R_{AA} of the HF decay leptons at both accelerators. Importantly, a fair description also emerges of the low- p_T elliptic flow, which is measured to be at the $\sim 10-15\%$ level for D mesons (slightly smaller for HF leptons) in non-central collisions at RHIC and the LHC,

with still rather significant uncertainties. The data favor scenarios in which the heavy quarks pick up substantial collectivity from the expanding QGP, which is then further augmented by hadronization through recombination (by several tens of percent), and by another 10-20% in the hadronic phase. The relative importance of the hadronization process in generating v_2 is another reflection of a strong HQ-medium coupling in the vicinity of T_{pc} . At first sight, the underlying HF transport coefficients appear to be quite different among current models. For example, comparing the low-momentum region of the MC@sHQ+EPOS (or Nantes) and TAMU models from Fig. 2 left, an appreciable discrepancy is found. The discrepancy is, however, smallest at the lowest temperatures, less than a factor of 2. It is further mitigated if one recalls that the charm-quark mass close to T_{pc} in the MC@sHQ+EPOS model ($m_c=1.5$ GeV) is smaller than in the TAMU model (where the in-medium mass grows as T_{pc} is approached from above, reaching up to $m_c \simeq 1.8$ GeV). In the conversion from A to the spatial diffusion coefficient D_s , the m_Q dependence of the former is approximately divided out, cf. eq. (2), which can be recast as $D_s \simeq T/m_Q A(p=0)$. This suggests that the coupling strength around T_{pc} is most important in building up the HF v_2 , which is not surprising since the bulk v_2 is largest from this stage on [39, 343] (the importance of recombination processes in the hadronization of the heavy quarks further corroborates this point). More quantitatively from Fig. 2, taking $T=0.2$ GeV, one finds $D_s(2\pi T) \simeq 2-3$ for the Nantes coefficients and $D_s(2\pi T) \simeq 3-4$ for the TAMU one. For the PHSD model, which also reproduces the D -meson R_{AA} and v_2 at the LHC reasonably well, the underlying spatial diffusion constant is somewhat larger, $D_s(2\pi T) \simeq 5-6$ (with $m_c=1.5$ GeV). However, the concrete implementation of heavy-light quark recombination differs significantly in the current models, both technically as well as in its impact on observables (the TAMU implementation tends to give larger effects from recombination than the one in MC@sHQ+EPOS, Duke and PHSD). This contributes significantly to the uncertainty in the model interpretations of the experimental data (such as the extraction of the transport coefficient).

Promising tools to discern different types of hadronization mechanisms and the nature of the interactions near T_{pc} are the R_{AA} and v_2 of HF hadrons with different quark composition and different mass. In particular, the production of mesons carrying a strange quark (D_s^+ and B_s^0) and of baryons (Λ_c^+ , Ξ_c^+ , Ξ_c^0 , Λ_b^0) at low and intermediate p_T has been suggested to encode pertinent information. The first measurement of the $D_s^+ R_{AA}$ at the LHC and a subsequent preliminary result at RHIC provide a hint for the relevance of recombination of charm with thermal strange quarks, although the current uncertainties do not allow for definite conclusions. A stronger signal for recombination of charm quarks, with anti-charm quarks, comes from the observed $J/\psi R_{AA}$ [345, 346] and v_2 [347] at the LHC. The larger data samples that will be collected in the next years will be most valuable to shed further light on the relevance heavy-light and heavy-heavy recombination processes.

Let us finally return to question of elastic vs. radiative HQ interactions in the QGP. The TAMU transport approach with non-perturbative elastic interactions only

approximately describes the R_{AA} and v_2 of D -mesons up to $p_T \simeq 5$ GeV (with significant deviations above), and the HF lepton observables, with a substantial beauty component, out to $p_T \simeq 10$ GeV. This may serve as an initial estimate of the regime where elastic interactions dominate the HQ coupling to the QCD medium. Interestingly, the BAMPs and MC@sHQ+EPOS approaches seem to do best in a simultaneous description of R_{AA} and v_2 toward higher p_T when the elastic HQ interactions in the QGP are maximized relative to the radiative ones. The former appear to be more effective in transferring collectivity from the expanding medium on heavy quarks than path length differences probed by energy loss mechanisms. On the other hand, theoretical calculations suggest that radiative contributions are important at high p_T , *e.g.*, for the observed mass dependence of energy loss. Hence, future measurements of the high- p_T v_2 will provide crucial information. Scattering processes of $2 \rightarrow 3$ and $3 \leftrightarrow 3$ type [348] may also play a role in future improvements of the theoretical models.

4. Conclusions and Outlook

The measurements of open heavy-flavor production in heavy-ion collisions at RHIC and the LHC have remarkably progressed in recent years. The pioneering measurements of semi-leptonic HF decays at RHIC are now augmented by D -meson measurements at both colliders, as well as beauty particles through their J/ψ decay products and b -jets. The nuclear modification factor exhibits large deviations from unity, and the accompanying elliptic flow substantial non-zero values, for all measured HF particles (data on beauty v_2 are not available yet), while control experiments in small systems yield $R_{pA} \simeq R_{dA} \simeq 1$. The main features of the data are in general understood and corroborate that HF particles acquire a substantial collective flow at low and intermediate momenta which requires a strong coupling to the QCD medium including recombination as hadronization mechanism. At the same time, high- p_T HF particles are significantly degraded in energy (beauty particles less than charm particles), which is most naturally associated with parton energy loss in the QGP.

Detailed comparisons of the experimental observations with various theoretical model calculations have been instrumental in deducing the above qualitative insights. Here, we have attempted to take the next step by extracting semi-quantitative estimates for the HF transport coefficients. In the low- p_T regime, the heavy-quark diffusion coefficient appears to lie in the range of $D_s(2\pi T) \simeq 2-5$ at temperatures of around $T \simeq 0.2$ GeV, which are arguably the most relevant ones to obtain the experimentally measured large charm- v_2 values. This result is not far from current estimates within quenched lattice QCD. The pertinent thermalization timescale of 3-6 fm/ c suggests that low- p_T charm particles are close to being thermalized in central AA collisions at RHIC and the LHC, and probably decouple slightly below T_{pc} . High- p_T suppression suggests an energy loss transport coefficient of approximately $\hat{q}/T^3 \simeq 10-15$ for a 10 GeV charm quark at temperatures of $T \simeq 0.35$ GeV, which tends to be larger than for light partons.

We also deduced that elastic scattering dominates the transport of charm (beauty) particles for $p_T \lesssim 5(15)$ GeV, and may remain important until much larger momenta.

The above estimates call for a more rigorous quantification of their uncertainties, including those caused by the medium evolution, hadronization process, and initial conditions. However, given that the current (statistical and systematic) uncertainties of the experimental data are still rather large in many cases, and that some observables (like beauty v_2 and heavy-baryon spectra) are not available yet, we see an excellent potential to further narrow down the latitude in the phenomenological modeling of HF transport in AA collisions at RHIC and the LHC. A base set of precision data on the R_{AA} and v_2 of D and B mesons, charm-strange mesons and charm baryons down to low p_T would go a long way toward disentangling different mechanisms, identifying their microscopic origin and obtaining reliable and accurate results for the temperature and momentum dependence of the charm and beauty transport coefficients in QCD matter. Accurate low- p_T measurements, including heavy baryons, are also essential to assess the total production yields of charm and beauty in URHICs, which are, *e.g.*, crucial for quantifying regeneration contributions in the quarkonium sector; current electron and D -meson measurements at RHIC show consistency with binary scaling within a $\sim 30\%$ accuracy. The experimental requirements for the above measurements are very likely to be met in the coming years through the larger data samples that, augmented with advanced detection methods, will become available at RHIC and the LHC.

Continued theoretical efforts will be required to firmly root the phenomenological analyses in finite-temperature QCD. Lattice results for the HF diffusion coefficient in full QCD are much anticipated and can serve as a benchmark for effective-theory calculations of this quantity. Such calculations provide a natural bridge between lattice-QCD and experiment, and can, in fact, draw constraints from a broad class of quantities that can be computed with good precision on the lattice, including heavy-quark free energies, correlation functions and susceptibilities. The latter, *e.g.*, are a well-known diagnostic tool for the prevalent degrees of freedom in the QCD medium, *i.e.*, whether charm propagates as individual quarks or as part of hadronic states. One is then automatically led into the quarkonium sector, which we did not discuss in the present review, but which obviously bears close connections to open heavy flavor, both theoretically and phenomenologically.

Future issues on the experimental side also include the role of HF transport in small colliding systems, at smaller (and higher) colliding energies, as well as correlation observables. For the former, pA collisions at the LHC found possible indications for a non-zero v_2 , while the R_{AA} appears to be only mildly modified, paralleling the more accurate observations for light-flavor hadrons. This could develop into quite a challenge for model calculations. At lower collision energies, in Au-Au reactions at $\sqrt{s}=62$ GeV, evidence has been found that the R_{AA} of semileptonic decay electrons is larger than at $\sqrt{s}=200$ GeV and 2.76 TeV, where the high- p_T suppression is comparable. In how far this finding is due to initial-state effects (*e.g.*, softer initial spectra and/or stronger Cronin effect) or final-state effects needs to be clarified, thereby providing further insights into

the impact of the QCD transition region on HF transport. High- p_T HF correlations hold, in principle, the potential for disentangling different mechanisms of energy loss, *i.e.*, how the energy dissipated by a heavy quark migrates into the medium. Current model calculations suggest that the discrimination power between, *e.g.*, elastic and radiative mechanisms requires a rather high experimental precision, which may be achievable with future LHC runs.

In conclusion, heavy-flavor physics in heavy-ion collisions remains one of the most promising areas in QCD matter research. In particular, it simultaneously incorporates two critical aspects, namely (i) taking advantage of upcoming precision data to quantitatively extract transport properties of the QCD medium while, (ii) taking advantage of controlled theoretical approaches to illuminate the in-medium properties of the fundamental QCD force in a non-perturbative regime. We believe that this opportunity will enable decisive progress in understanding the inner workings of the medium that filled the Universe in the first ~ 10 microseconds of its existence.

Acknowledgments

We thank Andrea Beraudo, Andrea Dainese and Min He for helpful comments on the ms., and Min He, Davide Caffarri and Diego Stocco for help with the figures. This work has been supported by the US National Science Foundation under grant no. PHY-1306359.

References

- [1] R. Stock (editor) *et al.*, *Relativistic Heavy-Ion Physics*, Landolt Börnstein **I-23**, Springer Verlag (Heidelberg 2010).
- [2] Y. Akiba *et al.*, arXiv:1502.02730 [nucl-ex].
- [3] P. Braun-Munzinger, V. Koch, T. Schaefer and J. Stachel, arXiv:1510.00442 [nucl-th].
- [4] B. I. Abelev *et al.* [STAR Collaboration], Phys. Rev. C **79** (2009) 034909.
- [5] B. Abelev *et al.* [ALICE Collaboration], Phys. Rev. Lett. **109** (2012) 252301.
- [6] S. Borsanyi, Z. Fodor, C. Hoelbling, S.D. Katz, S. Krieg, C. Ratti, K.K. Szabo [Wuppertal-Budapest Collaboration], JHEP **1009** (2010) 073.
- [7] T. Bhattacharya *et al.*, Phys. Rev. Lett. **113** (2014) 082001.
- [8] R. Rapp, Adv. High Energy Phys. **2013** (2013) 148253.
- [9] R. Rapp and H. van Hees, R. C. Hwa, X.-N. Wang (Ed.), Quark Gluon Plasma 4, World Scientific (2010) 111.
- [10] R. Averbeck, Prog. Part. Nucl. Phys. **70** (2013) 159.
- [11] A. Andronic *et al.*, arXiv:1506.03981 [nucl-ex].
- [12] P. Braun-Munzinger and J. Stachel, Landolt-Bornstein **23** (2010) 424.
- [13] L. Kluberg and H. Satz, Landolt-Bornstein **23** (2010) 372.
- [14] R. Rapp, D. Blaschke and P. Crochet, Prog. Part. Nucl. Phys. **65** (2010) 209.
- [15] A. Mocsy, P. Petreczky and M. Strickland, Int. J. Mod. Phys. A **28** (2013) 1340012.
- [16] G. S. Bali *et al.* [TXL and T(X)L Collaborations], Phys. Rev. D **62** (2000) 054503.
- [17] D. Banerjee, S. Datta, R. Gavai and P. Majumdar, Phys. Rev. D **85** (2012) 014510.
- [18] O. Kaczmarek, Nucl. Phys. A **931** (2014) 633.
- [19] P. Petreczky, Eur. Phys. J. C **62** (2009) 85.

- [20] A. Bazavov, F. Karsch, Y. Maezawa, S. Mukherjee and P. Petreczky, *Phys. Rev. D* **91** (2015) 054503.
- [21] F. Riek and R. Rapp, *New J. Phys.* **13** (2011) 045007.
- [22] G. D. Moore and D. Teaney, *Phys. Rev. C* **71** (2005) 064904.
- [23] C. P. Herzog, A. Karch, P. Kovtun, C. Kozcaz and L. G. Yaffe, *JHEP* **0607** (2006) 013.
- [24] S. S. Gubser, *Phys. Rev. D* **74** (2006) 126005.
- [25] J. Casalderrey-Solana and D. Teaney, *Phys. Rev. D* **74** (2006) 085012.
- [26] P. Danielewicz and M. Gyulassy, *Phys. Rev. D* **31** (1985) 53.
- [27] P. B. Gossiaux, *Nucl. Phys. A* **910-911** (2013) 301.
- [28] J. Uphoff, O. Fochler, Z. Xu and C. Greiner, *J. Phys. G* **42** (2015) 115106.
- [29] T. Koide and T. Kodama, *Phys. Rev. E* **83** (2011) 061111.
- [30] M. He, H. van Hees, P. B. Gossiaux, R. J. Fries and R. Rapp, *Phys. Rev. E* **88** (2013) 032138.
- [31] H. van Hees and R. Rapp, *Phys. Rev. C* **71** (2005) 034907.
- [32] H. van Hees, V. Greco and R. Rapp, *Phys. Rev. C* **73** (2006) 034913.
- [33] P. B. Gossiaux, V. Guiho and J. Aichelin, *J. Phys. G* **32** (2006) S359.
- [34] S. K. Das, J. e. Alam and P. Mohanty, *Phys. Rev. C* **82** (2010) 014908.
- [35] Y. Akamatsu, T. Hatsuda and T. Hirano, *Phys. Rev. C* **79** (2009) 054907.
- [36] W. M. Alberico, A. Beraudo, A. De Pace, A. Molinari, M. Monteno, M. Nardi and F. Prino, *Eur. Phys. J. C* **71** (2011) 1666.
- [37] F. Scardina, D. Perricone, S. Plumari, M. Ruggieri and V. Greco, *Phys. Rev. C* **90** (2014) 054904.
- [38] J. Uphoff, O. Fochler, Z. Xu and C. Greiner, *Phys. Lett. B* **717** (2012) 430.
- [39] S. K. Das, F. Scardina, S. Plumari and V. Greco, *Phys. Lett. B* **747** (2015) 260.
- [40] T. Song, H. Berrehrhah, D. Cabrera, J. M. Torres-Rincon, L. Tolos, W. Cassing and E. Bratkovskaya, *Phys. Rev. C* **92** (2015) 014910.
- [41] B. Svetitsky, *Phys. Rev. D* **37** (1988) 2484.
- [42] K. Aamodt *et al.* [ALICE Collaboration], *Phys. Lett. B* **696** (2011) 328.
- [43] S. S. Adler *et al.* [PHENIX Collaboration], *Phys. Rev. Lett.* **96** (2006) 032301.
- [44] A. Adare *et al.* [PHENIX Collaboration], *Phys. Rev. Lett.* **98** (2007) 172301.
- [45] A. Peshier, *Nucl. Phys. A* **888** (2012) 7.
- [46] P. B. Gossiaux and J. Aichelin, *Phys. Rev. C* **78** (2008) 014904.
- [47] E. Braaten and M. H. Thoma, *Phys. Rev. D* **44** (1991) 2625.
- [48] W. M. Alberico, A. Beraudo, A. De Pace, A. Molinari, M. Monteno, M. Nardi, F. Prino and M. Sitta, *Eur. Phys. J. C* **73** (2013) 2481.
- [49] O. Kaczmarek and F. Zantow, *Phys. Rev. D* **71** (2005) 114510.
- [50] H. Berrehrhah, E. Bratkovskaya, W. Cassing, P. B. Gossiaux, J. Aichelin and M. Bleicher, *Phys. Rev. C* **89** (2014) 054901.
- [51] T. Song, H. Berrehrhah, D. Cabrera, W. Cassing and E. Bratkovskaya, arXiv:1512.00891 [nucl-th].
- [52] S. Caron-Huot and G. D. Moore, *Phys. Rev. Lett.* **100** (2008) 052301.
- [53] E. Eichten, K. Gottfried, T. Kinoshita, K. D. Lane and T. M. Yan, *Phys. Rev. D* **21** (1980) 203.
- [54] A. Bazavov, Y. Burnier and P. Petreczky, *Nucl. Phys. A* **932** (2014) 117.
- [55] R. Brockmann and R. Machleidt, *Phys. Rev. C* **42** (1990) 1965.
- [56] R. Redmer, *Phys. Rep.* **282** (1997) 35.
- [57] P. A. Pantel, D. Davesne and M. Urban, *Phys. Rev. A* **91** (2015) 013627.
- [58] F. Riek and R. Rapp, *Phys. Rev. C* **82** (2010) 035201.
- [59] N. Brambilla, D. Gromes and A. Vairo, *Phys. Lett. B* **576** (2003) 314.
- [60] H. van Hees, M. Mannarelli, V. Greco and R. Rapp, *Phys. Rev. Lett.* **100** (2008) 192301.
- [61] K. Huggins and R. Rapp, *Nucl. Phys. A* **896** (2012) 24.
- [62] X. Zhao and R. Rapp, *Phys. Rev. C* **82** (2010) 064905.
- [63] Y. Liu, B. Chen, N. Xu and P. Zhuang, *Phys. Lett. B* **697** (2011) 32.
- [64] X. Zhao and R. Rapp, *Nucl. Phys. A* **859** (2011) 114.
- [65] M. He, R. J. Fries and R. Rapp, *Phys. Lett. B* **735** (2014) 445.

- [66] A. Emerick, X. Zhao and R. Rapp, *Eur. Phys. J. A* **48** (2012) 72.
- [67] M. Strickland and D. Bazow, *Nucl. Phys. A* **879** (2012) 25.
- [68] M. He, S.Y.F. Liu and R. Rapp, in preparation.
- [69] O. Kaczmarek, *PoS CPOD* **07** (2007) 043.
- [70] S. Y. F. Liu and R. Rapp, *Nucl. Phys. A* **941** (2015) 179.
- [71] Y. Burnier, O. Kaczmarek and A. Rothkopf, *Phys. Rev. Lett.* **114** (2015) 082001.
- [72] R. Sharma, I. Vitev and B. W. Zhang, *Phys. Rev. C* **80** (2009) 054902.
- [73] P. B. Gossiaux, J. Aichelin, T. Gousset and V. Guiho, *J. Phys. G* **37** (2010) 094019.
- [74] M. Nahrgang, J. Aichelin, P. B. Gossiaux and K. Werner, *Phys. Rev. C* **89** (2014) 014905.
- [75] J. Uphoff, O. Fochler, Z. Xu and C. Greiner, *Phys. Rev. C* **84** (2011) 024908.
- [76] M. He, R. J. Fries and R. Rapp, *Phys. Rev. C* **86** (2012) 014903.
- [77] Y. L. Dokshitzer and D. E. Kharzeev, *Phys. Lett. B* **519** (2001) 199.
- [78] N. Armesto, C. A. Salgado and U. A. Wiedemann, *Phys. Rev. D* **69** (2004) 114003.
- [79] N. Armesto, A. Dainese, C. A. Salgado and U. A. Wiedemann, *Phys. Rev. D* **71** (2005) 054027.
- [80] G. Y. Qin, J. Ruppert, C. Gale, S. Jeon, G. D. Moore and M. G. Mustafa, *Phys. Rev. Lett.* **100** (2008) 072301.
- [81] T. Lang, H. van Hees, J. Steinheimer, G. Inghirami and M. Bleicher, *Phys. Rev. C* **93** (2016) 014901.
- [82] S. Cao, G. Y. Qin and S. A. Bass, *Phys. Rev. C* **88** (2013) 044907.
- [83] S. Cao, G. Y. Qin and S. A. Bass, *Phys. Rev. C* **92** (2015) 024907.
- [84] S. Wicks, W. Horowitz, M. Djordjevic and M. Gyulassy, *Nucl. Phys. A* **783** (2007) 493.
- [85] M. Djordjevic, *Phys. Rev. C* **80** (2009) 064909.
- [86] M. Gyulassy, P. Levai and I. Vitev, *Nucl. Phys. B* **594** (2001) 371.
- [87] J. Aichelin, P. B. Gossiaux and T. Gousset, *Phys. Rev. D* **89** (2014) 074018.
- [88] J. F. Gunion and G. Bertsch, *Phys. Rev. D* **25** (1982) 746.
- [89] M. Nahrgang, J. Aichelin, P. B. Gossiaux and K. Werner, *Phys. Rev. C* **90** (2014) 024907.
- [90] T. Hilger, R. Thomas and B. Kampfer, *Phys. Rev. C* **79** (2009) 025202.
- [91] K. Suzuki, P. Gubler and M. Oka, arXiv:1511.04513 [hep-ph].
- [92] C. Fuchs, B. V. Martemyanov, A. Faessler and M. I. Krivoruchenko, *Phys. Rev. C* **73** (2006) 035204.
- [93] M. F. M. Lutz and C. L. Korpa, *Phys. Lett. B* **633** (2006) 43.
- [94] L. Tolos, A. Ramos and T. Mizutani, *Phys. Rev. C* **77** (2008) 015207.
- [95] M. Laine, *JHEP* **1104** (2011) 124.
- [96] M. He, R. J. Fries and R. Rapp, *Phys. Lett. B* **701** (2011) 445.
- [97] S. Ghosh, S. K. Das, S. Sarkar and J. e. Alam, *Phys. Rev. D* **84** (2011) 011503.
- [98] L. M. Abreu, D. Cabrera, F. J. Llanes-Estrada and J. M. Torres-Rincon, *Annals Phys.* **326** (2011) 2737.
- [99] L. Tolos and J. M. Torres-Rincon, *Phys. Rev. D* **88** (2013) 074019.
- [100] V. Ozvenchuk, J. M. Torres-Rincon, P. B. Gossiaux, L. Tolos and J. Aichelin, *Phys. Rev. C* **90** (2014) 054909.
- [101] S. K. Das, S. Ghosh, S. Sarkar and J. e. Alam, *Phys. Rev. D* **85** (2012) 074017.
- [102] L. M. Abreu, D. Cabrera and J. M. Torres-Rincon, *Phys. Rev. D* **87** (2013) 034019.
- [103] J. M. Torres-Rincon, L. Tolos and O. Romanets, *Phys. Rev. D* **89** (2014) 074042.
- [104] H. T. Ding, A. Francis, O. Kaczmarek, F. Karsch, H. Satz and W. Soeldner, *Phys. Rev. D* **86** (2012) 014509.
- [105] A. Francis, O. Kaczmarek, M. Laine, T. Neuhaus and H. Ohno, *Phys. Rev. D* **92** (2015) 116003.
- [106] M. He, R. J. Fries and R. Rapp, *Phys. Rev. Lett.* **110** (2013) 112301.
- [107] S. Mukherjee, P. Petreczky and S. Sharma, *Phys. Rev. D* **93** (2016) 014502.
- [108] M. Mannarelli and R. Rapp, *Phys. Rev. C* **72** (2005) 064905.
- [109] S.S. Gubser, *Phys. Rev. D* **76** (2007) 126003.
- [110] C. Peterson, D. Schlatter, I. Schmitt and P. M. Zerwas, *Phys. Rev. D* **27** (1983) 105.

- [111] M. Cacciari, M. Greco and P. Nason, JHEP **9805** (1998) 007.
- [112] M. Cacciari, P. Nason and R. Vogt, Phys. Rev. Lett. **95** (2005) 122001.
- [113] V. G. Kartvelishvili, A. K. Likhoded and S. R. Slabospitsky, Sov. J. Nucl. Phys. **33** (1981) 434 [Yad. Fiz. **33** (1981) 832].
- [114] R. C. Hwa, Phys. Rev. D **51** (1995) 85.
- [115] E. Braaten, Y. Jia and T. Mehen, Phys. Rev. Lett. **89** (2002) 122002.
- [116] R. Rapp and E. V. Shuryak, Phys. Rev. D **67** (2003) 074036.
- [117] Z. w. Lin and D. Molnar, Phys. Rev. C **68** (2003) 044901.
- [118] V. Greco, C. M. Ko and R. Rapp, Phys. Lett. B **595** (2004) 202.
- [119] D. Molnar, Acta Phys. Hung. A **22** (2005) 271.
- [120] L. Ravagli and R. Rapp, Phys. Lett. B **655** (2007) 126.
- [121] L. Ravagli, H. van Hees and R. Rapp, Phys. Rev. C **79** (2009) 064902.
- [122] A. Beraudo, A. De Pace, M. Monteno, M. Nardi and F. Prino, Eur. Phys. J. C **75** (2015) 121.
- [123] T. Sjostrand, S. Mrenna and P. Z. Skands, JHEP **0605** (2006) 026.
- [124] M. He, R. J. Fries and R. Rapp, Phys. Rev. C **85** (2012) 044911.
- [125] S. Takeuchi, K. Murase, T. Hirano, P. Huovinen and Y. Nara, Phys. Rev. C **92** (2015) 044907.
- [126] Y. Oh, C. M. Ko, S. H. Lee and S. Yasui, Phys. Rev. C **79** (2009) 044905.
- [127] P. M. Chesler, M. Lekaveckas and K. Rajagopal, JHEP **1310** (2013) 013.
- [128] S. K. Das, M. Ruggieri, S. Mazumder, V. Greco and J. e. Alam, J. Phys. G **42** (2015) 095108.
- [129] B. Schenke, P. Tribedy and R. Venugopalan, Phys. Rev. C **89** (2014) 024901.
- [130] M. He, unpublished (2014).
- [131] P. B. Gossiaux, S. Vogel, H. van Hees, J. Aichelin, R. Rapp, M. He and M. Bluhm, arXiv:1102.1114 [hep-ph].
- [132] P. F. Kolb and U. W. Heinz, In *Hwa, R.C. (ed.) et al.: Quark gluon plasma* 634-714 [nucl-th/0305084].
- [133] P. F. Kolb and R. Rapp, Phys. Rev. C **67** (2003) 044903.
- [134] W. Broniowski, W. Florkowski, M. Chojnacki and A. Kisiel, Phys. Rev. C **80** (2009) 034902.
- [135] C. Gale, S. Jeon, B. Schenke, P. Tribedy and R. Venugopalan, Phys. Rev. Lett. **110** (2013) 012302.
- [136] W. van der Schee, P. Romatschke and S. Pratt, Phys. Rev. Lett. **111** (2013) 22, 222302.
- [137] S. Pratt, Phys. Rev. Lett. **102** (2009) 232301.
- [138] S. Pratt, Nucl. Phys. A **830** (2009) 51C.
- [139] H. van Hees, C. Gale and R. Rapp, Phys. Rev. C **84** (2011) 054906.
- [140] H. van Hees, M. He and R. Rapp, Nucl. Phys. A **933** (2015) 256.
- [141] M. Nahrgang, J. Aichelin, S. Bass, P. B. Gossiaux and K. Werner, Nucl. Phys. A **931** (2014) 575.
- [142] B. Zhang, L. W. Chen and C. M. Ko, Phys. Rev. C **72** (2005) 024906.
- [143] D. Molnar, Eur. Phys. J. C **49** (2007) 181.
- [144] M. C. Abreu *et al.* [NA38 and NA50 Collaborations], Eur. Phys. J. C **14** (2000) 443.
- [145] R. Arnaldi *et al.* [NA60 Collaboration], Eur. Phys. J. C **59** (2009) 607.
- [146] C. Lourenco and H. K. Wöhri, Phys. Rept. **433** (2006) 127.
- [147] A. Adare *et al.* [PHENIX Collaboration], Phys. Rev. C **84** (2011) 044905.
- [148] L. Adamczyk *et al.* [STAR Collaboration], Phys. Rev. D **86** (2012) 072013.
- [149] B. Abelev *et al.* [ALICE Collaboration], JHEP **1207** (2012) 191.
- [150] R. Aaij *et al.* [LHCb Collaboration], Nucl. Phys. B **871** (2013) 1.
- [151] C. Albajar *et al.* [UA1 Collaboration], Phys. Lett. B **256** (1991) 121 [Phys. Lett. B **262** (1991) 497].
- [152] D. Acosta *et al.* [CDF Collaboration], Phys. Rev. D **71** (2005) 032001.
- [153] A. Adare *et al.* [PHENIX Collaboration], Phys. Rev. Lett. **103** (2009) 082002.
- [154] B. B. Abelev *et al.* [ALICE Collaboration], Phys. Lett. B **738** (2014) 97.
- [155] B. Abelev *et al.* [ALICE Collaboration], Phys. Lett. B **721** (2013) 13.
- [156] S. S. Adler *et al.* [PHENIX Collaboration], Phys. Rev. C **71** (2005) 034908 [Phys. Rev. C **71**

- (2005) 049901].
- [157] S. Chatrchyan *et al.* [CMS Collaboration], Phys. Rev. Lett. **109** (2012) 152303.
- [158] K. A. Olive *et al.* [Particle Data Group Collaboration], Chin. Phys. C **38** (2014) 090001.
- [159] B. I. Abelev *et al.* [STAR Collaboration], Phys. Rev. Lett. **98** (2007) 192301 [Phys. Rev. Lett. **106** (2011) 159902].
- [160] B. Abelev *et al.* [ALICE Collaboration], Phys. Rev. D **86** (2012) 112007.
- [161] G. Aad *et al.* [ATLAS Collaboration], Phys. Lett. B **707** (2012) 438.
- [162] H. Agakishiev *et al.* [STAR Collaboration], Phys. Rev. D **83** (2011) 052006.
- [163] A. Adare *et al.* [PHENIX Collaboration], Phys. Rev. C **86** (2012) 024909.
- [164] B. Abelev *et al.* [ALICE Collaboration], Phys. Rev. Lett. **109** (2012) 112301.
- [165] A. Adare *et al.* [PHENIX Collaboration], Phys. Lett. B **670** (2009) 313.
- [166] A. Adare *et al.* [PHENIX Collaboration], Phys. Rev. C **91** (2015) 014907.
- [167] M. M. Aggarwal *et al.* [STAR Collaboration], Phys. Rev. Lett. **105** (2010) 202301.
- [168] B. Abelev *et al.* [ALICE Collaboration], JHEP **1211** (2012) 065.
- [169] J. Adam *et al.* [ALICE Collaboration], JHEP **1507** (2015) 051.
- [170] V. Khachatryan *et al.* [CMS Collaboration], Eur. Phys. J. C **71** (2011) 1575.
- [171] R. Aaij *et al.* [LHCb Collaboration], Eur. Phys. J. C **71** (2011) 1645.
- [172] R. Aaij *et al.* [LHCb Collaboration], JHEP **1402** (2014) 072.
- [173] D. Buskulic *et al.* [ALEPH Collaboration], Phys. Lett. B **295** (1992) 396.
- [174] O. Adriani *et al.* [L3 Collaboration], Phys. Lett. B **317** (1993) 467.
- [175] P. Abreu *et al.* [DELPHI Collaboration], Phys. Lett. B **341** (1994) 109.
- [176] B. Abelev *et al.* [ALICE Collaboration], JHEP **1201** (2012) 128.
- [177] B. Abelev *et al.* [ALICE Collaboration], Phys. Lett. B **718** (2012) 279.
- [178] CMS Collaboration [CMS Collaboration], CMS-PAS-HIN-15-005.
- [179] V. Khachatryan *et al.* [CMS Collaboration], Phys. Rev. Lett. **116** (2016) 032301.
- [180] S. Chatrchyan *et al.* [CMS Collaboration], Phys. Rev. Lett. **113** (2014) 132301 [Phys. Rev. Lett. **115** (2015) 029903].
- [181] R. J. Glauber in Lectures in Theoretical Physics, NY, 1959, Vol. 1, 315.
- [182] M. L. Miller, K. Reygers, S. J. Sanders and P. Steinberg, Ann. Rev. Nucl. Part. Sci. **57** (2007) 205.
- [183] P. Braun-Munzinger and K. Redlich, Eur. Phys. J. C **16** (2000) 519.
- [184] B. W. Zhang, C. M. Ko and W. Liu, Phys. Rev. C **77** (2008) 024901.
- [185] S. Batsouli, S. Kelly, M. Gyulassy and J. L. Nagle, Phys. Lett. B **557** (2003) 26.
- [186] A. Andronic, P. Braun-Munzinger, K. Redlich and J. Stachel, Phys. Lett. B **571** (2003) 36.
- [187] I. Kuznetsova and J. Rafelski, Eur. Phys. J. C **51** (2007) 113.
- [188] P. R. Sorensen and X. Dong, Phys. Rev. C **74** (2006) 024902.
- [189] G. Martinez-Garcia, S. Gadrat and P. Crochet, Phys. Lett. B **663** (2008) 55 [Phys. Lett. B **666** (2008) 533].
- [190] J. Adams *et al.* [STAR Collaboration], Phys. Rev. C **72** (2005) 014904.
- [191] S. S. Adler *et al.* [PHENIX Collaboration], Phys. Rev. Lett. **91** (2003) 182301.
- [192] B. B. Abelev *et al.* [ALICE Collaboration], JHEP **1506** (2015) 190.
- [193] J. Y. Ollitrault, Phys. Rev. D **46** (1992) 229.
- [194] M. Gyulassy, I. Vitev and X. N. Wang, Phys. Rev. Lett. **86** (2001) 2537.
- [195] E. V. Shuryak, Phys. Rev. C **66** (2002) 027902.
- [196] M. H. Thoma and M. Gyulassy, Nucl. Phys. B **351** (1991) 491.
- [197] R. Baier, Y. L. Dokshitzer, A. H. Mueller, S. Peigne and D. Schiff, Nucl. Phys. B **484** (1997) 265.
- [198] D. Molnar and S. A. Voloshin, Phys. Rev. Lett. **91** (2003) 092301.
- [199] M. Nahrgang, J. Aichelin, S. Bass, P. B. Gossiaux and K. Werner, Phys. Rev. C **91** (2015) 1, 014904.
- [200] J. Uphoff, F. Senzel, Z. Xu and C. Greiner, Phys. Rev. C **89** (2014) 064906.
- [201] S. Cao, G. Y. Qin and S. A. Bass, Nucl. Phys. A **932** (2014) 38.

- [202] T. Renk, Phys. Rev. C **89** (2014) 054906.
- [203] G. Aad *et al.* [ATLAS Collaboration], Phys. Rev. Lett. **105** (2010) 252303.
- [204] S. Chatrchyan *et al.* [CMS Collaboration], Phys. Rev. C **84** (2011) 024906.
- [205] A. Adare *et al.* [PHENIX Collaboration], Phys. Rev. C **89** (2014) 034915.
- [206] A. Adare *et al.* [PHENIX Collaboration], Phys. Rev. C **83** (2011) 044912.
- [207] G. Wang [STAR Collaboration], J. Phys. G **35** (2008) 104107.
- [208] D. Thomas [ALICE Collaboration], J. Phys. Conf. Ser. **509** (2014) 012079.
- [209] B. L. Combridge, Nucl. Phys. B **151** (1979) 429.
- [210] M. L. Mangano, P. Nason and G. Ridolfi, Nucl. Phys. B **373** (1992) 295.
- [211] B. A. Kniehl, G. Kramer, I. Schienbein and H. Spiesberger, Phys. Rev. D **71** (2005) 014018.
- [212] B. A. Kniehl, G. Kramer, I. Schienbein and H. Spiesberger, Eur. Phys. J. C **41** (2005) 199.
- [213] M. Luszczak, R. Maciula and A. Szczurek, Phys. Rev. D **79** (2009) 034009.
- [214] R. Maciula and A. Szczurek, Phys. Rev. D **87** (2013) 094022.
- [215] S. Catani, M. Ciafaloni and F. Hautmann, Nucl. Phys. B **366** (1991) 135.
- [216] T. Sjostrand, S. Mrenna and P. Z. Skands, Comput. Phys. Commun. **178** (2008) 852.
- [217] G. Corcella, I. G. Knowles, G. Marchesini, S. Moretti, K. Odagiri, P. Richardson, M. H. Seymour and B. R. Webber, JHEP **0101** (2001) 010.
- [218] S. Frixione, P. Nason and B. R. Webber, JHEP **0308** (2003) 007.
- [219] S. Frixione, P. Nason and G. Ridolfi, JHEP **0709** (2007) 126.
- [220] S. Wicks, W. Horowitz, M. Djordjevic and M. Gyulassy, Nucl. Phys. A **784** (2007) 426.
- [221] M. Djordjevic and M. Djordjevic, Phys. Lett. B **734** (2014) 286.
- [222] J. Xu, J. Liao and M. Gyulassy, Chin. Phys. Lett. **32** (2015) 092501.
- [223] J. Xu, J. Liao and M. Gyulassy, arXiv:1508.00552 [hep-ph].
- [224] A. Bhattacharya, R. Enberg, M. H. Reno, I. Sarcevic and A. Stasto, JHEP **1506** (2015) 110.
- [225] R. Gauld, J. Rojo, L. Rottoli and J. Talbert, JHEP **1511** (2015) 009.
- [226] A. Adare *et al.* [PHENIX Collaboration], Phys. Rev. Lett. **97** (2006) 252002.
- [227] M. Cacciari, S. Frixione, N. Houdeau, M. L. Mangano, P. Nason and G. Ridolfi, JHEP **1210** (2012) 137.
- [228] P. M. Nadolsky, H. L. Lai, Q. H. Cao, J. Huston, J. Pumplin, D. Stump, W. K. Tung and C.-P. Yuan, Phys. Rev. D **78** (2008) 013004.
- [229] M. Klasen, C. Klein-Bsing, K. Kovarik, G. Kramer, M. Topp and J. Wessels, JHEP **1408** (2014) 109.
- [230] B. B. Abelev *et al.* [ALICE Collaboration], Phys. Rev. D **91** (2015) 012001.
- [231] B. Abelev *et al.* [ALICE Collaboration], Phys. Lett. B **708** (2012) 265.
- [232] P. Bolzoni and G. Kramer, Nucl. Phys. B **872** (2013) 253 [Nucl. Phys. B **876** (2013) 334].
- [233] B. A. Kniehl, G. Kramer, I. Schienbein and H. Spiesberger, Eur. Phys. J. C **72** (2012) 2082.
- [234] J. Pumplin, H. L. Lai and W. K. Tung, Phys. Rev. D **75** (2007) 054029.
- [235] R. Aaij *et al.* [LHCb Collaboration], arXiv:1510.01707 [hep-ex].
- [236] M. L. Mangano and J. Rojo, JHEP **1208** (2012) 010.
- [237] M. Cacciari, M. L. Mangano and P. Nason, Eur. Phys. J. C **75** (2015) 610.
- [238] G. Aad *et al.* [ATLAS Collaboration], arXiv:1512.02913 [hep-ex].
- [239] D. Acosta *et al.* [CDF Collaboration], Phys. Rev. Lett. **91** (2003) 241804.
- [240] R. Aaij *et al.* [LHCb Collaboration], JHEP **1306** (2013) 064.
- [241] V. Khachatryan *et al.* [CMS Collaboration], Phys. Rev. Lett. **106** (2011) 112001.
- [242] G. Aad *et al.* [ATLAS Collaboration], Eur. Phys. J. C **71** (2011) 1846.
- [243] S. Chatrchyan *et al.* [CMS Collaboration], JHEP **1204** (2012) 084.
- [244] R. Aaij *et al.* [LHCb Collaboration], JHEP **1510** (2015) 172.
- [245] V. Khachatryan *et al.* [CMS Collaboration], JHEP **1103** (2011) 136.
- [246] S. Bjelogrić [ALICE Collaboration], Nucl. Phys. A **931** (2014) 563.
- [247] B. Abelev *et al.* [ALICE Collaboration], Phys. Lett. B **712** (2012) 165.
- [248] J. Adam *et al.* [ALICE Collaboration], JHEP **1509** (2015) 148.

- [249] S. Chatrchyan *et al.* [CMS Collaboration], JHEP **1404** (2014) 103.
- [250] M. Arneodo, Phys. Rept. **240** (1994) 301.
- [251] S. Malace, D. Gaskell, D. W. Higinbotham and I. Cloet, Int. J. Mod. Phys. E **23** (2014) 1430013.
- [252] K. J. Eskola, H. Paukkunen and C. A. Salgado, JHEP **0904** (2009) 065.
- [253] M. Hirai, S. Kumano and T.-H. Nagai, Phys. Rev. C **76** (2007) 065207.
- [254] D. de Florian and R. Sassot, Phys. Rev. D **69** (2004) 074028.
- [255] F. Gelis, E. Iancu, J. Jalilian-Marian and R. Venugopalan, Ann. Rev. Nucl. Part. Sci. **60** (2010) 463.
- [256] M. Lev and B. Petersson, Z. Phys. C **21** (1983) 155.
- [257] X. N. Wang, Phys. Rev. C **61** (2000) 064910.
- [258] B. Z. Kopeliovich, J. Nemchik, A. Schafer and A. V. Tarasov, Phys. Rev. Lett. **88** (2002) 232303.
- [259] S. Gavin and J. Milana, Phys. Rev. Lett. **68** (1992) 1834.
- [260] S. J. Brodsky and P. Hoyer, Phys. Lett. B **298** (1993) 165.
- [261] I. Vitev, Phys. Rev. C **75** (2007) 064906.
- [262] F. Arleo and S. Peigne, JHEP **1303** (2013) 122.
- [263] S. Chatrchyan *et al.* [CMS Collaboration], Phys. Lett. B **718** (2013) 795.
- [264] B. Abelev *et al.* [ALICE Collaboration], Phys. Lett. B **719** (2013) 29.
- [265] B. B. Abelev *et al.* [ALICE Collaboration], Phys. Lett. B **726** (2013) 164.
- [266] G. Aad *et al.* [ATLAS Collaboration], Phys. Rev. Lett. **110** (2013) 182302.
- [267] K. Dusling and R. Venugopalan, Phys. Rev. D **87** (2013) 051502.
- [268] A. Adare *et al.* [PHENIX Collaboration], Phys. Rev. Lett. **111** (2013) 202301.
- [269] B. B. Abelev *et al.* [ALICE Collaboration], JHEP **1412** (2014) 073.
- [270] E. G. Ferreira, Phys. Lett. B **749** (2015) 98.
- [271] X. Du and R. Rapp, Nucl. Phys. A **943** (2015) 147.
- [272] A. Adare *et al.* [PHENIX Collaboration], Phys. Rev. Lett. **109** (2012) 24, 242301.
- [273] A. Adare *et al.* [PHENIX Collaboration], Phys. Rev. Lett. **112** (2014) 252301.
- [274] I. Helenius, K. J. Eskola, H. Honkanen and C. A. Salgado, JHEP **1207** (2012) 073.
- [275] A. M. Sickles, Phys. Lett. B **731** (2014) 51.
- [276] A. Beraudo, A. De Pace, M. Monteno, M. Nardi and F. Prino, arXiv:1512.05186 [hep-ph].
- [277] J. Adam *et al.* [ALICE Collaboration], Phys. Lett. B **754** (2016) 81.
- [278] B. B. Abelev *et al.* [ALICE Collaboration], Phys. Rev. Lett. **113** (2014) 23, 232301.
- [279] V. Khachatryan *et al.* [CMS Collaboration], Phys. Lett. B **754** (2016) 59.
- [280] S. Li [ALICE Collaboration], Nucl. Phys. A **931** (2014) 546.
- [281] H. Fujii and K. Watanabe, Nucl. Phys. A **920** (2013) 78.
- [282] Z. B. Kang, I. Vitev, E. Wang, H. Xing and C. Zhang, Phys. Lett. B **740** (2015) 23.
- [283] R. Auerbeck, N. Bastid, Z. C. del Valle, P. Crochet, A. Dainese and X. Zhang, arXiv:1107.3243 [hep-ph].
- [284] Y. Xu, S. Cao, G. Y. Qin, W. Ke, M. Nahrgang, J. Auvinen and S. A. Bass, arXiv:1510.07520 [nucl-th].
- [285] J. Adam *et al.* [ALICE Collaboration], arXiv:1602.07240 [nucl-ex].
- [286] J. Adam *et al.* [ALICE Collaboration], Phys. Rev. C **91** (2015) 6, 064905.
- [287] J. Huang, Z. B. Kang and I. Vitev, Phys. Lett. B **726** (2013) 251.
- [288] Z. Conesa del Valle, E. G. Ferreira, F. Fleuret, J. P. Lansberg and A. Rakotozafindrabe, Nucl. Phys. A **926** (2014) 236.
- [289] R. Gauld, Phys. Rev. D **93** (2016) 1, 014001.
- [290] C. Marquet, Nucl. Phys. A **796** (2007) 41.
- [291] T. Lappi and H. Mantysaari, Nucl. Phys. A **908** (2013) 51.
- [292] Z. B. Kang, I. Vitev and H. Xing, Phys. Rev. D **85** (2012) 054024.
- [293] J. Adam *et al.* [ALICE Collaboration], Phys. Lett. B **753** (2016) 126.
- [294] L. Adamczyk *et al.* [STAR Collaboration], Phys. Rev. Lett. **113** (2014) 14, 142301.
- [295] W. A. Horowitz and M. Gyulassy, Phys. Lett. B **666** (2008) 320.

- [296] W. A. Horowitz, AIP Conf. Proc. **1441** (2012) 889.
- [297] M. Djordjevic, Phys. Rev. Lett. **112** (2014) 042302.
- [298] M. Djordjevic, M. Djordjevic and B. Blagojevic, Phys. Lett. B **737** (2014) 298.
- [299] A. Adil and I. Vitev, Phys. Lett. B **649** (2007) 139.
- [300] K. Adcox *et al.* [PHENIX Collaboration], Phys. Rev. Lett. **88** (2002) 192303.
- [301] S. S. Adler *et al.* [PHENIX Collaboration], Phys. Rev. Lett. **94** (2005) 082301.
- [302] A. Adare *et al.* [PHENIX Collaboration], Phys. Rev. C **91** (2015) 044907.
- [303] A. Adare *et al.*, arXiv:1509.04662 [nucl-ex].
- [304] J. Adam *et al.* [ALICE Collaboration], Phys. Lett. B **753** (2016) 41.
- [305] S. Sakai [ALICE Collaboration], Nucl. Phys. A **904-905** (2013) 661c.
- [306] The ATLAS collaboration, ATLAS-CONF-2015-053.
- [307] A. Adare *et al.* [PHENIX Collaboration], Phys. Rev. C **90** (2014) 3, 034903.
- [308] M. He, R. J. Fries and R. Rapp, Phys. Rev. C **91** (2015) 2, 024904.
- [309] A. Adare *et al.* [PHENIX Collaboration], Phys. Rev. Lett. **109** (2012) 152301.
- [310] S. S. Adler *et al.* [PHENIX Collaboration], Phys. Rev. C **74** (2006) 024904.
- [311] L. Adamczyk *et al.* [STAR Collaboration], arXiv:1405.6348 [hep-ex].
- [312] S. Cao, G. Y. Qin and S. A. Bass, J. Phys. G **40** (2013) 085103.
- [313] M. Volkl [ALICE Collaboration], arXiv:1412.2670 [nucl-ex].
- [314] B. Abelev *et al.* [ALICE Collaboration], JHEP **1209** (2012) 112.
- [315] B. Abelev *et al.* [ALICE Collaboration], Phys. Rev. Lett. **111** (2013) 102301.
- [316] B. B. Abelev *et al.* [ALICE Collaboration], Phys. Rev. C **90** (2014) 034904.
- [317] J. Adam *et al.* [ALICE Collaboration], JHEP **1511** (2015) 205.
- [318] J. Adam *et al.* [ALICE Collaboration], arXiv:1509.06888 [nucl-ex].
- [319] J. Adam *et al.* [ALICE Collaboration], arXiv:1509.07287 [nucl-ex].
- [320] Z. Ye [STAR Collaboration], Nucl. Phys. A **931** (2014) 520.
- [321] W. A. Horowitz and M. Gyulassy, Nucl. Phys. A **872** (2011) 265.
- [322] A. Dainese *et al.*, arXiv:1602.04120 [nucl-ex].
- [323] R. Baier, Nucl. Phys. A **715** (2003) 209.
- [324] R. Vogt [Hard Probes Collaboration], Int. J. Mod. Phys. E **12** (2003) 211.
- [325] J. Rafelski and B. Muller, Phys. Rev. Lett. **48** (1982) 1066 [Phys. Rev. Lett. **56** (1986) 2334].
- [326] P. Koch, B. Muller and J. Rafelski, Phys. Rept. **142** (1986) 167.
- [327] B. B. Abelev *et al.* [ALICE Collaboration], Phys. Lett. B **736** (2014) 196.
- [328] B. Abelev *et al.* [ALICE Collaboration], Phys. Lett. B **720** (2013) 52.
- [329] B. Abelev *et al.* [ALICE Collaboration], Phys. Lett. B **719** (2013) 18.
- [330] M. Gyulassy and M. Plumer, Phys. Lett. B **243** (1990) 432.
- [331] S. Chatrchyan *et al.* [CMS Collaboration], JHEP **1205** (2012) 063.
- [332] CMS Collaboration [CMS Collaboration], CMS-PAS-HIN-12-014.
- [333] A. Buzzatti and M. Gyulassy, Nucl. Phys. A **904-905** (2013) 779c.
- [334] M. He, R. J. Fries and R. Rapp, Nucl. Phys. A **910-911** (2013) 409.
- [335] P. B. Gossiaux, M. Nahrgang, M. Bluhm, T. Gousset and J. Aichelin, Nucl. Phys. A **904-905** (2013) 992c.
- [336] G. Aad *et al.* [ATLAS Collaboration], Phys. Lett. B **719** (2013) 220.
- [337] CMS Collaboration [CMS Collaboration], CMS-PAS-HIN-12-004.
- [338] A. Banfi, G. P. Salam and G. Zanderighi, JHEP **0707** (2007) 026.
- [339] A. H. Mueller and P. Nason, Phys. Lett. B **157** (1985) 226.
- [340] M. L. Mangano and P. Nason, Phys. Lett. B **285** (1992) 160.
- [341] S. S. Gubser, Nucl. Phys. B **790** (2008) 175.
- [342] K. M. Burke *et al.* [JET Collaboration], Phys. Rev. C **90** (2014) 1, 014909.
- [343] R. Rapp, J. Phys. G **36** (2009) 064014.
- [344] M. Nasim [STAR Collaboration], arXiv:1512.09352 [nucl-ex].
- [345] B. Abelev *et al.* [ALICE Collaboration], Phys. Rev. Lett. **109** (2012) 072301.

- [346] B. B. Abelev *et al.* [ALICE Collaboration], Phys. Lett. B **734** (2014) 314.
- [347] E. Abbas *et al.* [ALICE Collaboration], Phys. Rev. Lett. **111** (2013) 162301.
- [348] W. Liu and C. M. Ko, arXiv:nucl-th/0603004.